UNIVERSITY OF SOUTHERN QUEENSLAND

MONITORING THE DEPTH OF ANAESTHESIA USING SIMPLIFIED ELECTROENCEPHALOGRAM (EEG)

A dissertation submitted by

Tai Nguyen-Ky,

M. Eng. (Hon.), Ho Chi Minh City University of Technology, 2000

MBA (Hon.), Ho Chi Minh City University of Technology, 1996

B. Eng. (Hon.), Ho Chi Minh City University of Technology, 1991

For the award of

Doctor of Philosophy

February 2011

To my family

Abstract

Anaesthesia is administered routinely every day in hospitals and medical facilities. Numerous methods have been devised and implemented for monitoring the depth of anaesthesia (DoA) in order to guarantee the safety of patients. Monitoring the depth of anaesthesia provides anaesthesia professionals with an additional method to assess anaesthetic effects and patient responses during surgery. The measurement of depth of anaesthesia benefits patients and helps anaesthetists such as "reduction in primary anaesthetic use, reduction in emergence and recovery time, improved patient satisfaction and decreased incidence of intra-operative awareness and recall" (Kelley S. D.).

Clinical practice uses autonomic signs such as heart rate, blood pressure, pupils, tears, and sweating to determine depth of anaesthesia. However, clinical assessment of DoA is not valuable in predicting the response to a noxious stimulusand may vary depending on disease, drugs and surgical technique. Currently available DoA monitoring devices have been criticised in the literature, such as being redundant (Schneider, 2004), not responsive to some anaesthetic agents (Barr G., 1999), and time delay (Pilge S., 2006).

This research proposes new methods to monitor the depth of anaesthesia (DoA) based on simplified EEG signals. These EEG signals were analysed in both the time domain and the time-frequency domain. In the time domain, the Detrended Fluctuation Analysis (DFA), detrended moving average (DMA) and Chaos methods

are modified to study the scaling behaviour of the EEG as a measure of the DoA. In the frequency domain, fast Fourier transform (FFT) and filter bank are used to identify difference states of anaesthesia. In the time-frequency domain, discrete wavelet transforms (DWT) and power spectral density (PSD) function are applied to pre-process EEG data and to monitor the DoA.

Firstly, a new de-noising algorithm is proposed with a threshold T_{WE}, which is a function of wavelet entropy and the window length m for an EEG segment. Secondly, the anaesthesia states are identified into awake, light, moderate, deep and very deep anaesthesia states. Finally, the DoA indices are computed using:

- Modified DFA method (MDFA I),
- Modified DFA-Lagrange method (MDFA II),
- Modified detrended moving average method (MDMA),
- Modified Chaos method, combined Chaos and MDMA method,
- Wavelet-power spectral density.

Simulation results demonstrate that our new methods monitor the DoA in all anaesthesia states accurately. These proposed methods and indices present a good responsive to anaesthetic agent, reduce the time delay when patient's hypnotic state changes (from 12 to 178 seconds), and can estimate a patient's hypnotic state when signal quality is poor.

Certification of Dissertation

I certify that the ideas, experimental work, results and analyses, software and conclusions reported in this dissertation are entirely my own effort, except where otherwise acknowledged. I also certify that the works is original and has not been previously submitted for any other award, except where otherwise acknowledged.

_____ _____

Tai Nguyen-Ky, Candidate Date

ENDORSEMENT

_____ _____

A/ Prof. Peng (Paul) Wen, Principle supervisor Date

_____ _____

A/ Prof. Yan Li, Associate supervisor Date

Acknowledgements

This research is supported by Australia Research Council (ARC) Discovery Program grant DP0665216.

I would like to express my deepest appreciation to Associate Professor Peng (Paul) Wen and Associate Professor Yan Li for their valuable support, advice and effective guidance. They have introduced me to this attractable field of biomedical research and have made the completion of this dissertation possible. I am also very thankful to Dr Robert Gray, a senior anaesthetist, for his clinical knowledge and expertise in anaesthesia.

I would like to thank Prof. Thanh Tran-Cong, Prof. Nguyen Thuc Loan for their support and encouragement. I wish to thank Prof. Frank Bullen, Dean of Faculty of Engineering and Surveying, Pro Vice Chancellor (Research), for his support. I wish to thank all the lecturers and staffs of the Faculty of Engineering and Surveying, Centre for Systems Biology (CSBi), Computational Engineering Research Centre (CESRC), University of Southern Queensland (USQ) for their academic and administrative assistance. I thank all my colleagues for their cooperation and discussions. I am also thankful to my friends, Ms Jeanette and Mr Andreas Helwig, for their comments and corrections.

Finally, I wish to thank my parents, my brothers and my sisters for their continuing support and encouragement. I am especially thankful to my wife, Pham Thi Cuc for her love, patience, and understanding.

Related Publications

During Dissertation Period

1. Nguyen-Ky, T., Wen, P., Li, Y., *et al.* (2010d). "Measuring and reflecting depth of anaesthesia using wavelet and power spectral density techniques." *IEEE Transactions on Information Technology in Biomedicine, accepted 2011*.

2. Nguyen-Ky, T., Wen, P. and Li, Y. (2010c). "An improved de-trended moving average method for monitoring the depth of anaesthesia." *IEEE Transactions on biomedical engineering*, 57(10): 2369-2378.

3. Nguyen-Ky, T., Wen, P. and Li, Y. (2010b). "Improving the accuracy of depth of anaesthesia using modified detrended fluctuation analysis method." *Biomedical Signal Processing and Control* 5(1): 59-65.

4. Nguyen-Ky, T., Wen, P. and Li, Y. (2010a). "De-noising a raw eeg signal and measuring depth of anaesthesia for general anaesthesia patients." *The 2010 IEEE/ICME International Conference on Complex Medical Engineering (CME2010) in Gold Coast, Australia.*

5. Nguyen-Ky, T., Wen, P. and Li, Y. (2009b). "Theoretical basis for identification of different anaesthetic states based on routinely recorded EEG during operation." *Computers in Biology and Medicine* 39(1): 40-45.

6. Nguyen-Ky, T., Wen, P. and Li, Y. (2009a). "Monitoring the depth of anaesthesia using discrete wavelet transform and power spectral density." *Proceeding of the fourth International Conference on Rough Sets and Knowledge Technology (RSKT2009), Gold Coast, Australia*. (*The best student paper award*)

7. Nguyen-Ky, T., Wen, P. and Li, Y. (2008). "Modified detrended fluctuation analysis method in depth of anaesthesia assessment application." *Proceeding of the 2008 International Conference on bioinformatics & computational biology, Las Vegas, Nevada, USA*: 279-284.

Contents

List of Frequently used Acronyms and Abbreviations

ANN	Artificial Neural Network
ANOVA	Analysis of Variance
AP	Affine Projection
AWL	Adaptive Window Length
BIS	Bispectrum Index
BS	Burst Suppression
BSR	Burst Suppression Ratio
cdf	cumulative distribution function
CDoA	Chaos Depth of Anaesthesia
CsDoA	Chaos-s Depth of Anaesthesia
CFAM	Central Function Analysing Monitor
Ch-MDMA	Chaos-Modified Detrended Moving Average
CSI	Cerebral State Index
CWTs	Continuous Wavelet Transforms
DB	Daubechies Wavelet.
df	degrees of freedom
DFA	Detrended Fluctuation Analysis
DMA	Detrended Moving Average
DoA	Depth of Anaesthesia

DSP	Digital Signal Processing
DTFT	Discrete-Time Fourier Transform
DWT	Discrete Wavelet Transform
ECGs	Electrocardiograms
EEA	Error Estimation Algorithm
EEG	Electroencephalogram
EMG	Electromyogram
EOG	Electrooccluglams
FFT	Fast Fourier Transform
fMRI	functional Magnetic Resonance Imaging
HMSPs	High Magnitude Specified Peaks
IFT	Isolated Forearm Technique
LMS	Least Mean Squares
LOC	Lower Oesophageal Contractility
LOC	Loss of Consciousness
MAC	Minimum Alveolar Concentration
MAC	Monitored Anesthesia Care
MaPS	Maximum Power Spectrums
MDFA1	Modified Detrended Fluctuation Analysis 1
MDFA2	Modified Detrended Fluctuation Algorithm 2
MDMA	Modified Detrended Moving Average
MLAEP	Mid-Latency Auditory Evoked Potentials
MS	Mean Squares
MUSIC	Multiple Signal Classification
NEEA	New Error Estimate Algorithm

OAA/S	Observer’s Assessment of Alertness/Sedation
OMT	Ocular Micro Tremor
PCA	Patient Controlled Analgesia
PET	Positron Emission Tomography
PRST	Pressure, Rate, Sweating and Tear
PSD	Power Spectral Density
PSI	Patient State Index
RE	Response Entropy
RLS	Recursive Least Squares
SC	Skin Conductance
SE	State Entropy
SMI	Set-Membership Identification
SM-NLMS	Set-Membership Normalized Least Mean-Squares
SPECT	Single Photon Emission Computed Tomography
SQI	Signal Quality Index
SS	Sum of Squares
TCR	Time to Correct Response
USB	Universal Serial Bus
WDoA	Wavelet DoA
WT	Wavelet Transform

List of Tables

List of Figures

Chapter 1

Introduction

Anaesthesia is the term given to the loss of feeling or sensation. This is a method of decreasing sensitivity to pain in a patient while surgery is being performed. Anaesthesia may be accomplished without the loss of consciousness, or with partial or total loss of consciousness. There are two kinds of anaesthesia: general anaesthesia, which affects the entire body and causes a loss of consciousness, and local anaesthesia which is accomplished using drugs that temporarily block the sensation of pain in a certain area of the body while the patient remains awake. This thesis is only concerned with general anaesthesia. There are three phases to general anaesthesia:

- induction: placing the patient in an initial state of unconsciousness;
- maintenance: keeping the patient unconscious while the procedure is performed;
- emergence: allowing the patient to emerge back into consciousness.

Pharmacological methods are used for preparation of medical procedures. Drugs can be administered by injection into muscle or under the skin with a needle, intravenously (by needle into a vein), or with a gas mask for inhalation. Creams, gels, liquids can directly be applied onto the area being treated.

The administration and monitoring of anaesthesia require both knowledge and practice. Vital signs and other monitoring parameters are assessed continuously throughout the procedure.

There are many reasons underlying an increased risk of underdose and overdose in surgery which could include inadequate drug dosing, poor monitoring, failure to refill the anaesthetic machine's vaporisers, insufficient training, unfamiliarity with techniques used, machine misuse and malfunction.

Monitoring the depth of anaesthesia will help anesthesiologists to adjust the anaesthetic under administration, and to prevent the incidence of awareness and anaesthetic overdose during surgery. DoA monitor systems provide anaesthesia professionals with an additional method to assess anaesthetic effects and patient responses during surgery. A robust measurement of depth of anaesthesia will benefit patients in recovery time and help anaesthetists in primary anaesthetic use (Yentis, 2009; Taylor, 1993; Kelley).

1.1 ANAESTHESIA AWARENESS

Awareness during anaesthesia occurs when a patient is underdose, does not have enough anaesthetic or analgesic to prevent consciousness or waking up during surgery (Brice, 1970). In this situation, the patient may feel the pain or pressure of surgery, hear conversations, or feel as if they can not breathe. Although currently there is no evidence that monitoring the depth of unconsciousness prevents awareness, it is conceivable that by maintaining a sufficient depth of anaesthesia, awareness prevention will be achieved (Sebel, 2004).

The overall incidence of intraoperative awareness with recall is about 0.2–3% but it may be more than 40% in certain high risk patients (Andrew, 2005; Kuizenga, 2001; Mathews, 2005) such as those with multiple trauma; those undergoing caesarean section or cardiac surgery and haemodynamically unstable patients. Intraoperative awareness is a medico-legal liability for anaesthetists as it may be

interpreted as a failure to adequately anaesthetise. It has the potential to cause severe postoperative psychosomatic dysfunction (Moerman, 1993; Sandin, 2000; Lennmarken, 2002; Sebel, 2004; Brice, 1970). Thus, inadequate anaesthesia is not desirable, and a robust measurement of depth of anaesthesia will benefit patients and help anaesthetists.

1.2 ANAESTHETIC OVERDOSE

Whenever a patient undergoes surgery, they can be at a risk of overdose. If a dose of anaesthetic is injected too quickly or the injections are given too closely together, an overdose may happen to a patient. "There are a number of reasons that may lead to an overdose including:

- incorrect labeling on anaesthetic,
- confusing two different anaesthetics,
- injecting too quickly or/and too much anaesthetic at a given time,
- improperly timing durations between injections,
- combining incompatible anaesthetics. "

(http://www.articlesbase.com/personal-injury-articles/anesthesia-overdose-risks-and-medical-malpractice-2254011.html)

These types of errors can result in a variety of injuries that may leave a patient with a serious brain injury, nerve damage, paralysis, or a spinal cord injury. The patient can suffer other serious complications such as a heart attack; stroke or even death. Clinical investigations and individual cases have reported the accidental overdose of anaesthic (Musshoff, 2005; Isbister, 2001; Cork, 1990; Bøggild-Madsen, 1978; Cork, 1990). Musshoff reported a case about the patient died as a result of a drug overdose during patient-controlled analgesia (PCA). This report is a further example that

human errors play a crucial role in the safety of medical equipment (Musshoff, 2005). Notcutt *et al.* reported two incidents when a PCA pump has accidentally delivered the whole contents of the syringe of diamorphine (60 mg) over a period of approximately 1 hour (Notcutt, 1992).

1.3 THE PROCESS OF ANAESTHESIA

Clinical monitoring is essential for safe patient care during anaesthesia by an anaesthetist. Appropriate equipments are used to assist the anaesthetist such as oxygen analyser, pulse oximeter, breathing system disconnection, electrocardiograph, temperature monitor, carbon dioxide monitor, neuromuscular function monitor, continuous blood pressure monitor, and other equipment.

"In anaesthetic room and operating theatre, the patient's consent form and other details are checked. An intravenous cannula is put into a vein and secured. Anaesthetic machines are use to administer the injection of medicine, the flow of oxygen and anaesthetic gases" (Kane S., 2003).

A guide dose is pre-calculated based on the patient's body weight and age. However, it must be modified according to the previous history of anaesthesia, the physical status of the patient, the type and complexity of the surgery, and may be changed at different points in the operation. During the operation period, the anaesthetist's task is to observe the patient directly, and maintain the depth of anaesthesia by administering anethetics. At the end of the operation, administration of the anaesthetic stops, the patient gradually regains consciousness and is transferred to the recovery room.

1.4 MONITOR THE DEPTH OF ANAESTHESIA

Anaesthetists seek an early warning of a patient's level of hypnosis in real time. A number of methods have been developed over the years to determine depth of anaesthesia such as:

- clinical signs: systolic blood pressure, heart rate, sweating and tears (PRST);
- spontaneous surface electromyogram (SEMG);
- heart rate variability (HRV);
- the minimum alveolar concentration (MAC);
- lower oesophageal contractility (LOC);
- isolated forearm technique;
- EEG signals.

EEG signals are used as a clinical monitoring tool during anaesthesia. Results from both human and animal studies demonstrate that changes in EEG with anaesthesia primarily reflect hypnotic information (Terri, 2005; Rampil, 1992; 1993; Andrew, 2005; Kuizenga, 2001; Bruhn, 2006; Agarwal, 2004). Several DoA monitoring devices based on EEG signals have been developed in the past few years such as the Cerebral State Index, the Patient State Index, the state entropy, the Narcotrend index, and the BIS Index.

1.5 BRAIN RHYTHMS AND EEG SIGNAL

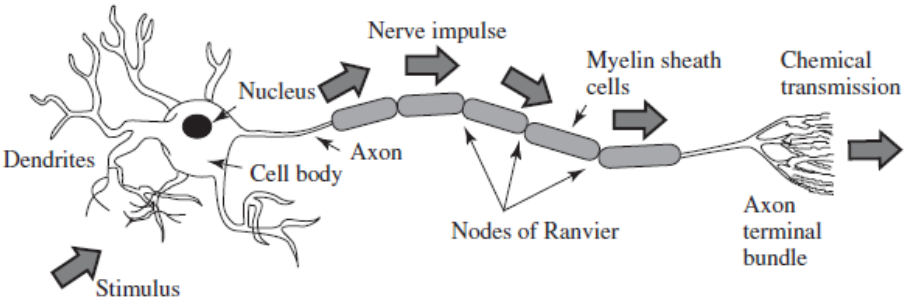

Figure 1.1: Structure of a neuron (Attwood, 1989)

The fundamental unit of the brain is the neuron - the scientific term for a single brain cell. A neuron communicates to other neurons via electrical impulses and chemical secretions. Electrical inputs to one neuron come from many others, each having a specific amount of influence, or weight, on the neuron (Figure 1.1). When neuronal networks are activated, they produce a noticeable change in voltage, which can be captured by a special apparatus called an electroencephalograph (EEG). These changes appear as wriggling lines along the time axis in a typical EEG record (Attwood, 1989, Sanei, 2007, Joseph, 2003; Bischoff, 2000).

EEGs show continuous oscillating electric activity. The amplitude and the patterns are determined by the overall excitation of the brain which in turn depends on the activity of the reticular activating system in the brain stem. The amplitude on the surface of the brain is about 1-2 mV, those on the surface of the scalp range up to 100 μV, and frequencies range from 0.3 to 100 Hz. Higher frequencies are measured and are of research interest, but are as yet poorly understood (eg fast ripples at 200 Hz). The physiological interest lies between 0.3 and 64 Hz. There are five major brain rhythms and frequency bands: alpha, beta, gamma, delta and theta

(Rundshagen, 2004). They are distinguished by their different frequency ranges (Alkire, 1998).

- *Delta waves* have a frequency range between 0.5 and 4 Hz with an amplitude less than 100 μV at sedation and light anaesthesia;
- *Theta waves* have a frequency range between 4 to 8 Hz with an amplitude less than 100 μV. They occur mainly in the parietal and temporal regions in sleep;
- *Alpha waves* contain frequencies between 8 and 13 Hz with amplitude less than 10 μV at awake state. Closing the eyes has a strong activating to alpha rhythms;
- *Beta waves* have a frequency range of 13 to 30 Hz. They have their maximum amplitude (less than 20 μV) on the parietal and frontal regions of the scalp. There are two types: beta I waves, lower frequencies which disappear during mental activity, and beta II waves, higher frequencies which appear during tension and intense mental activity;
- *Gamma waves* have frequencies between 30 and 100 Hz with an amplitude less than 2 μV peak-to-peak when the person is attending or some sensory stimulation (Rampill 1998).

Chapter 2

A Literature Review Of DoA Assessment

2.1 CLINICAL VIEWPOINT

Anaesthesia is the largest single hospital specialty and has service delivery requirements not only in operating theatres, but also in intensive care units, high dependency units, accident and emergency, obstetric units and pain clinics.

Before 1846, the mechanism of anaesthesia was studied by physicians and scientists to explore the effect of the drugs on the central nervous system. Morton had a demonstration of surgical anaesthesia in Boston, on October 16, 1846. A French physiologist, Francois Magendie (1783-1855), played a significant role among early studies of drug action. Physicians recognized that anaesthetized patients exhibited an orderly sequence of clinical signs, starting with a disturbance of consciousness, followed by a loss of reflex activity, and finally a paralysis of respiratory and cardiac activity. Anaesthesia results are explained in clinically observable effects, at multiple levels: the brain and spinal cord, the dorsal horn of the

spinal cord, the synapse, the cell membrane with its associated receptors and proteins, individual receptors, and individual molecules (Joseph, 2003).

2.1.1 Clinical endpoint

Despite 150 years of general anaesthesia practice, there is still no accepted scientific definition of hypnosis and consciousness, let alone a gold standard for the quantification and measurement of these endpoints. Currently, there are no mechanistic, physiological standards in defining consciousness or unconsciousness. The difficulty of tackling DoA is for anaesthetists to determine what constitutes 'adequate' anaesthesia for an individual patient. The clinical observations used to assess anaesthetic adequacy all lack sensitivity and specificity for the presence or absence of consciousness. There is growing evidence of dose-related harmful effects of anaesthetic agents, and some evidence shows that excessive anaesthetic doses contribute to mortality rates (Terri, 2005; Maj-Lis, 2009; Monk, 2008; Kim, 2002; Kortelainen, 2008; Van, 2006).

Anaesthetic endpoints commonly used in experimental studies of mechanism include:

- Unconsciousness is loss of response to verbal commands: loss of right reflex in vertebrates, and loss of movement in response to a noxious stimulus.
- Amnesia is a condition in which memory is disturbed or lost. Memory in this context refers either to stored memories or to the process of committing something to memory.
- Analgesia means loss of painful sensation before immobility.
- Immobility is any disease or disability case in that there are extremely limits patient’s activity.

2.1.2 Anaesthetic drugs

Anaesthetics are available in two formulations: gases (vapours) and injections (intravenous anaesthetics). The most commonly used anaesthetic technique is to induce anaesthesia intravenously, then maintain it with anaesthetic gases. There is no one anaesthetic agent that can produce all of unconsciousness, amnesia, analgesia and immobility. Several agents are used together in an anaesthetic procedure. A typical anaesthetic procedure has four parts: premedication, induction, maintenance and recovery. The quantities of anaesthetic agents are calculated by anaesthetists for each individual patient. Modern medicine uses multiple agents to invoke clinical anaesthesia. These agents are known to have unique and stereotypical effects on EEG activity.

Administration of sub-anaesthetic drug concentrations causes EEG activation. This is characterized by increased or decreased power of EEG signal in different frequency bands (Kuizenga, 2001; Zhong, 2005; Anderson, 2004; Poirier, 1998; Nieminen, 2002; Gibbs, 1937, Glass, 1998). "Modern general anaesthetic techniques typically involve the co-application of a hypnotic drug, an analgesic drug and a muscle relaxant. The combinations of drugs are typically depending on using drugs, their relative concentrations with respect to each other, and bolus or continuously intravenous dose" (Urban, 2002). Dates of introduction of anaesthetic drugs are presented in Figure 2.1.

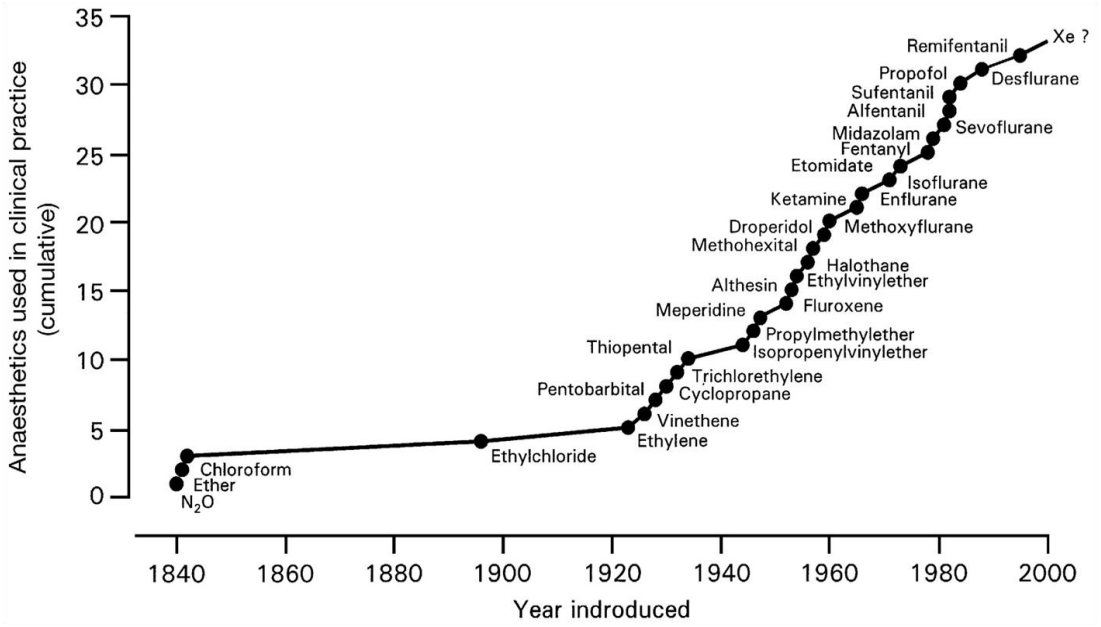

Figure 2.1: Dates of introduction of anaesthetic drugs (Urban, 2002)

2.1.3 Clinical monitoring

Clinical monitoring is the most common practice to estimate the depth of anaesthesia, such as:

1. Pupil size: in general, when the depth of anaesthesia is increasing, the pupil size tends to decrease, although the degree of constriction varies with different anaesthetic drugs, and the pupil may dilate during very deep anaesthesia (Taylor, 1993; Bajekal, 2004).
2. Cardiovascular changes: heart rate tends to decrease with increasing depth of anaesthesia.
3. Sweating and lacrimation may be found during light anaesthesia. Lacrimation is more sensitive index of light anaesthesia than sweating (Taylor, 1993).
4. Response to verbal commands: the isolated foream technique (IFT) (Russell, 1993) and the time to correct response (TCR) test are used (Breckenridge, 1983; Taylor, 1993). These methods are limited as patient recall is affected by drugs

and unreliable. Therefore, TCR test can be discounted. The IFT test requires the co-operation of the patient and can not use during surgery.

5. Clinical scoring system: PRST score

Adequacy of anaesthesia was assessed using a "pressure, rate, sweating and tear" as the PRST score (Table 2.1). The scores of 0-2 are allocated for each of the four components (Russell, 1993; Panousis, 2009).

Table 2.1: PRST scoreing indices

Index	Condition	Score
Systolic Arterial Pressure (mmHg)	Less than control +15 mm Hg Less than control +30 mm Hg More than control +30 mm Hg	0 1 2
Heart Rate (beats/min)	Less than control +15 bpm Less than control +30 bpm More than control +30 bpm	0 1 2
Sweat	Nil Skin moist to touch Visible beads of sweat	0 1 2
Tears or Lacrimation	No excess tears when eyelids open Excess tears visible when eyelids open Tear overflow from closed eyelids	0 1 2

6. Clinical scoring system: OAA/S score

The Observer's Assessment of Alertness/Sedation (OAA/S) score is presented in Table 2.2. The final score is the sum of the responsiveness, speech, facial expression, and eyes component. Therefore, a "wide-awake" score = 20/20 and a

"deeply sedated" score = 9/20 (1 [responsiveness] + 2 [speech] + 3 [faces] + 3 [eyes]) (Doufas, 2001).

Table 2.2: The Observer's Assessment of Alertness/Sedation (OAA/S)

Responsiveness	Score
Responds readily to name spoken in normal tone	5
Lethargic response to name spoken in normal tone	4
Responds only after name is spoken loudly and repeatedly or both	3
Responds only after mild prodding or shaking	2
Does not respond to mild prodding or shaking	1

2.2 DoA MONITORING EQUIPMENTS

2.2.1 Instrumental monitoring

Some instruments have been developed in an attempt to monitor depth of anaesthesia by indirect monitors or direct measurement of cerebral electrical activity.

1. Skin Conductance (SC): the MEDSTORM AS 2005 monitor achieves the SC with three single uses Ag/AgCl paediatric ECG electrodes attached to the palmar surface of the hand (Ledowski, 2006; 2007).
2. Digital Plethysmography: Plethysmographic measurements are valuable noninvasive methods for characterizing haemodynamic changes during treatment with vasoactive drugs. Especially in testing the response to nitrates and nitratelike compounds, digital pulse plethysmography is frequently used (Stengele, 1996; Grote, 2003; Dorlas, 1985)
3. Lower Oesophageal Contraction (LOC): Lower oesophageal contractility monitoring has recently been described as a monitor of the depth or adequacy

of anaesthesia. The musculature of the lower oesophagus is non-striated and remains fully active despite full skeletal muscle paralysis (Evans, 1984;1987; Isaac, 1989; 1990). Minimum alveolar concentration (MAC) is the most widely used method to compare anaesthetic drug potencies. MAC is reduced by other depressant drugs, α-methyldopa, reserpine, hypothermia/hypotension, extremes of ages. MAC is increased in children, hyperthermia, hyperthyroidism, chronic alcoholism (Merkel, 1963; Eger, 1965; Kaul, 2002; Yentis, 2009).

4. Ocular microtremor (OMT): OMT is a fine physiologic tremor of the eye related to neuronal activity in the reticular formation of the brainstem (Heaney, 2004; Bojanic, 2001; Coakley, 1977).
5. Electromyogram (EMG): The integrated EMG recordings from the frontalis muscle have been used as a means of monitoring light anaesthesia (Sleigh, 2001; Horner, 1991; Renna, 2002).
6. Electroencephalogram (EEG): The EEG is a recording of the brain's electrical activity from the surface of the scalp. The recordings are the summation of volume conductor fields produced by millions of interconnecting neurones. The neurone components producing the currents are the dendrites, axons and cell bodies (Sanei, 2007; Moca, 2009; Lemere, 1938; Martin, 1959)

Several equipments based on EEG signals have been developed for monitoring the DoA such as Cerebral State Index, Patient State Index, state entropy, Narcotrend Index, and BIS Index. The algorithms of these monitors are different and not fully published. The basic principles are described as the following:

2.2.2 The Cerebral State Index

The Cerebral State Index (CSI) is calculated using a fuzzy logic combination of four sub-parameters of the EEG signals in:

- time domain (Brust Suppression): $BS\% = \frac{t_{BS}}{30\,\mathrm{sec}\,onds}$, and
- frequency domain: ($\beta_{ratio} = \log \frac{E_{30-42.5Hz}}{E_{11-21Hz}}$, $\alpha_{ratio} = \log \frac{E_{30-42.5Hz}}{E_{6-12Hz}}$, β_{ratio}- α_{ratio})

analysis (Jensen, 2005). The diagram for the calculation of the CSI Index is presented in Figure 2.2. $E_{x\text{-}y}$ is the sum of the spectral power in the band extending from frequency *x* to *y*; and t_{BS} is the Brust Suppression time.

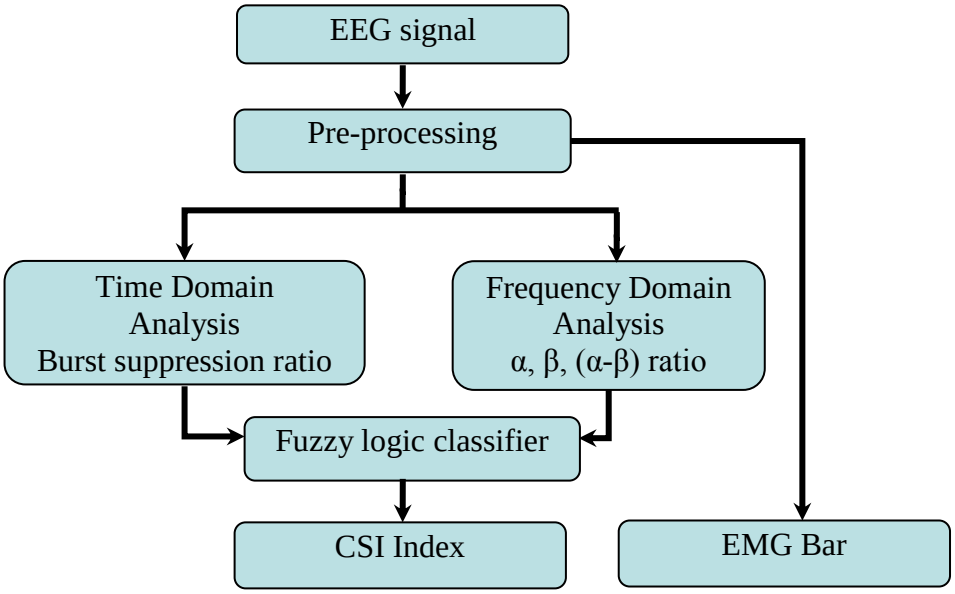

Figure 2.2: The diagram for the calculation of the CSI Index.

2.2.3 The Patient State Index

The Patient State Index (PSI) is the result of a complex computation that combines weighted quantitative EEG parameters reflecting many dimensions of brain electrical activities such as: changes in power in various EEG frequency bands, changes in symmetry and synchronization between critical brain regions, and the

inhibition/activation of regions of the frontal cortex (Drover, 2006; Prichep, 2004). Algorithm and instrument diagram of the PSI index are presented in Figure 2.3.

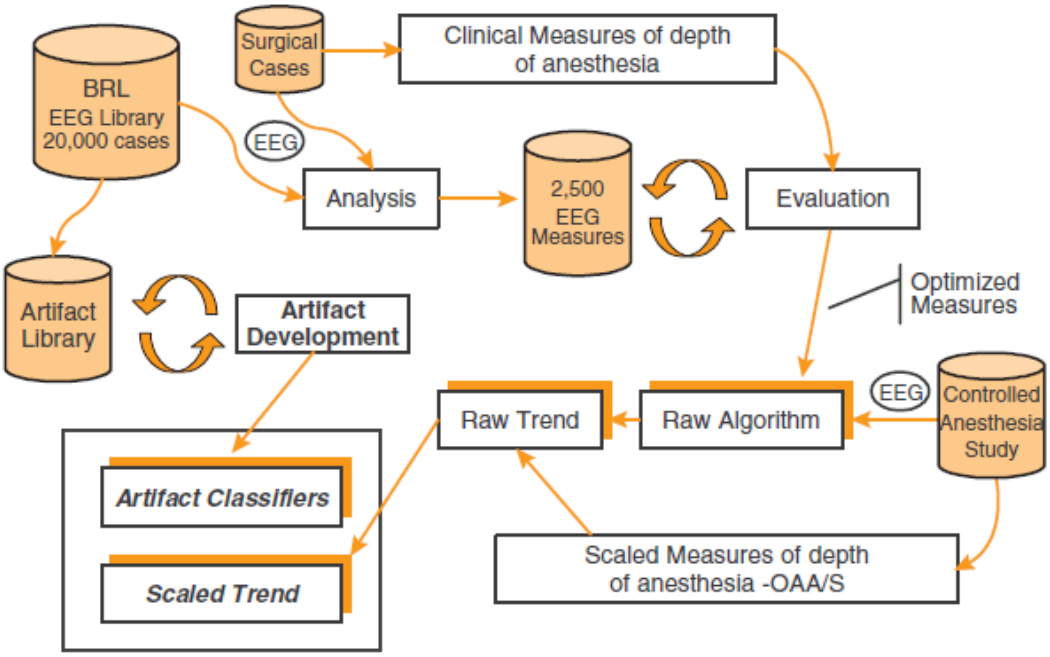

Figure 2.3: Algorithm and instrument diagram of the PSI index (Drover, 2006).

2.2.4 The state entropy

The state entropy (SE) is computed over the EEG-dominant part of the spectrum (0.8–32 Hz), with the time window from 60.16 to 15 seconds. The response entropy (RE) is computed over a frequency range from 0.8 to 47 Hz with the time windows from 15 to 1.92 seconds. (Viertiö-Oja, 2004). The spectral entropy (S) is corresponding to the frequency range $[f_1, f_2]$**.** Call $N[f_1, f_2]$ be the total number of frequency components in the range $[f_1, f_2]$, R_{low} is the frequency range from 0.8 Hz to 32 Hz, R_{high} is the frequency range from 32 Hz to 47 Hz, and $R_{low+high}$ is the frequency range from 0.8 Hz to 47 Hz.

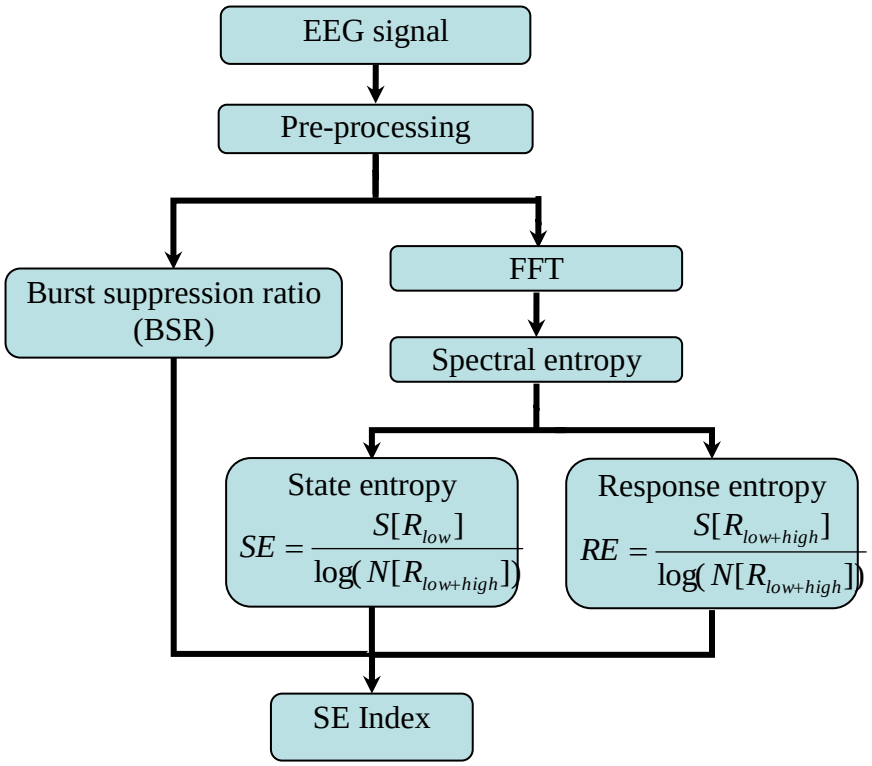

Figure 2.4: The SE Index diagram.

2.2.5 BIS Index

BIS Index is calculated from following four parameters: (1) burst suppression ratio (BSR); (2) quazi suppression index; (3) relative β ratio and (4) synchfastslow (Rampil, 1998; Pomfrett, 1998).

- Burst Suppression Ratio (*BSR*) by time domain analysis. *BSR* is a time domain EEG parameter to recognize those periods longer than 0.50 second, during which the EEG voltage does not exceed approximately +/- 5.0μV.
- *Quazi* suppression index also by time domain analysis. It was designed to detect burst suppression in the presence of wandering baseline voltage.
- Relative β ratio ($logP_{30\text{-}47Hz}/P_{11\text{-}20Hz}$) by power spectral analysis, with $P_{x\text{-}y}$ is the sum of the spectral power in the band extending from frequency x to y.

- *SynchFastSlow* ($logB_{0.5\text{-}47Hz}/B_{40\text{-}47Hz}$) by bispectral analysis, with $B_{x\text{-}y}$ is the sum of the bispectrum activity in the area subtended from frequency *x* to *y*.

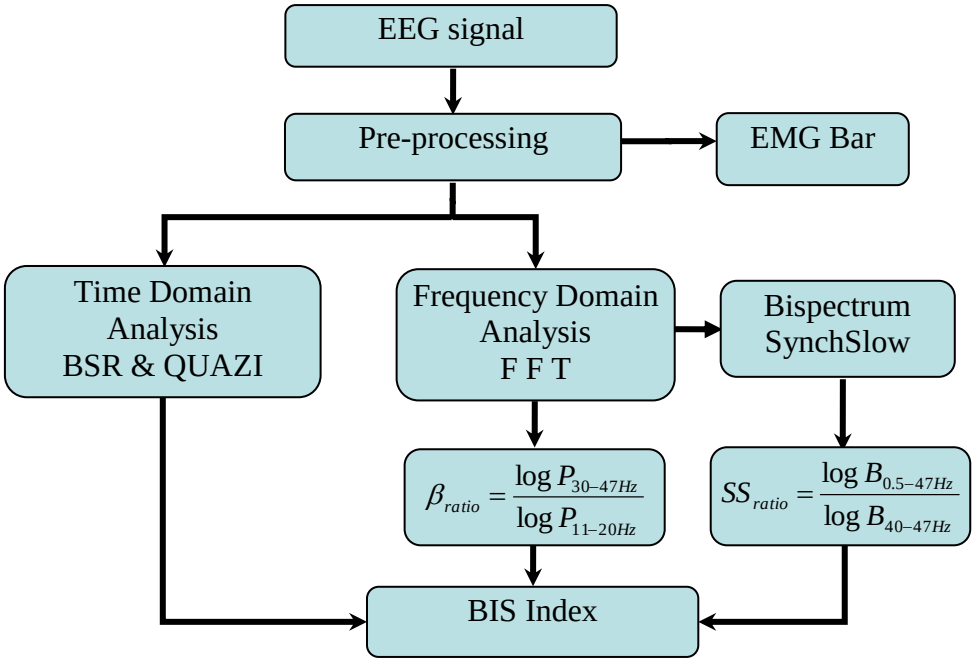

Figure 2.5: The block diagram of the BIS algorithm

2.2.6 Narcotrend Index

The EEG signals are sampled at 128 samples per second with a 12-bit resolution, and a bandpass filtered of 0.5–45 Hz. Trace segments are the units of classification with a length of 20 s. "The preceding 20 second period is classified every 5 s, yielding an overlap of 75% of the recorded data at every time point. From the traces, numerous quantitative features were extracted from the time and the frequency domain, such as spectral parameters, entropy measures and autoregressive parameters." (Kreuer, 2006; Bauerle, 2004).

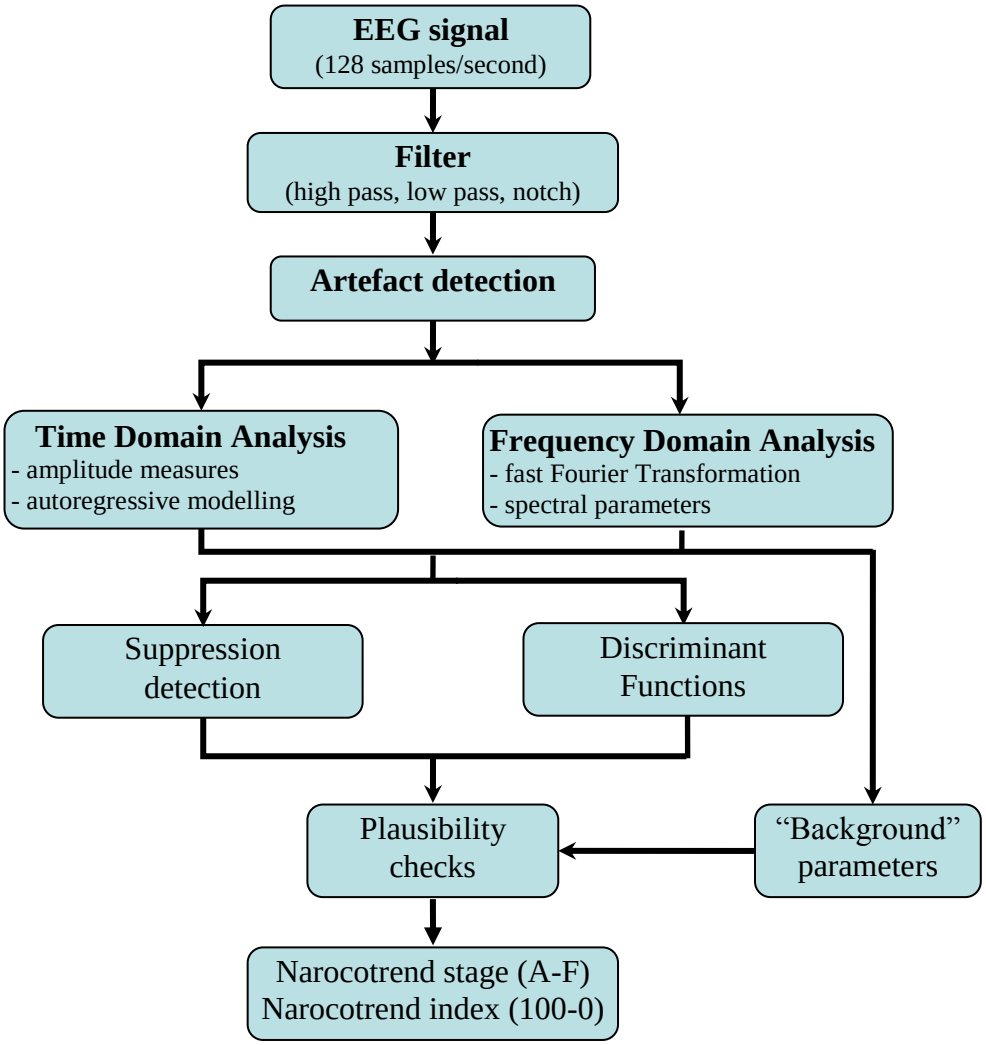

Figure 2.6: Narcotrend algorithm (Kreuer, 2006)

2.3 BASIC METHODS AND TECHNIQUES

2.3.1 Fast Fourier transform

A fast Fourier transform (FFT) is an efficient algorithm to compute the discrete Fourier transform (DFT) and the inverse. A DFT decomposes a sequence of values into components of different frequencies. The discrete-time Fourier transform of a sequence *x(n)* is define as

$$X(e^{jw}) = \sum_{n=-\infty}^{\infty} x(n) e^{-jwn} \tag{2.1}$$

The time index *n* is disctrete, and ω is the normalized frequency. There are *N* input *x(n)*. The transform pair of the discrete Fourier transform (DFT) is defined as

$$X(k) = \sum_{n=0}^{N-1} x(n) W_N^{nk} \quad \leftrightarrow \quad x(n) = \frac{1}{N} \sum_{k=0}^{N-1} X(k) W_N^{-nk}, \tag{2.2}$$

where $W = e^{-j2\pi/N}$. The DFT can be seen as the discrete-time Fourier transform of a periodic signal with period *N*.

$$\boldsymbol{x} = \begin{bmatrix} x(0) \\ x(1) \\ \vdots \\ x(N-1) \end{bmatrix}, \quad \boldsymbol{X} = \begin{bmatrix} X(0) \\ X(1) \\ \vdots \\ X(N-1) \end{bmatrix}, \tag{2.3}$$

$$\mathbf{W} = [W_N^{kn}] = \begin{bmatrix} 1 & 1 & \cdots & 1 \\ 1 & W_N & \dots & W_N^{N-1} \\ \vdots & \vdots & & \vdots \\ 1 & W_N^{N-1} & \dots & W_N^{(N-1)(N-1)} \end{bmatrix}. \tag{2.4}$$

The relationship between $\boldsymbol{x}$ and $\boldsymbol{X}$ can be expressed as

$$X = Wx \quad \leftrightarrow \quad x = \frac{1}{N} W^{\mathrm{H}} X \tag{2.5}$$

For a complex-valued input signal *x(n)* of length *N* the implementation of the DFT matrix *W* requires N^2 complex multiplications. The fast Fourier transform factorizes *W* into a matrix that require a lower implementation cost than the direct DFT. Each stage of FFT requires *N/2* complex multiplications and *N* additions (Brigham, 1988; Mertins 1999).

2.3.2 Filter banks

Filter banks are used for the spectral decomposition and composition of a signal. Multi-rate filter banks are used in a variety of applications from communications (multicarrier modulation) to data compression (speech, audio, image, and video), and feature detection. Figure 3.4 shows a general *M*-channel filter

bank. A analysis filter bank is used to decompose the input signal into M sub-band signals. The sub-band signal carries information on the input signal in each frequency band. Down-sampling and up-sampling are indicated by factor *N* (Mertins 1999).

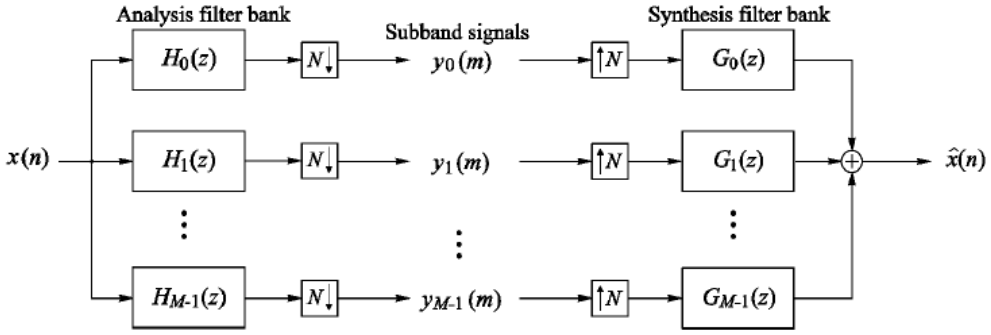

Figure 2.7: M-channel filter bank (Mertins 1999).

2.3.3 Wavelet transform

The problem in EEG-based assessment of anaesthetic state is that the characteristics of EEG signals in every state of anaesthesia are unknown. To find the characteristic parameters, we use wavelet transform (WT) for decomposition and reconstruction of the EEG signals. Fourier transformation has no time response nor time resolution because it defines the presence of a particular frequency within a sample window. Sinusoids are not assumed to be localized in time. It is only the resolution of an exact frequency that depends on the length of a finite window. Wavelet transformation is able to detect both time and frequency responses of finite duration signal components but with limited frequency content over their duration (Daubechies, 1992; Mallat, 1999; Vetterli, 1992). The wavelet transform of signal *x(t)* is defined as

$$C(a,\, b) = \int_R x(t)\psi_{a,b}(t)\, dt = \int_R x(t)\frac{1}{\sqrt{a}}\psi(\frac{t-b}{a})\, dt \ , \qquad (2.6)$$

where *C(a, b)* are the WT coefficients of signal *x(t)*,

a is a scale parameter,

b is a translation parameter,

$\psi(.)$ is the wavelet function,

$a \in R^{+} - \{0\}, b \in R$ for continuous analysis,

$a = 2^{j}$, $b = k2^{j}, (j,k) \in Z^{2}$ for discrete analysis, j is the decomposition level.

Wavelet transforms are classified into discrete wavelet transforms (DWTs) and continuous wavelet transforms (CWTs). The continuous wavelet transform has two drawbacks: redundancy and impracticality. These problems are solved by making the transform parameters (*a, b*) discrete. The discrete wavelet transform (DWT) is used to reduce redundancy in WT of EEG signals. WT in (3.12) is highly redundant when parameters (*a, b*) are continuous. Therefore the transforms are presented in the time-frequency domain with discrete values, corresponding to their continuous basic functions (Vetterli, 1992; Mallat, 1989).

In DWT method, the input EEG signals are filtered separately by a low-pass filter (*g*) and a high-pass filter (*h*) as follows (Mallat, 1989; 1999):

$$A_j(n) = \sum_{l=-\infty}^{+\infty} g(l-2n) A_{(j-1)}(l), \tag{2.7}$$

$$D_j(n) = \sum_{l=-\infty}^{+\infty} h(l-2n) A_{(j-1)}(l). \tag{2.8}$$

Here $A_j(n)$ and $D_j(n)$ are the approximation and the detail at level *j*. A DWT decomposes a given EEG input *x* into a number of coefficient sets. Each of these sets contains a time series which represents the activities of the signal in a particular frequency band with sampling frequency (f).

$$WT:\ x \rightarrow \left\{ \begin{array}{ll} D_1 & band:\left[\frac{f}{4},\frac{f}{2}\right] \\ D_2 & band:\left[\frac{f}{8},\frac{f}{4}\right] \\ \vdots & \\ D_j & band:\left[\frac{f}{2^{j+1}},\frac{f}{2^{j}}\right] \\ \vdots & \\ D_J & band:\left[\frac{f}{2^{J+1}},\frac{f}{2^{J}}\right] \\ A_J & band:\left[0,\frac{f}{2^{J+1}}\right] \end{array} \right\},\ j=1,...,J. \tag{2.9}$$

If we label the first decomposition as A_1 and D_1, then the decomposition of A_1 could be labelled as A_2 and D_2. The original signal (x) can be reconstructed to signal (x') from the approximation and detail coefficients by a synthesis filter bank (h', g') as shown in Figure 3.5. We have:

$$\begin{aligned} x' &= A_1 + D_1 = A_2 + D_2 + D_1 = A_J + D_J + D_{J-1} + \cdots + D_1 \\ &= \sum_{j=1}^{J} D_j + A_J \end{aligned} \quad . \tag{3.10}$$

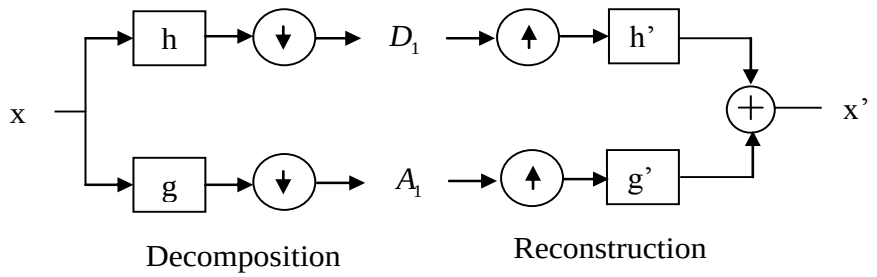

Figure 2.8: Decomposition and reconstruction of signals in DWT.

2.3.4 Power Spectral Density (PSD) and Eigenvector method

The basic theory of eigenvector-based method and the MUSIC method are first introduced by Schmidt and Franks in (Schmidt, 1986) and further presented by Marple (Marple, 1987) and Haykin (Haykin, 1991). A brief description of these methods is provided below.

For a time index n, the autocorrelation of $x[n]$ at two different time indices n_1 and n_2 is $r_{xx}[n_1, n_2] = \varepsilon\{x[n_1]x^*[n_2]\}$. A vector x is a conjugate symmetric if $Jx=x^*$, where J is the reflection matrix. The power spectral density (PSD) is the discrete-time Fourier transform (DTFT) of the autocorrelation sequence

$$P_{xx}(f) = T\sum_{m-\infty}^{\infty} r_{xx}[m]e^{(-j2\pi fmT)} \tag{2.11}$$

where $m = n_2 - n_1$, f is frequency, and T is period. The PSD function describes how the variance of a random process is distributed with frequency. The inverse of DTFT is:

$$r_{xx}[m] = \int_{-1/2T}^{1/2T} P_{xx}(f)e^{(-j2\pi fmT)}df \tag{2.12}$$

The autocorrelation sequence of p complex sinusoids of random phase in additive complex white noise is defined as:

$$r_{xx}[k] = \int_{i=1}^{p} P_i e^{(-j2\pi f_i mT)} + \xi\delta[k], \tag{2.13}$$

where P_i is the power of the i^{th} sinusoid and ξ is the noise variance. The N^{th}-order Toeplitz autocorrelation matrix of dimension $(N+1)x(N+1)$ is:

$$R_N = \begin{pmatrix} [r_{xx}[0]] & \cdots & r_{xx}^*[N] \\ \vdots & \ddots & \vdots \\ r_{xx}[N] & \cdots & r_{xx}[0] \end{pmatrix} \tag{2.14}$$

The N^{th}-order autocorrelation matrix for the case of p real sinusoids in white noise is:

$$R_N = \sum_{i=1}^{p} \frac{P_i}{2}\left[s_i s_i^H + s_i^* s_i^T\right] + \xi I = Q_N + G_N \tag{2.15}$$

$$s_i = \begin{bmatrix} 1 \\ e^{j2\pi f_i T} \\ \vdots \\ e^{j2\pi f_i NT} \end{bmatrix} \tag{2.16}$$

with $Q_N = \sum_{i=1}^{p} \frac{P_i}{2}\left[s_i s_i^H + s_i^* s_i^T\right]$ and $G_N = \xi I$. The eigendecomposition of the signal matrix is:

$$Q_N = \sum_{i=1}^{p} \lambda_i v_i v_i^H \quad . \tag{2.17}$$

In (3.17), the eigenvectors are orthonormal ($v_j v_i^H = 0$ if $i \neq j$ or $v_j v_i^H = 1$ if $i=j$) and the eigenvalues decrease ($\lambda_1 \geq \lambda_2 \geq \ldots \geq \lambda_{N+1}$). The noise subspace eigenvectors $v_{p+1},\ldots,v_N$ of an autocorrelation matrix of p total eigenvectors and N principal eigenvectors theoretically are orthogonal to the sinusoidal signal vectors, so that their linear combinations with arbitrary weighting α_k is:

$$\sum_{k=N+1}^{p} \alpha_k \left| E^H(f) v_k \right|^2 = E^T(f) \left(\sum_{k=N+1}^{p} \alpha_k v_k v_k^H \right) E(f), \tag{2.18}$$

where the complex sinusoid vector *E(f)* is

$$E^T(f) = \left[1,\ e^{j2\pi fT}, \cdots, e^{j2\pi fNT}\right]. \tag{2.19}$$

The frequency estimator function is:

$$P(f) = \frac{1}{\sum_{k=N+1}^{p} \alpha_k \left| E^H(f) v_k \right|^2} \tag{2.20}$$

E(f) will be zero whenever $E(f_i) = s_i$. This means that at $f = f_i$, the frequency estimator function will have infinite value. Selecting $\alpha_k = 1$ for all k yields the MUSIC algorithm frequency estimation based strictly on the noise subspace

eigenvectors with uniform weighting. Choosing $\alpha_k=1/\lambda_k$ yields the eigenvector frequency estimator which weighs each noise subspace eigenvector by the inverse of its associated eigenvalue.

$$P_{ev}(f) = \frac{1}{E^H(f)\left(\sum_{k=N+1}^{p} \alpha_k v_k v_k^H\right)E(f)}, \tag{2.21}$$

The eigenvector method produces fewer spurious peaks than MUSIC for a given choice of order p due to the use of inverse eigenvalue weighting (Marple, 1987; Eriksson, 1994; Johnson, 1982). The extracted wavelet coefficients give a compact representation of signals which shows the energy distribution of the given signals in time and frequency domains.

2.4 STATEMENT OF THE PROBLEMS FOR MONITORING THE DOA

Clinical signs may vary over a wide range depending on disease, drugs and surgical technique. Heart rate, blood pressure, lacrimatiom, sweat and ocular signs are not valuable in predicting response to a noxious stimulus (Schneider, 1997). Clinical investigations and individual cases report that some patients were aware during anaesthesia at times when there were no abnormalities: blood pressure and heart rate in a normal range (Moerman, 1993; Hug, 1990; Hilgenberg, 1981).

Numerous methods are devised and implemented for purpose of monitoring the depth of anaesthesia based on EEG signals. However, none of them are reliable. The Cerebral State Index (CSI) monitoring was not consistent with the clinical observations in the different stages of deep anaesthesia (Anderson, 2006; 2005). Narcotrend did not adequately detect the transition between awareness and

unconsciousness in surgical patients (Schneider, 2004a). The Bispectrum (BIS) index, the most popular, has also recently received some criticism, such as being redundant (Schneider, 2004b), not responsive to some anaesthetic agents such as ketamine and nitrous oxide (Johansen, 2000; Barr G., 1999), and not robust across patients (Tempe, 2004; Hall, 1998). In addition, the BIS monitor is unable to give an accurate estimate of the patient's hypnotic state when signal quality is poor (Aspect, 2008; BIS, 2008).

Although the basic principles and algorithms used in the above EEG monitoring devices are completely different, most of them are based on EEG signals analysis in the frequency domain. The analyses of the EEG signals in the frequency domain are restricted because they only capture the information relevant to frequency without any reference to time. Fourier transform has no time response or time resolution because it finds the presence of continuous infinite-time sinusoids of a particular frequency within a sample window. Sinusoids are not localized in time. The criticism of using the frequency domain here is somewhat harsh, since in practice it is always accessed via the FFT which uses data with a finite time extent. So while the criticism is correct theoretically, the practical use of the frequency domain does imply time resolution equal to the size of the window of data used in the FFT.

Moreover, none of these methods have extracted information from the raw EEG for continuously evaluating the DoA. They did not show reliable aneathetic efficacy during routine procedures. Time domain analysis is used for the detection of epochs that represent electrical suppression of EEG signal. It only happens in the case of very deep of anaesthesia. Therefore, these analyses can not be used for light anaesthesia detecting. A limitation of these above methods is a lag in the processing

time for analyse EEG signal and computing the DoA index. Pilge *et al.* studied the processing delays in the Cerebral State Monitor (CSM), the Narcotrend monitor, and BIS monitor. They found that the time delays are from 14 to 155 seconds for these monitors. In the transition case from "general anaesthesia" to "awake", the delay times were 15, 65 and 30 seconds for CSM, Narcotrend, and BIS, respectively (Pilge, 2006).

Recently, several EEG based parameters and algorithms have been developed for a better monitoring the DoA. Ortolani *et al.* used an artificial neural network (ANN) to estimate the depth of anaesthesia. Comparison with corresponding BIS, they claimed that neural networks could be trained to predict anaesthesia depth directly from the raw EEG (Ortolani, 2002). However, this method did not extracte information from the raw EEG for continuously evaluating the DoA.

Another new approach for quantifying the relationship between brain activity patterns and depth of anaesthesia was presented by Zhang *et al.* (Zhang, 2001) which analysed the spatio-temporal patterns in the EEG using Lempel-Ziv complexity analysis. An OAA/S scores were considered asleep and awake staes. Twenty-seven patients were studied under general anaesthesia. Compared with other methods, such as approximate entropy, spectral entropy and median frequency, the proposed method not only demonstrated better performance across all of the patients but also presented an algorithm which was easy to implement for real-time use. However, they only discriminated the awake and asleep states.

The entropy and complexity of the EEG have been proposed as measures of depth of anaesthesia and sedation (Ferenets, 2006). Entopy is independent of absolute amplitude and frequency scales of the EEG signal. This technology may be

not reliant on a large comparative database. The response entropy (RE) may be affected by EMG.

Another approach based on the analysis of a single-channel EEG signal using stationary wavelet transform was applied to study the cortical activity during general anaesthesia (Zikov, 2006). The wavelet coefficients calculated from the EEG are pooled into a statistical representation. The results showed that the wavelet-based anaesthetic value and BIS were well correlated during periods of steady-state. This method only used the γ-band (32-64 Hz). Therefore, the EEG information in the other bands may be lost.

Rezek *et al.* presented a model that generalized an autoregressive class of poly-spectral models by having a semi-parametric description of the residual probability density. Their results only indicated that in two out of three anaesthetic agents, better classification could be achieved with higher-order spectral. Their analysis also suggested that propofol had the strongest effect on the EEG signal. However, they did not give a new DoA index (Rezek, 2007).

Several studies have tried to detect long-range temporal correlations in EEG using detrended fluctuation analysis (DFA) and demonstrated convincingly that the dynamics of EEG had long-range temporal correlations (Jospin, 2007; Lee, 2002; Pan, 2004). The DFA is also used to study the scaling behaviour of the EEG as a measure of the level of consciousness (Jospin, 2007). This result only shows the relation of scaling behaviour and the level of consciousness rather than an index for monitoring DoA.

To investigate the effect of box sizes in DFA method, Gifani *et al.* managed to find the optimum fractal-scaling exponent by selecting the best domain of box

sizes (Gifani, 2007). With the original DFA method, their results could not discriminate between light anaesthesia and moderate anaesthesia states.

Chapter 3

Research Aims

3.1 DATA ACQUISITION

3.1.1 Ethics clearance

The study was approved by the University of Southern Queensland Human Research Ethics Committee (No: H09REA029) and the Toowoomba and Darling Downs Health Service District Human Research Ethics Committee (No: TDDHSD HREC 2009/016).

3.1.2 Anaesthesia process

The EEG data were collected at the Toowoomba St Vincent's Hospital by a senior anaesthetist, who is a member of our research group. He or his assistants asked whether relevant patients were willing for them to collect the data after explained the purposes and the procedures of the data collection. They will then be recruited through a consent form. The anaesthetist or assistant clearly explain to the patients more details in consent form and help the patients to fill it. The participants would print their full name and sign in the consent form. If they have any concerns, questions, or wish to withdraw once they have participated in this study, they could

do that after talked with their doctors. The consent forms would be kept separately from their completed personal information and only doctors could access to the consent forms.

Total 25 adult patients were involved in this project. All patients underwent general anaesthesia induced with clinically appropriate doses of conventional pharmaceuticals including midazolam; alfentanil; fentanyl and propofol. Intravenous morphine, clonidine, parecoxib and paracetamol were used as indicated for post-operative analgesia. The airway was supported by endotracheal intubation or by laryngeal mask airway insertion as indicated clinically. Patient demographic characteristics and mean drug doses (when used) are shown in Table 3.1.

Table 3.1: Patient demographics and intraoperative drug usage

	Mean ± SD or Number
Age (yr)	59 ± 16
Weight (kg)	98 ± 32
Gender (F/M)	10/15
Midazolam (mg)	4 ± 1
Alfentanil (μg)	850 ± 150
Propofol (mg)	170 ± 60
Parecoxib (mg)	40
Fentanyl (μg)	135 ± 35

Anaesthesia was maintained with desflurane or sevoflurane in combination with air or nitrous oxide. Skeletal muscle paralysis was variable but always reversed with neostigmine and atropine or glycopyrrolate. The time stamps, the BIS values, all intravenous dosing, and significant intra-operative events were recorded by the

attending anesthetist. Assessment of loss of consciousness (LOC) was clinically carried out with lack of response to verbal and tactile stimulus. Loss of the lash reflex was used in case of doubt.

3.1.3 Equipment for collecting the EEG signal

We made pre- and intra-operative use of the proprietary BIS VISTA™ monitor (BIS VISTA Version 3.00, Algorithm Version BIS 4.1, Aspect Medical Systems; Johansen, 2006). Raw EEG data were obtained through the four adhesive forehead electrodes/sensors used clinically for BIS monitoring. The BIS VISTA monitoring system is shown in Figure 3.1.

Figure 3.1: The BIS VISTA monitoring system (Service information manual, Aspect Medical Systems, Inc.)

Different types of electrodes are used in the EEG recording systems, such as:

- Disposable (gel-less, and pre-gelled types)
- Reusable disc electrodes (gold, silver, stainless stell, or tin)
- Headbands and electrode caps

- Saline-based electrodes
- Needle electrodes.

The BIS VISTA system has been designed to operate with BIS Quatro electrodes. "The BIS Quatro electrode offers enhanced performance in deep anaesthetic states and improved resistance to interference from noise sources, such as high frequency/electromyography conditions. This electrode features an improved design compared with the BIS Standard Sensor for easy connection, which enables the BIS system to automatically configure its settings for specific patient populations and applications. The BIS Quatro electrode contains an electronic memory device that allows information about the sensor, such as lot code, expiration date and type of sensor, to be stored on the sensor and to be retrieved by the BIS monitor, BIS Module Kit, or BIS system. Before the electrode placement, the skin was cleaned with alcohol and abraded to ensure electrical conductivity. These electrodes were placed diagonally on the forehead with electrode No. 1 at the centre of the forehead, approximate 2 inches (5 cm) above the bridge of the nose, electrode No. 4 directly above eyebrow, No. 2 between No. 1 and No. 4, No. 3 on the temple, between the corner of the eye and hairline. Connecting the sensor to the patient interface cable (PIC), the impedance test should complete successfully, with low impedance values. Typical values using the test sensor are less than 5 kΩ." (BIS sensor for Aspect Medical Systems, Inc.)

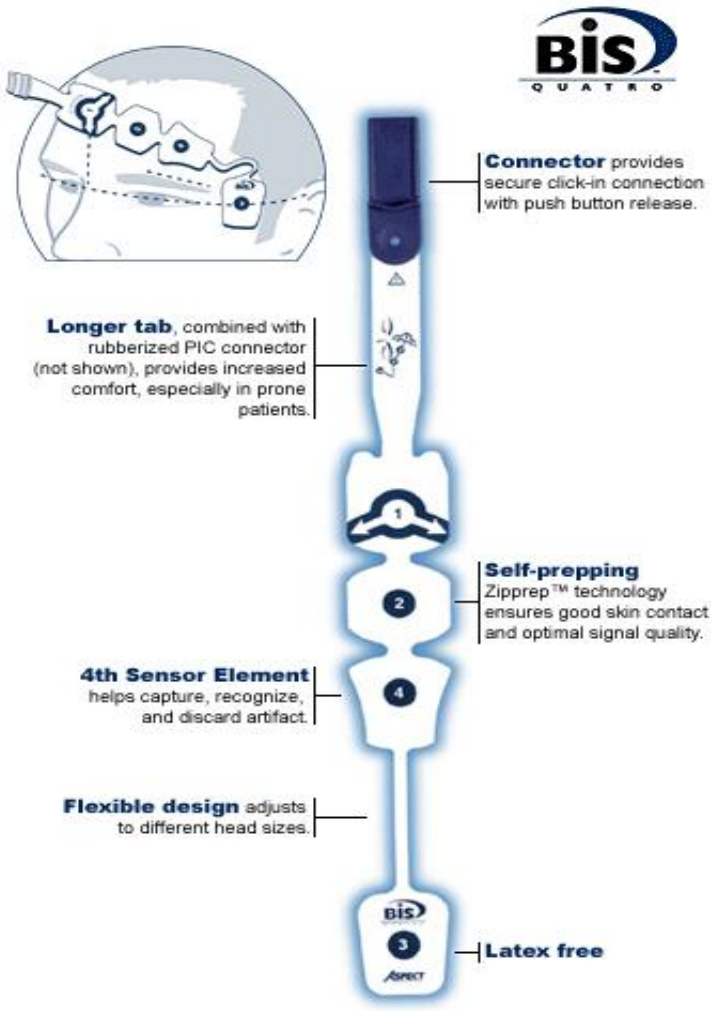

Figure 3.2: BIS Quatro electrodes (BIS sensor for Aspect Medical Systems, Inc.)

3.1.4 Data format

The downloaded data were included:

- Live Data: EEG, BIS and other processed variable information
- BIS History Data: BIS and other processed variables from the BISx
- Monitor Error Logs: Critical events and any monitor errors.

In this study, live data is used as the raw EEG signals and to extract EEG variables, as well as impedance and other events. BIS index is displayed as a single value and updated every second, which is calculated from data gathered over the past

15-30 seconds of EEG recording. The root *filename* for Live Data is LMMDDHHMM**,** where MM is the month (01-12), DD is the day (01-31), HH is the hour (00-23), and MM is the minute (00-59). Files are stored in *filename* directory (LMMDDHHMM).

Exported data files are created as soon as export is initiated (BIS, 2008). Data logging, however, occurs only when a sensor is inserted. A new directory (if started on a different minute than the previous export) and set of files is created when a valid sensor is inserted.

Live data provides *processed data* with a name of *filename*.spa and *raw data* with a name of *filename*.r2a. Data are transferred and stored in a computer for the off-line analysis.

- In the *processed data*, BIS index is updated every second. Signal Quality Index (SQI) is a measure of the signal quality for the EEG channel source(s) that is calculated based on impedance data, artifact, and other variables. It is not affected by Suppression Ratio.
- The *raw data* include a binary file documenting two channels of the unfiltered EEG signals. (Aspect, 2008).

Data were exported to a Universal Serial Bus (USB) drive and transferred to a portable computer for off-line analysis. Each EEG sample is a 16-bit signed integer in units of 0.05μV. Data are sampled at 128 times per second for each channel. The Raw EEG binary data file cannot be opened or read by normal text editors.

It is possible to use a Hex editor to display the file contents in "Hexadecimal" format. Freeware Hex Editor Neo is a program which allows us to view, modify, and analyze binary files and hexadecimal data. The details are available online (http://www.hhdsoftware.com/free-hex-editor).

3.2 RESEARCH OBJECTIVES

This research aims to develop new methods to monitor the DoA based on routinely recorded EEG during operations using the time domain, the frequency domain and the time-frequency domain analysis techniques. The objectives of this research are:

1. To de-noise and analyse the raw EEG signals;
2. To identify and classify the depth of anaesthesia states into awake, light, moderate, deep and very deep anaesthesia states;
3. To compute the DoA values:
   - in the time domain and frequency domain using fast Fourier transforms, filter banks and the Modified Detrended Fluctuation Analysis method;
   - in the time domain using further Modified Detrended Fluctuation Analysis and Lagrange methods;
   - in the time domain using the modified Detrended Moving Average method;
   - in the time domain using the modified Chaos method;
   - in the time-frequency domain using power spectral densities (PSD) and wavelet (WDoA) methods;
4. To estimate a patient's hypnotic state in the case of poor signal quality;
5. To reflect and minimize the time delay of DoA monitor.

3.3 METHODOLOGIES

We are going to investigate these EEG signals to monitor the DoA in both the time domain and the time-frequency domain as a measure of the level of consciousness. The Detrended Fluctuation Analysis (DFA), the detrended moving

average (DMA) and Chaos methods are modified to study the scaling behavior of the EEG in the time domain. The FFT and filter banks are used to identify difference states of anaesthesia in frequency domain. In the time-frequency domain, the discrete wavelet transforms (DWT) and power spectral density (PSD) function are applied to pre-process EEG data. The concepture framework of this study is presented in Figure 3.3. Based on these above techniques, five new methods are proposed in this thesic for monitoring the DoA as the following:

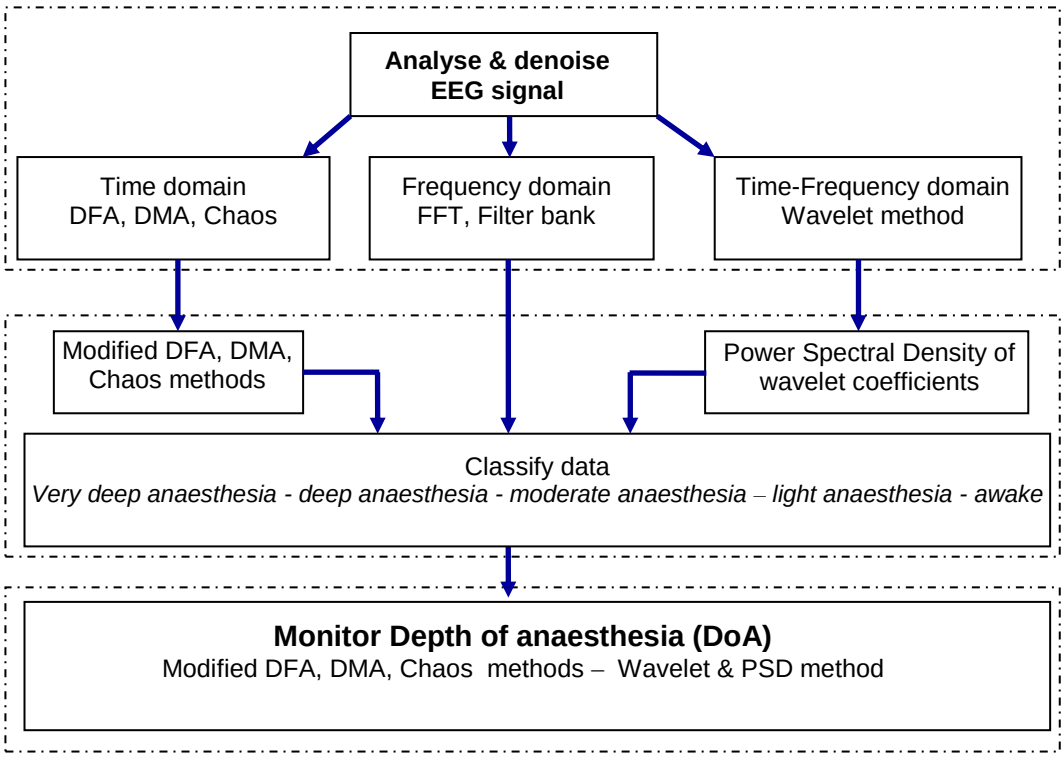

Figure 3.3: Diagram for methodologies.

Method I

A Modified Detrended Fluctuation Analysis (MDFA I) method is presented in Chapter 5. The DFA algorithm finds a trend on the integrated EEG signals. The integrations on EEG signals are divided in segments of length s. These segments are called box sizes. This trend is iteratively searched on different sizes of boxes over the signals. When the trend is found in each box, it is subtracted from the integrated signals. FFT and filter bank methods are designed to identify anaesthesia states and to separate EEG signals into five components. In MDFA I, the box sizes are reduced gradually from awake state, light anaesthesia, moderate anaesthesia, deep anaesthesia and very deep anaesthesia states. The simulation results demonstrate that the MDFA I can clearly discriminate five above anaesthesia states and the DoA values are close to the BIS values (Nguyen-Ky 2009b).

Method II

Another modified detrended fluctuation analysis (MDFA II) method is proposed in Chapter 6 to improve the monitoring accuracy of the depth of anaesthesia (DoA). MDFA II method first is used to classify anaesthesia state levels into awake, light, moderate, deep and very deep states. Then five zones are built up using linear regression method from very deep anaesthesia state to awake state, corresponding to different box sizes. Finally, the Lagrange method is applied to compute the DoA. Simulation results demonstrate that the new technique monitors the DoA in all anaesthesia states accurately (Nguyen-Ky 2010b).

Method III

A modified Detrended Moving Average (MDMA) method is proposed to assess the DoA in chapter 7. The MDMA method can distinguish the patient's clinical states from awake to deep anaesthesia more accurately than the original DMA method. The MDMA method was investigated by computing the scaling exponent α (F_α) and minimum lnF_{MDMA} value (F_{min}). A close correlation is found between our results (F_{min}, F_α) and BIS Index with $r(F_{min}) = 0.9346$, $r(F_\alpha) = 0.9458$ and $r^2(F_{min}) = 0.9183$, $r^2(F_\alpha) = 0.8855$ (Nguyen-Ky 2010c).

Method IV

To study the EEG signal in time-frequency domain to monitor the DoA, a new method is proposed in chapter 8 for constructing a wavelet-based depth of anaesthesia (WDoA) index. This method is based on discrete wavelet transform (DWT) and power spectral density (PSD) function. DWT is applied to pre-process EEG data. To assess DoA with accuracy, the PSD with eigenvector method is chosen as a feature function for six levels of the coefficients in DWT. To reduce the time delay for monitoring the DoA, an adaptive window length (AWL) technique is proposed to compute the length of the sliding window (Nguyen-Ky 2010d).

Method V

Chaos method is used to analysis of EEG signals in chapter 9. Two new indices CDoA and CsDoA for monitoring the DoA using the modified Hurst exponents to calculate the average rescaled range over multiple regions of the data. A combination of Chaos and MDMA methods (Ch-MDMA) is applied for monitoring the DoA. Comparing with BIS trends, covering the whole scale from 100 to 0 with a

full recording time, CDoA, CsDoA and Ch-MDMA trends are close to BIS trend in this time range.

3.4 THESIS OUTLINE

This thesis is presented as follows:

- Chapter 1 includes five major topics: definition and process of anaesthesia, intraoperative awareness and anaesthetic overdose, monitor the depth of anaesthesia, and brain rhythms and EEG signal.
- Chapter 2 presents a literature review od DoA assessment which include clinical viewpoint, DoA monitoring, basic method and techniques such as the FFT, filter banks, the wavelet transform, PSD and the eigenvector method, and the statement of the problems for monitoring the DoA.
- Chapter 3 introduces research aims with the data acquisition, the research objective, the methodologies and the thesis outline.
- Chapter 4 focuses on the de-noising of raw EEG signals. This chapter is organised into two parts, describing an adaptive filter for noise cancelation and a wavelet-entropy adaptive noise canceller.
- Chapter 5 presents a new method to improve the DoA estimation accuracy using the fast Fourier transform (FFT), filter banks and the modified de-trended fluctuation analysis (DFA) method. It demonstrates that the modified DFA method (MDFA I) can clearly discriminate among awake states, light anaesthesia, moderate anaesthesia and deep anaesthesia states based on the EEG data.

- Chapter 6 presents another modified DFA method (MDFA II) and Lagrange method to improve the monitoring accuracy of the depth of anaesthesia.
- Chapter 7 applies the modified de-trended moving average (MDMA) method to monitor DoA. The results show that this method reflects the state of consciousness of a patient undergoing general anaesthesia faster than BIS and agrees with clinical observation.
- Chapter 8 proposes a wavelet-based depth of anaesthesia (WDoA) index. This method is based on the discrete wavelet transform (DWT) and power spectral density (PSD) function. WDoA and BIS indices are compared through the whole BIS scale from 100 to 0 with full recording of surgery time.
- Chapter 9 applies the modified Chaos, combined Chaos and MDMA methods for monitoring the DoA.
- Chapter 10 provides a summary of the main outcomes and contributions of the research.

Chapter 4

De-noising raw EEG signal

The EEG signals are mainly affected by eye blinks, electrocardiograms (ECGs), and electro-oclugram (EOG). An attempt is made to remove ECG patterns, but it is not always successful because recognition requires a detectable repetitive waveform. If any ECG is detected (as a glitch) but not removed, then that epoch of data is considered unusable in BIS. Electromyographic (EMG) is not considered as an artefact, but if the EMG is large enough to trigger some of the other artefact detectors, it will cause the Signal Quality Indicator (SQI) to decrease (BIS, 2008). As an introduction in Section 3.1.2, electrode No. 1 will measure more EEG and less EMG than electrode No. 3. So electrode No. 3 can be used as a noise reference to cancel noise from electrode No. 1. In this case, an adaptive noise cancelation can be used for de-noising. This chapter focuses on an adaptive filter and a wavelet-entropy adaptive noise canceller.

4.1 ADAPTIVE FILTER FOR NOISE CANCELATION

The EEG signals vary in time. Therefore, noise removal must be adaptive and track the changing signal characteristics. Most adaptive noise removal algorithms are based on the least mean squares (LMS) or the recursive least squares (RLS)

algorithms (James, 1997; Oikonomou, 2007). Figure 4.1 presents a block diagram of an adaptive filter for noise cancellation (Haykin, 1991).

Let the EEG signal be $\{ x_i, i=1,..., n \}$. This signal has been corrupted by additive noise:

$$y_i = x_i + e_i, \tag{4.1}$$

where e_i is additive noise and it is an independent identically distributed normal variable with zero mean and variance σ^2. The weighting coefficients w_i of the adaptive filter are adjustable.

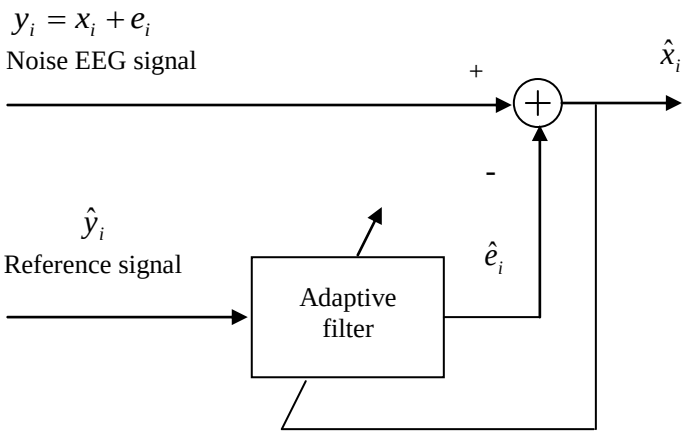

Figure 4.1: An adaptive noise canceller

The reference signal $\hat{y}_i$ is employed as the input to the adaptive filter. The adaptive filter output

$$\hat{e}_i = \hat{Y}_i^T W_i = W_i^T \hat{Y}_i, \tag{4.2}$$

with $\hat{Y}_i = [\hat{y}_0, \hat{y}_1, \ldots, \hat{y}_{i-1}]^T$ and $W_i = [w_0, w_1, \ldots, w_{i-1}]^T$.

The adaptive algorithm adjusts the weights w_i of the adaptive filter combiner to minimize mean-square error.

The EEG signal after de-noise is:

$$\hat{x}_i = y_i - \hat{e}_i = x_i + (e_i - \hat{e}_i). \tag{4.3}$$

From (4.3), the noise of the system in Figure 4.1 is defined as

$$e = e_i - \hat{e}_i. \tag{4.4}$$

The adaptive filter attempts to minimize the mean-square value of $\hat{x}_i$. The EEG signal x_i is essentially unaffected by the adaptive noise canceller. A cost function is defined for the optimum design of the adaptive filter as:

$$J(W) = E\left[\left|\hat{x}_i\right|^2\right] = E\left[\left|y_i - W_i^T \hat{Y}_i\right|^2\right], \tag{4.5}$$

where E is the expectation operator. The filter is optimized by finding the W vector to minimize the cost function. Minimizing the mean-square value of $\hat{x}_i$ is equivalent to minimize the mean-square value of the noise of the system $e = e_i - \hat{e}_i$.

Set-membership identification (SMI) theory is a well-established paradigm in the area of system identification that exploits the assumption of a bounded noise process added to a linear-in-parameter model (Gollamudi, 1998). The set-membership filtering criterion is to find W that satisfies:

$$\left|\hat{x}_i\right|^2 \le \delta^2 \tag{4.6}$$

With the minimum noise signal δ, the filter lengths N_i are computed so that the error signal may approximate the minimum noise signal.

The error estimate algorithm (EEA)

$$\hat{x}_i = y_i - \hat{e}_i \tag{4.7}$$

$$w_{i+1} = w_i - \mu_i \hat{y}_i \hat{x}_i \tag{4.8}$$

$$\mu_i = F_{i+1} = \left[F_i - \frac{F_i \hat{y}_i \hat{y}_i^T F_i}{1 + \hat{y}_i^T F_i \hat{y}_i} \right] \tag{4.9}$$

where μ_i is defined in the affine projection (AP) algorithm (Sicuranza., 2004). The length of the adaptive filter is computed by

$$N_i = \begin{cases} N_i + 1 & if \quad |\hat{x}_i| > \delta, \\ N_i & if \quad |\hat{x}_i| \le \delta. \end{cases} \tag{4.10}$$

The new error estimate algorithm (NEEA)

Using the same equations (4.7) to (4.10), the bound δ was computed as:

$$\delta^* = \frac{\delta}{\left(1 - \frac{\delta}{|\hat{x}_i|}\right) + 1} \tag{4.11}$$

$$N_i = \begin{cases} N_i + 1 & if \quad |\hat{x}_i| > \delta^*, \\ N_i & if \quad |\hat{x}_i| \le \delta^*. \end{cases} \tag{4.12}$$

The optimum value N_i of the filter lengths is computed in (4.10) and (4.12) (Nguyen-Ky, 2007; 2010).

4.2 WAVELET-BASED DE-NOISING

In Figure 4.1, the reference signal $\hat{y}_i$ is derived from a sensor or set of sensors supplying the noise EEG signal y_i (Haykin, 1991). The reference signal carries significant information about the noise and its statistical properties (Sanei, 2007). However, it is difficult to record the EEG reference signal during surgery in the operating room. Therefore, we present a new wavelet-based de-noising algorithm which removes the spikes and the low frequency noise from raw EEG signals. This algorithm includes a new threshold T_{WE}, which is a function of the wavelet entropy for an EEG segment.

4.2.1 Wavelet threshold

In wavelet method, the selection of the levels of decomposition is depending on the dominant frequency components of the EEG signals. They are chosen in such a way that the range of the resulting frequency correlates with the five EEG rhythms: δ-band, θ-band, α-band, β-band, and γ-band.

In order to select a basis function that matches the frequency characteristics of a spike, we decompose EEG signals into six sub-bands to obtain the desired frequency resolution. The corresponding frequency sub-bands of a decomposed signal are presented in Table 4.1 and Figure 4.2. In Table 4.1, the component D_6 and D_5 decompositions are within the δ-band; and D_4, D_3, D_2, D_1 decompositions are within the θ-band, α-band, β-band, and γ-band, respectively.

Table 4.1: Frequencies corresponding to decomposition levels

Subband *j*	Decomposed signal	Frequency band	Clinical band
1	D_1	32-64 (Hz)	γ-band
2	D_2	16-32 (Hz)	β-band
3	D_3	8-16 (Hz)	α-band
4	D_4	4-8 (Hz)	θ-band
5	D_5	2-4 (Hz)	δ-band
6	D_6	0-2 (Hz)	δ-band

The detail coefficients contain the main component of noise and the signal wavelet transforms. The wavelet-threshold de-noising method filters each coefficient from the sub-bands with a threshold function. There are two thresholding methods

frequently used (hard threshold and soft-threshold) and D_J^* is obtained from threshold D_J. The hard threshold function is

$$D_J^* = \begin{cases} D_J & if \quad |D_J| > T \\ 0 & if \quad |D_J| \le T \end{cases}. \tag{4.13}$$

And the soft-threshold function is

$$D_J^* = \begin{cases} sign(D_J)(|D_J| - T) & if \quad |D_J| > T \\ 0 & if \quad |D_J| \le T \end{cases} \tag{4.14}$$

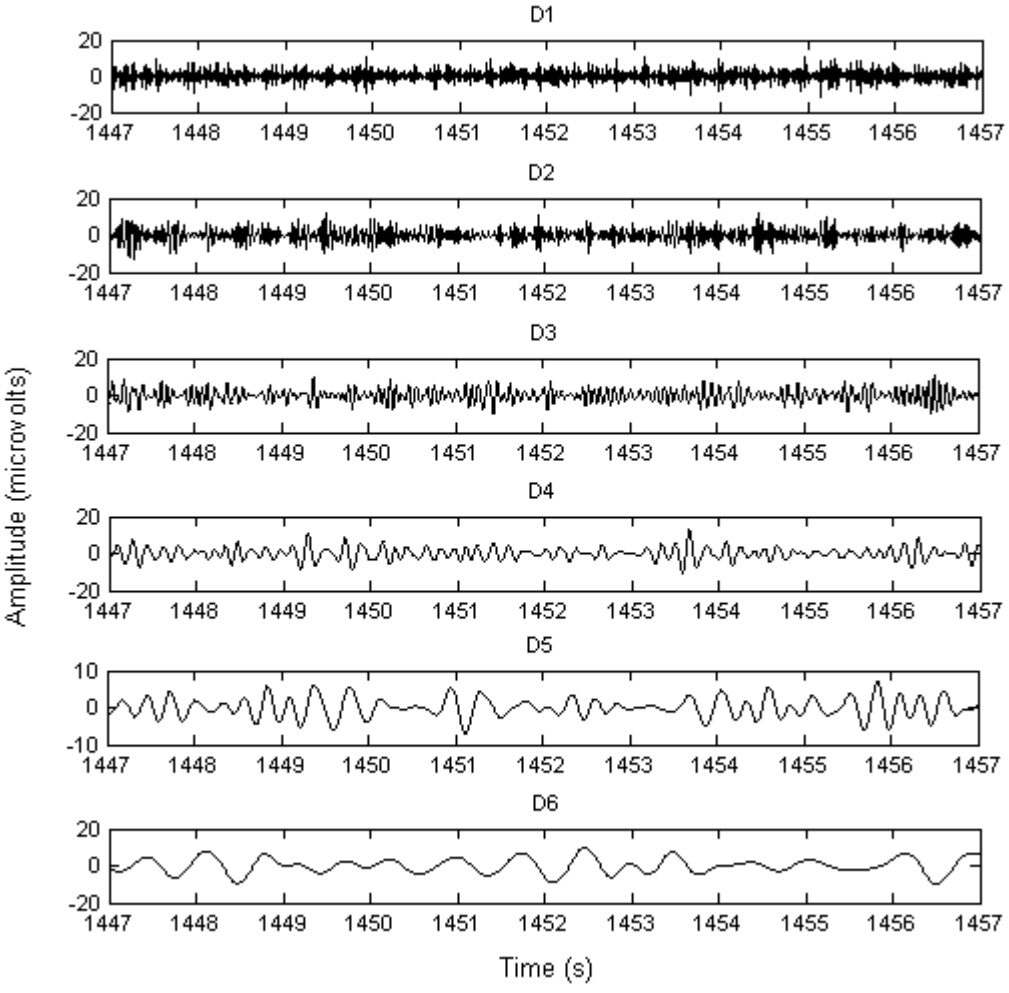

Figure 4.2: Six levels of decomposition EEG signal.

To obtain the hard-threshold, wavelet coefficient D_J with an absolute value below the threshold T is replaced with 0. A wavelet coefficient with an absolute value above the threshold is kept as it is. For the soft-threshold, a coefficient with a magnitude above the threshold is "shrunk", otherwises it is replaced with 0.

Noise decreases as the threshold value increases and vice versa. Noise may persist in the signal if too small a threshold value is chosen. It is thus important to select an optimum threshold value. Donoho and Johnstone proposed a simple thresholding procedure for recovering signal from noisy data (Donoho, 1994). They proposed a threshold as:

$$T_{DoNOHO} \sim \sigma_J \sqrt{2\log(n)}\,. \tag{4.15}$$

The noise level is

$$\sigma_J = median(|D_J|)/0.6745 \tag{4.16}$$

The threshold value is a trade-off between closeness of fitness and smoothness. A small threshold yields a result close to the coefficient (D_J), but the result may still be noisy. On the other hand, a large threshold may cause some coefficients to become zero (D_1^* and D_2^* in Figure 4.3). Therefore, an optimised threshold should be selected.

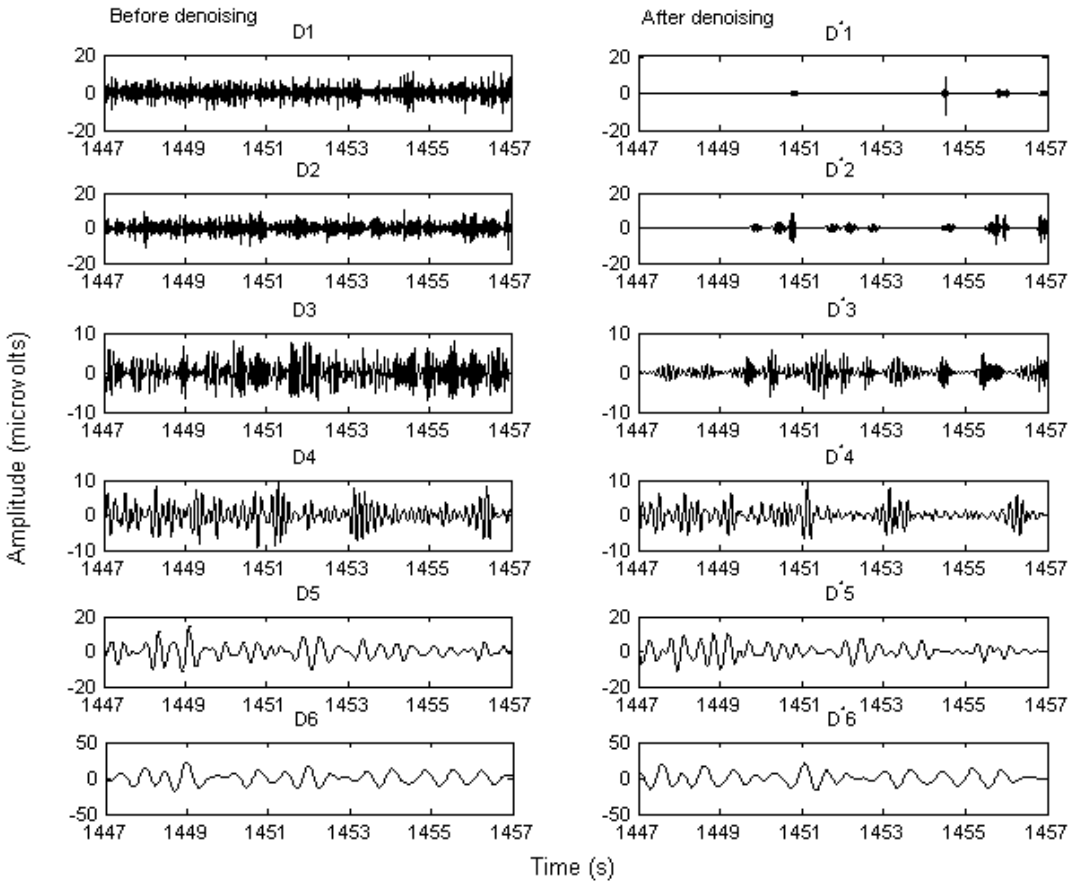

Figure 4.3: Detail coefficients of y_i before and after de-noising.

4.2.2 Wavelet entropy threshold

Entropy based methods have been applied to analyze EEG data (Rosso, 2001; Yordanova, 2002; Shannon, 1984; Aydin, 2009; Banjanin, 2001, Bhagat, 2009; Coifman, 1992; He, 2007; Sang, 2010). The entropy measures the predictability of future amplitude values of EEG based on the probability distribution of amplitude values already observed in time domain. The wavelet entropy has been developed to calculate EEG power in different bands, to measure how wide the power distributes in frequency bands, and to reduce the effect of changed amplitude of EEG signal in time domain. The energy is defined at each time instance *k* of coefficients D_J and window length *m* as:

$$E_{m,j}(k) = \sum_{j=1}^{J} \left| D_j(k) \right|^2 . \tag{4.17}$$

The total energy of wavelet coefficients is given by

$$E_{m,total} = \sum_{j=1}^{J} \sum_{k=1}^{m} \left| D_j(k) \right|^2 = \sum_{j} E_{m,j} . \tag{4.18}$$

The relative wavelet energy is:

$$p_{m,j} = \frac{E_{m,j}}{E_{m,total}} . \tag{4.19}$$

With the definition of entropy given by Shannon (Shannon, 1984), the wavelet entropy can be defined as:

$$E_m = -\sum_{j} p_{m,j} . \log p_{m,j} . \tag{4.20}$$

We propose a new threshold T_{WE} which is a function of wavelet entropy and window length m for an EEG segment. T_{WE} is given as:

$$T_{WE} = \left(\log E_m \sqrt{\frac{\log(m \log(m))}{2}} - V_{offset} \right) \times G . \tag{4.21}$$

where G and V_{offset} are two values calculated in the offline analysis. Empirically, values like $G=10$ and $V_{offset}=8$ produced the best results (Nguyen-Ky, 2010a; Nguyen-Ky, 2010c).

4.2.3 Wavelet-based de-noising algorithm

We denote $\Phi^{T_{WE}}$ as the function of the wavelet threshold T_{WE}. To reduce noise, we propose the wavelet-based de-noising algorithm as the followings:

- *Apply the DWT to the raw EEG signal and obtain the empirical wavelet coefficients*
- *Apply the threshold nonlinearity function in (4.13) or (4.14) to the noisy empirical wavelet coefficients, with the new threshold T_{WE} in (4.21).*

- *Estimate the low frequency signal (e_i) which is seen as a carrier signal for the true EEG signal. Compute the inverse wavelet transform of the processed wavelet coefficients, we have:*

$$\Phi^{T_{WE}}: \quad y_i \rightarrow \Phi^{T_{WE}}(D_j(y_i)) = \hat{e}_i, \tag{4.22}$$

where $D_j(y_j)$ is the detail coefficients of y_j.

- *Compute the output EEG signal after de-noising using (4.1) and (4.22),*

$$\hat{x}_i = y_i - \hat{e}_i. \tag{4.23}$$

Figure 4.4 demonstrates the results of our threshold T_{WE} and the wavelet-based de-noising algorithm. Raw EEG signal is shown in Figure 4.4(a). Figures 4.4(b) and 4.4(c) show the low frequency noise and spike noise in the case using hard-threshold. Figures 4.4(d) and 4.4(e) show the low frequency noise and spike noise in the case using soft-threshold. Figures 4.4(f) and Figure 4.4(h) present the resulted EEG signals after de-noising the low frequency noise using hard-threshold and soft-threshold. The EEG signals after de-noising the spike noise using hard-threshold and soft-threshold are presented in Figure 4.4(g) and Figure 4.4(i). In Figure 4.4(g), obviously the output EEG signal is almost noiseless.

Methods of removing noise such as the *Minimax* threshold; *SureShrink* threshold and Universal threshold have been previously reported (Donoho, 1994; 1995a). *Minimax* uses pre-computed thresholds to minimize a constant term in the upper bound for the minimax risk of estimating a function (Donoho, 1994). The *SureShrink* threshold is an adaptive threshold selection using the principle of Stein's unbiased risk estimation. The Universal threshold achieves minimax convergence rates up to a logarithmic penalty over a wide range of function classes (Donoho, 1995b).

A comparison of the proposed method with the SureShink and Minimax threshold methods is presented in Figure 4.5. The raw EEG signal was presented in Figure 4.5(a). Figures 4.5(b) and 4.5(c) show the plots of EEG signal using SureShink and Minimax thresholds. The resulted EEG signal using SureShink and Minimax thresholds still have low frequency noise and high offset voltages. Using our new threshold T_{WE} and the wavelet-based de-noising algorithm, the EEG signal is reproduced almost noiselessly in Figure 4.5(d).

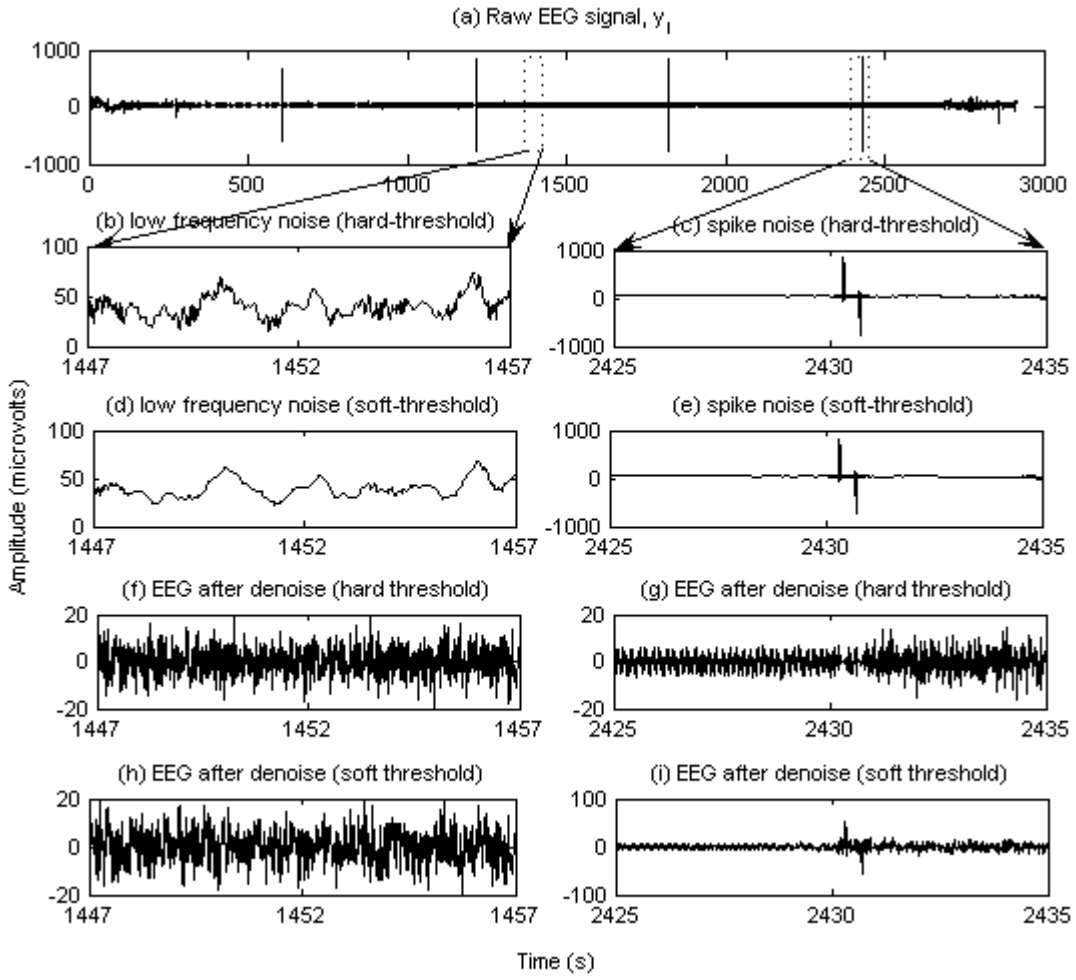

Figure 4.4: (a) Raw EEG signal;

(b) Low frequency noise using hard-threshold;

(c) Spike noise using hard-threshold;

(d) Low frequency noise using soft-threshold;

(e) Spike noise using soft-threshold;

(f) EEG signal after de-noising the low frequency noise by hard-threshold;

(g) EEG signal after de-noising the spike noise by hard-threshold;

(h) EEG signal after de-noising the low frequency noise by soft-threshold;

(i). EEG signal after de-noising the spike noise by soft-threshold.

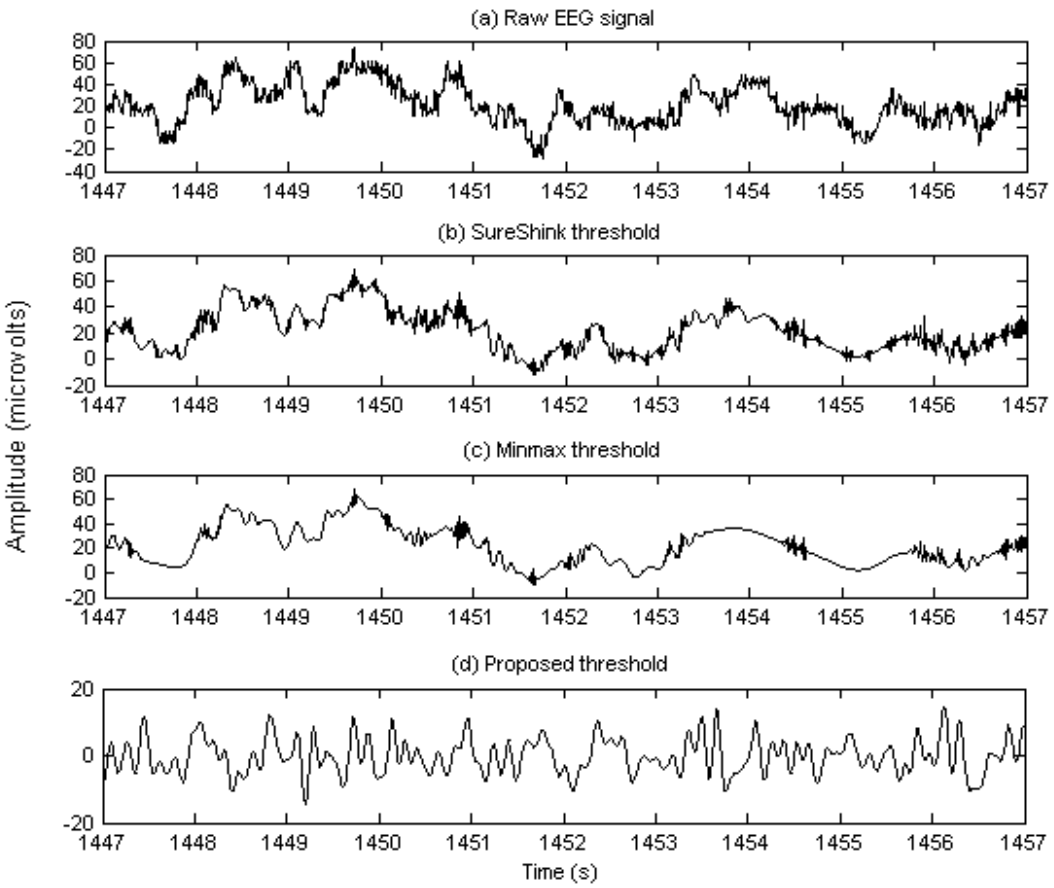

Figure 4.5: Comparison of three methods for de-noising.

(a) Raw EEG signal.

(b) EEG signals after de-noising with SureShink threshold (Matlab toolbox).

(c) EEG signals after de-noising with Minimax threshold (Matlab toolbox)...

(d) EEG signals after de-noising with proposed threshold using wavelet-based denoising algorithm.

Chapter 5

Monitoring DoA using Modified De-trended Fluctuation Analysis (MDFA I) Method I

This chapter introduces de-trended fluctuation analysis (DFA) method and its application for signal processing and monitoring the DoA. A new method is proposed to improve the DoA accuracy using modified de-trended fluctuation analysis method, fast Fourier transform (FFT) and filter banks. A brief review about DFA method, its applications in DoA, and their problems are presented. Then the DFA method is modified and applied to identify different stages of anaesthesia. The optimum box sizes are chosen corresponding to five states of DoA: very deep anaesthesia, deep anaesthesia, moderate anaesthesia, light anaesthesia and awake. Comparing to the original DFA method in (Jospin, 2007), the modified DFA (MDFA I) method can clearly discriminate among awake state, light anaesthesia, moderate anaesthesia and deep anaesthesia states.

5.1 INTRODUCTION TO DE-TRENDED FLUCTUATION ANALYSIS

Scalp electrodes record signals containing both EEG and EMG. The amplitude of EEG decreases as frequency increase, whereas for EMG there is little energy at low frequencies, it rises significantly around 10-40 Hz and is large and relatively constant beyond 40 Hz (well beyond 100 Hz). Integration of signals effectively amplifies high frequencies, so integrating scalp recordings emphasises EMG over EEG. Fractal analysis is used to characterize complex time serie based on the time-evolutionary properties. In fractal analysis, detrended fluctuation analysis has been applied to detect the correlation of long-range temporal in a nonstationary time series (Bardet, 2008; Blesic, 1999; Kantelhardt, 2001). The DFA algorithm aggregated the process by finding a trend from the integrated EEG signals. The integrations *Y(i)* on EEG signals are divided into boxes of equal length *s*. The length of the segments is called box size. This trend is iteratively searched on different sizes of boxes over the signals using a polynomial function $p_v(i)$. In each box, the local trend is subtracted from the integrated signals. Finally, the root mean square (rms) fluctuation *F(s)* for the integrated and detrended signal is calculated for each box *s*. The procedure is summarised as follows:

1) Determine the profile:

$$Y(i) = \sum_{k=1}^{i} [x_k - \langle x \rangle], \qquad i = 1,..., L \tag{5.1}$$

of the time series x_i of EEG sample of length *L*, where <*x*> is the average of the time series, that is

$$\langle x \rangle = \frac{1}{L} \sum_{k=1}^{L} x_k \tag{5.2}$$

2) Cut the profile *Y(i)* into L_s=[*L*/*s*], non-overlapping segments of equal length *s*.

Since the recorded length L needs not to be a multiple of the considered time scale s, a short part at the end of the profile will remain. In order not to discard this part of the record, the same procedure is repeated starting from the other end of the record. Thus, $2L_s$ segments are obtained altogether.

3) Calculate the local trend for each segment ν by a least-square fit of the data. Then we define the detrending time series for segment duration s, denoted by $Y_s(i)$, as the differences between the original time series and the fits:

$$Y_s(i) = Y(i) - p_\nu(i) \tag{5.3}$$

where $p_\nu(i)$ is the fitting polynomial in the ν*th* segment, $\nu = 1,\ldots, 2L_s$. Linear, cubic, or higher order polynomials can also be used in the fitting procedure (DFA1, DFA2, and higher order DFA). Since the detrending of the time series is done by the subtraction of the fits from the profile, these methods differ from their capabilities of eliminating trends in the data. In *mth* order DFA, trend's order of m in the profile and order of $m-1$ in the original record are eliminated.

4) Calculate the variance for each of the $2L_s$ segments:

$$F_s^2(\nu) = \left\langle Y_s^2(i) \right\rangle = \frac{1}{s}\sum_{i=1}^{s} Y_s^2[(\nu-1)s + i] \tag{5.4}$$

of the detrended time series $Y_s(i)$ by averaging over all data points i in the ν*th* segment. Finally, we average over all segments and take the square root to obtain the DFA fluctuation function:

$$F(s) = \left[\frac{1}{2L_s}\sum_{\nu=1}^{2L_s} F_s^2(\nu)\right]^{\frac{1}{2}} \tag{5.5}$$

This computation is repeated over all time scales (segment/box sizes) to provide a relationship between $F(s)$, the average fluctuation as a function of segment size, and the segment size s. Typically, $F(s)$ increases with s. A power-law relation

between the average root-mean-square fluctuation function *F(s)* and the box size *s* indicates the presence of scaling:

$$F(s) \propto s^{\alpha} \tag{5.6}$$

where α is the slope of the line observed in the log-log representation of *F(s)* in the function of *s*.

The fluctuations in a signal can be characterized by the scaling exponent α. If $\alpha = 0.5$, there is no correlation and the signals are uncorrelated (white noise); if $\alpha < 0.5$, the signal is anti-correlated; if $\alpha > 0.5$, the signal is correlated. Since we use a polynomial fit of order *m*, we denote the algorithm as DFA-*m*.

Furthermore, we note that for stationary signals x_k with long-range power-law correlations, the value of the scaling exponent α is related to the exponent β in the power spectrum $S(f) = f^{-\beta}$, of signals x_k, where $\beta = 2\alpha - 1$ (Ferree, 2002; 2003). Since the power spectrum is the Fourier transform of the autocorrelation function, one can find the following relationship between the autocorrelation exponent γ and the power spectrum exponent β: $\gamma = 1 - \beta = 2 - 2\alpha$, where γ is defined by the autocorrelation function $C(\tau) = \tau^{-\gamma}$ and should satisfy $0 < \gamma < 1$ (Bardet, 2008).

5.2 APPLICATION OF DFA METHOD IN SIGNAL PROCESSING

DFA method was used to study the long-range power-law correlations for Deoxyribonucleic acid (DNA) sequences (Peng, 1994; Buldyrev, 1998; 1995). In these papers, patchy nucleotide sequences were analysed by DFA method using two classes: long-range power-law correlations and none long-range power-law correlations. DNA walk for a control sequence were correlated with the changed values of the power-law exponent α and the box size ℓ.

DFA method was used to investigate the effect of sleep stages and sleep apnea on autonomic activity by analysing heart rate variability (HRV) (Penzel, 2003). In Figure 5.1, DFA method can distinguish "light sleep", "deep sleep", "REM sleep", and "wakefulness" from the averages of the heartbeat inputs. The power-law exponents (α) correspond to the slopes of the curves. This result shows that DFA method can be used for the detection of long-range correlations in noisy (artifacts) and nonstationary time series (EEG signals). DFA method can be used to analyse EEG signals for classification the states of DoA.

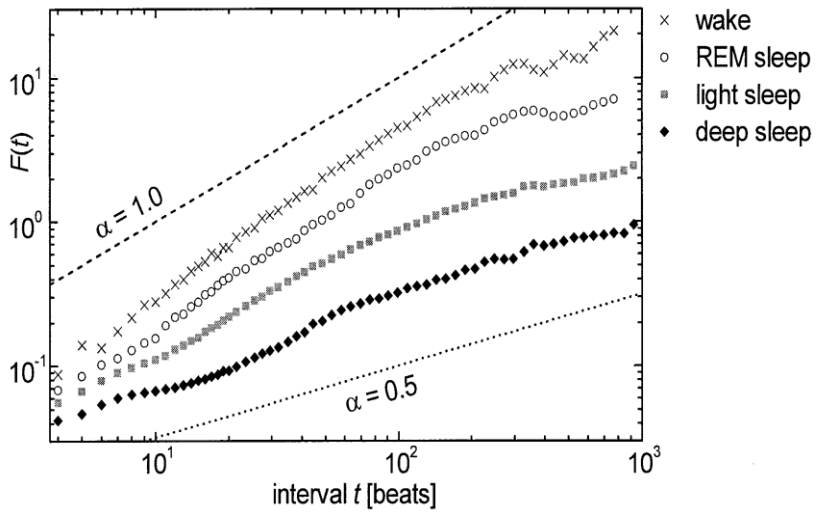

Figure 5.1: The slopes of the curves *F(t)* correspond to the value of the fluctuation scaling exponent α for the three sleep stages and compared to the result for wake during the night (Penzel, 2003).

An application of detrended fluctuation analysis to gearbox fault diagnosis was presented by De Moura et al. (De Moura, 2009) in mechanical system. Grau-Carles used DFA method to investigate long-range power-law correlations in US, UK, Japanese, German, French and Spanish stock markets using daily data and applying a recently developed residual analysis (Grau-Carles, 2001). Using DFA method, Alvarez-Ramirez *et al* studied the long-term memory dynamics for continent

and ocean temperature records in the recent 125 years for both Northern hemisphere (NH) and Southern hemisphere (SH) (Alvarez-Ramirez, 2008).

5.3 APPLICATION OF DFA IN EEG SIGNAL ANALYSING AND DoA

The DFA was applied to study the scaling behaviour of the EEG as a measure of the level of consciousness (Jospin, 2007). Three indexes (α_1, α_2, and α_3) are used to characterize the patient state. The exponent α_i is the slope of fluctuation F on the time scale t, with $F=t^{\alpha}$. One classical fractal is a random walk, a walk with completely uncorrelated steps. The root-mean-square (RMS) displacement from the origin in the case of a random walk grows in a power-law fashion as $t^{1/2}$, with t being the elapsed time from the beginning of the walk. Walks with correlated steps behave differently: a purposeful walk grows as t^1 and a back-and-forth walk as t^0. This method allows real-time implementation and enables its application in monitoring devices.

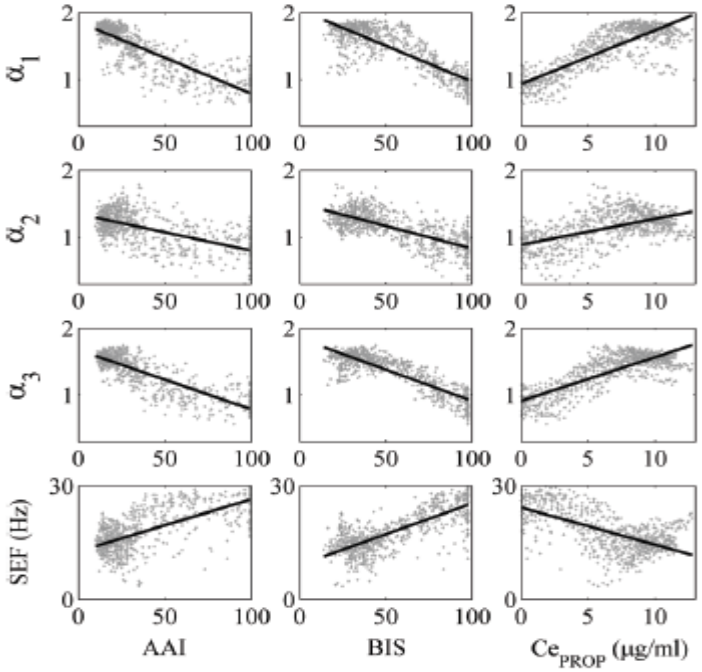

Figure 5.2: The scatter plot of the DFA indexes (α_1, α_2, and α_3) versus three monitor DoA indexes (AAI, BIS, Ce_{PROP}). (Jospin, 2007)

Figure 5.2 presents a comparison between DFA indexes (α_1, α_2, and α_3) with other DoA indexes (AAI, BIS, Ce_{PROP}). The spectral edge frequency (SEF) is a spectral parameter of the total EEG power. This result indicates that the DFA method can be used to monitor the DoA. However, this result only shows the relation of scaling behaviour and the level of consciousness rather than an index for monitoring DoA.

To investigate the effect of box sizes in DFA method, Gifani *et al* gave comprehensive reviews about the fractal and self-similarity properties of the EEG signals (Gifani, 2007). They managed to find the optimum fractal-scaling exponent by selecting the best domain of box sizes, which have meaningful changes with different depth of anaesthesia (Figure 5.3). However, with the original DFA method, their results could not discriminate between light anaesthesia and moderate anaesthesia states. Therefore, the result of light anaesthesia was not shown in the Figure 5.4.

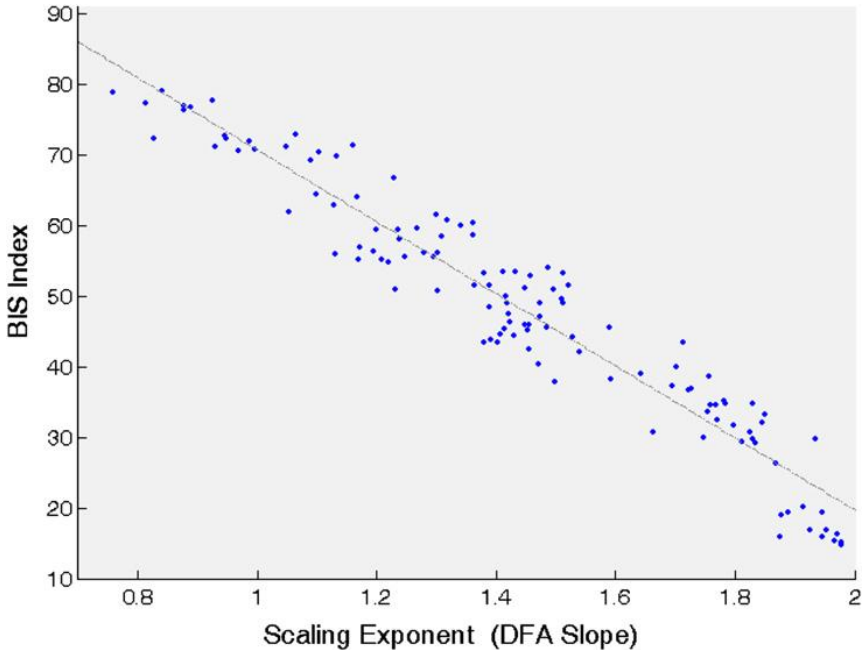

Figure 5.3: BIS index versus fractal-scaling exponent for optimal range of box size. (Gifani, 2007)

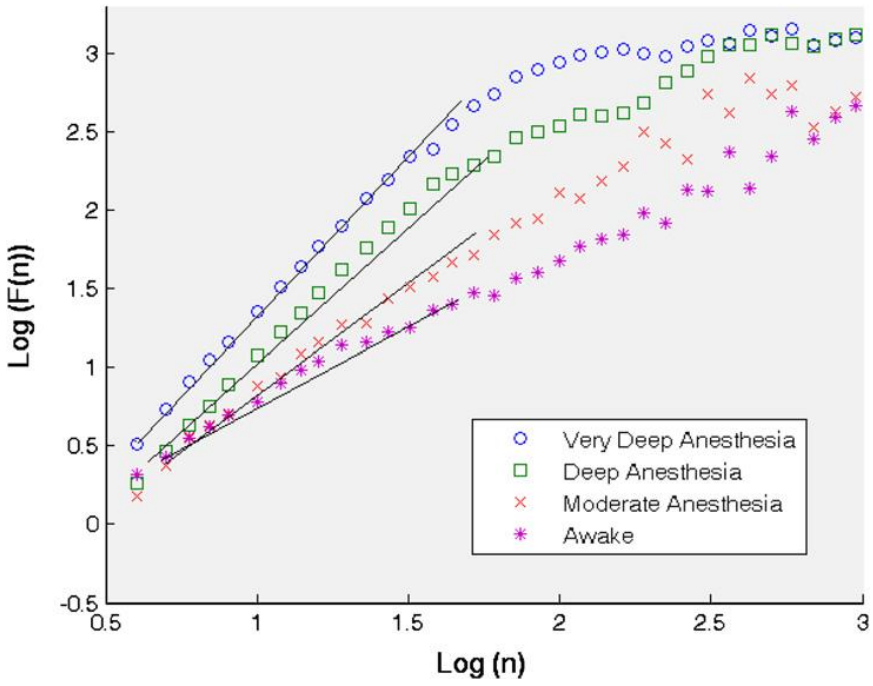

Figure 5.4: Fluctuation versus box size in logarithmic scale (Gifani, 2007).

5.4 USING DFA METHOD TO IDENTIFY DIFFERENT STATES OF ANAESTHESIA

The collected EEG time series in Figure 5.5 have five anaesthetic states. Very deep anaesthesia and deep anaesthesia states have the BIS values from 0 to 40, moderate anaesthesia state from 40 to 60, light anaesthesia state from 60 to 80 and awake state from 80 to 100. In Figure 5.5, these states are labelled as *A*, *B*, *C*, *D* and *E* having the BIS values 15, 30, 50, 80 and 97, respectively (Gifani, 2007). The rate of fluctuation *Y(i)* decreases when the patient's brain states change from anesthetized state to awaked situation.

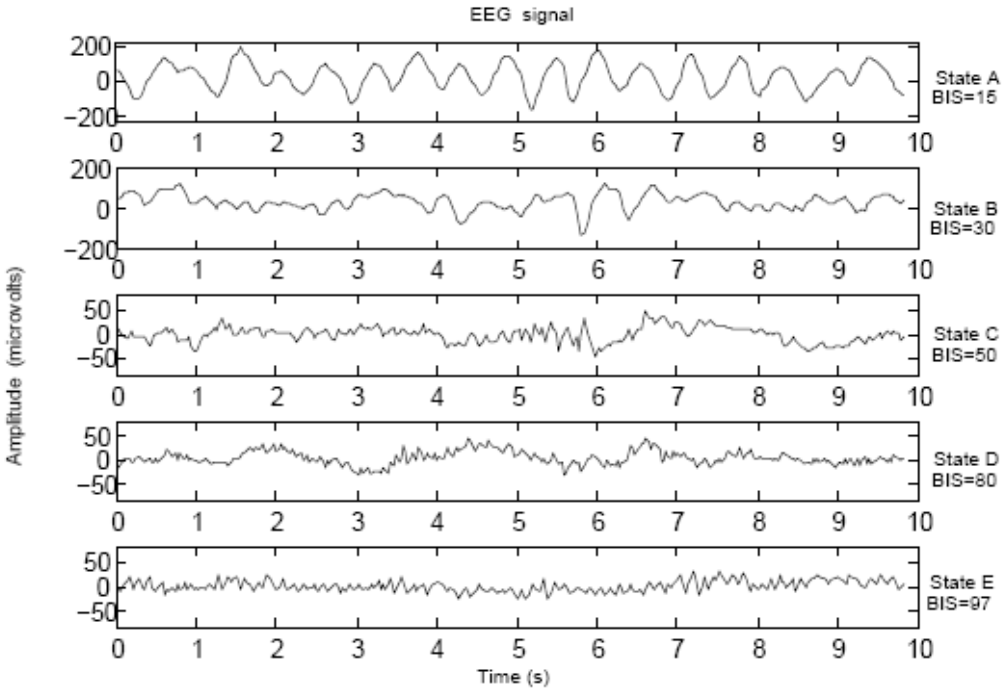

Figure 5.5: The collected EEG time series from five states of anaesthesia. These states are labelled as *A*, *B*, *C*, *D* and *E* having the BIS values 15, 30, 50, 80 and 97, respectively. Very deep anaesthesia have the BIS values from 0 to 20, deep anaesthesia states have the BIS values from 20 to 40, moderate anaesthesia state from 40 to 60, light anaesthesia state from 60 to 80 and awake state from 80 to 100.

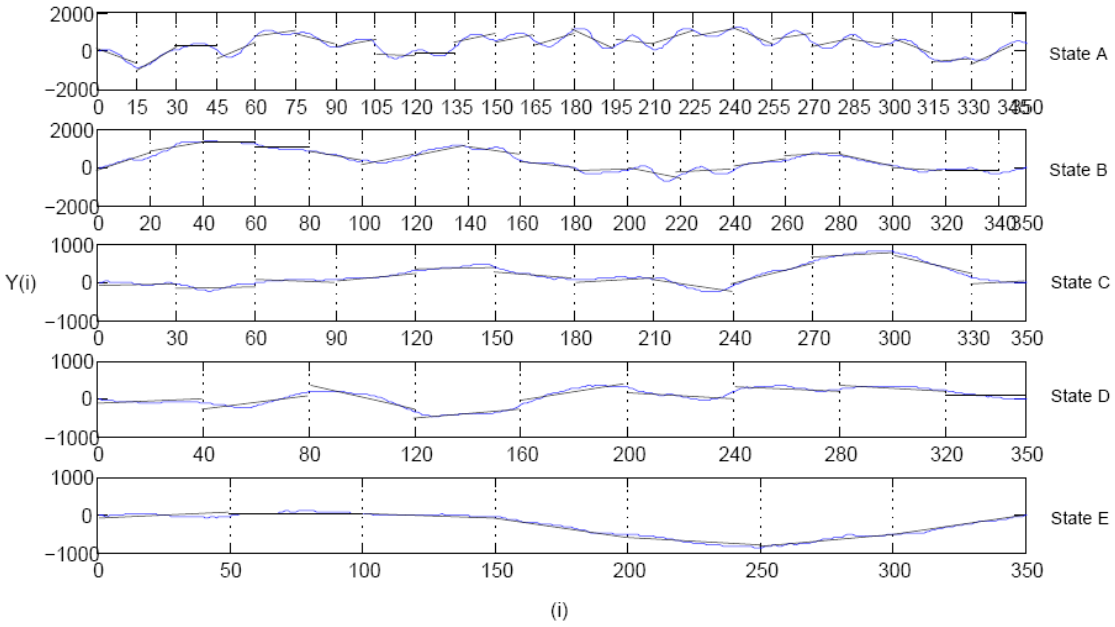

Figure 5.6: Integrated and fitted lines on EEG samples of the time series.

In Figure 5.6, the fluctuation of *Y(i)* is reduced from state A (very deep of anaesthesia) to state E (awake). The integration signals with higher amplitudes and lower fluctuations which correspond to less brain activity (state *A* in Figure 5.5) have resulted in a more wavy output *Y(i)* in Figure 5.6. The integration signals with high fluctuations and low amplitudes which correspond to high brain activity (state *E* in Figure 5.5) have smoothed output *Y(i)* in Figure 5.6.

In DFA, one first builds a walk by integrating the original time series, and then calculates a measure of the amplitude of the fluctuations from a simple linear trend as shown in Figure 5.6. The root mean square fluctuations, *F*, can be expected to depend on the time scale *t*; this is characterized by the exponent α as the slope of this relationship on $F = t^{\alpha}$. The exponent characterizes the correlations in the original time series (Jospin, 2007). The exponent of fractal walks may have any nonnegative value. The main particularity of DFA is trying to filter out non-fractal behaviour by de-trending the time series. We apply the DFA method to identify the five anaesthetic states. In Figure 5.7, we can identify four of the five different states of anaesthesia. With the same value *s*, we have $F_{stateA} > F_{stateB} > F_{stateC} > F_{stateE}$. When the BIS values increase from the state *A* (BIS=15) to state *E* (BIS=97) then the DFA values decrease from F_{stateA} to F_{stateE}. These results are consistent with the results in (Jospin, 2007; Rezek, 2007; Gifani, 2007).

However, we can also see the values of states *C* and *D* are overlapped in DFA method in Figure 5.7. It is almost impossible to distinguish those two states. Figure 5.4 only presented the four states: very deep anaesthesia, deep anaesthesia, moderate anaesthesia and awake (Gifani, 2007). These states are corresponding to states A, B, C and E in this study. State D (light anaesthesia with BIS=80) was not studied in Fig. 5.4 because the curve of state D was overlap with the curve of state C, as shown in

Fig. 5.7. This is a limitation of the original DFA method in this case. Therefore, a modified DFA method is presented in section 5.6.

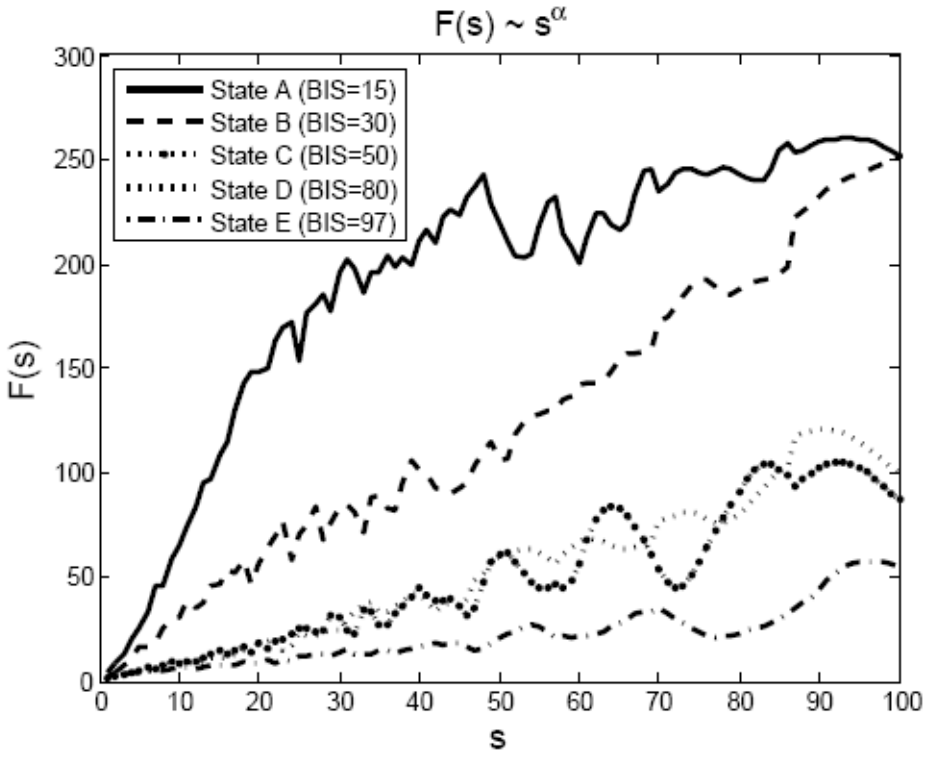

Figure 5.7: The DFA fluctuation function $F(s)$ versus s. Four of the five different states of anaesthesia can identify. With the same value *s*, we have $F_{stateA} > F_{stateB} > F_{stateC} > F_{stateE}$. When the BIS values increase from the state *A* (BIS=15) to state *E* (BIS=97) then the DFA values decrease from F_{stateA} to F_{stateE}.

5.5 IDENTIFY THE STATES OF ANAESTHESIA USING FAST FOURIER TRANSFORM AND FILTER BANK METHODS

5.5.1 Fast Fourier Transform

The fast Fourier transform (FFT) is a discrete Fourier transform algorithm which reduces the computations (Brigham, 1974; Ferree, 2003). The power spectrum obtained from FFT provides a characteristic representation of the contributing

frequencies to an underlying signal. Observing the distinct peaks on the power spectrum, we canderive quantitative connotation to facilitate comparisons between individuals and groups.

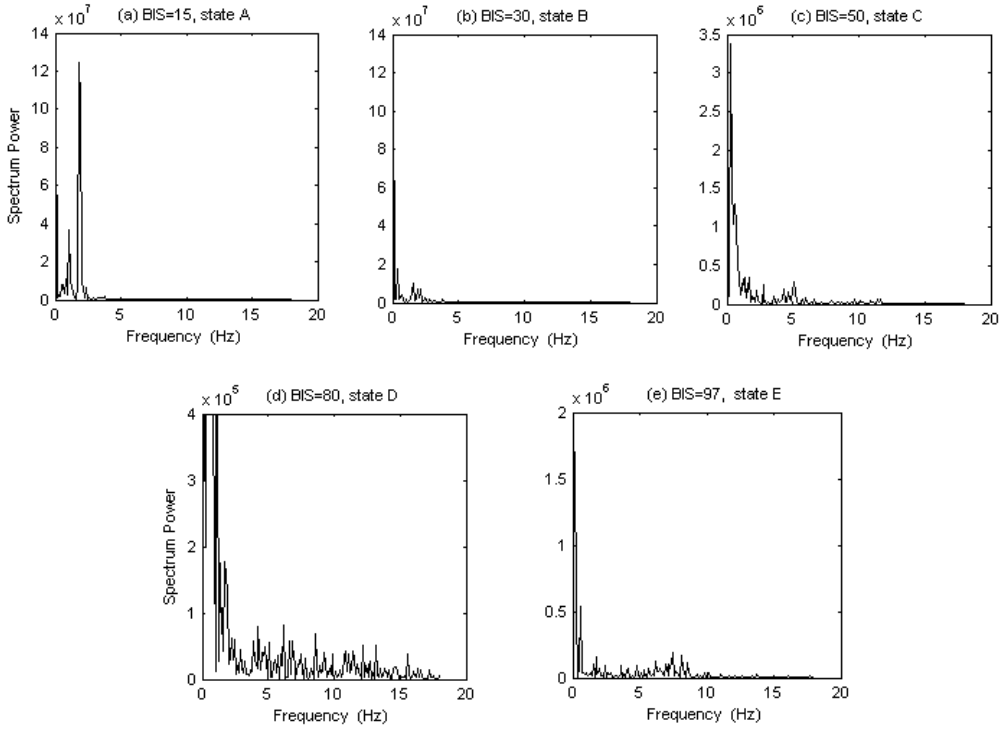

Figure 5.8: The power spectrum obtained from FFT of EEG signal of:

(a) State A; (b) State B;

(c) State C; (d) State D;

(e) State E.

Spectral analysis of the given raw EEG data reveals five principal frequency zones:

- Figure 5.8(a): state *A* (frequency ≤ 2.2 Hz),
- Figure 5.8(b): state *B* (frequency ≤ 4 Hz),
- Figure 5.8(c): state *C* (frequency ≤ 5.2 Hz),
- Figure 5.8(d): state *D* (2 Hz ≤ frequency ≤ 18 Hz),
- Figure 5.8(e): state *E* (frequency ≤ 8.5 Hz).

In the case of state *D*, the distinct peaks have the wide frequency band from 2 Hz to 18 Hz. Therefore, a filter bank is designed to identify the EEG signals in different states of DoA.

5.5.2 Filter banks

Based on the results of FFT analysis, we design the FFT-filter bank with five band-pass filters in Figure 5.9. The power spectrum of the input signal has the local highest values in frequency zones: *1.5-2.2 Hz*, *3-4 Hz*, *4-5.2 Hz*, *5.2-6.2 Hz* and *6.2-8.5 Hz*. A filter bank with five finite impulse response (FIR) filters is applied to identify these frequency zones. The bandpass filters were designed with the five passbands ω_1=[0.075 0.183], ω_2=[0.183 0.250], ω_3=[0.250 0.300], ω_4=[0.3 0.35], and ω_5=[0.35 0.45]. ω_n is a number between 0 and 1, where 1 corresponds to the Nyquist frequency. Each bandpass filter returns row vector *b* containing the (*n+1*) coefficients of an order n lowpass FIR filter. This is a Hamming-window based, linear-phase filter with normalized cutoff frequency ω_n. The output filter coefficients, *b*, are ordered in descending powers of *z*: $B(z) = b(1) + b(2)z^{-1} + \ldots + b(n+1)z^{-n}$ (Matlab signal processing toolbox)."

Every zone is corresponding to different state (*A*, *B*, *C*, *D* or *E)* which has different power spectrum values.

In Figure 5.9(a), at the band-pass filter 1, the spectrum of state *A* has the highest power. In Figure 5.9(b), state *B* has the power higher than those in states *C*, *D* and *E* at the band-pass filter 2. In Figure 5.9(c), the state *C* has the power higher than those in states *B*, *D* and *E* at the band-pass filter 3 while the state *D* has the power higher than those in states *B*, *C* and *E* at the band-pass filter 4 (Figure 5.9(d)),

and the spectrum of state *E* has the highest power at the band-pass filter 5 in Figure 5.9(e).

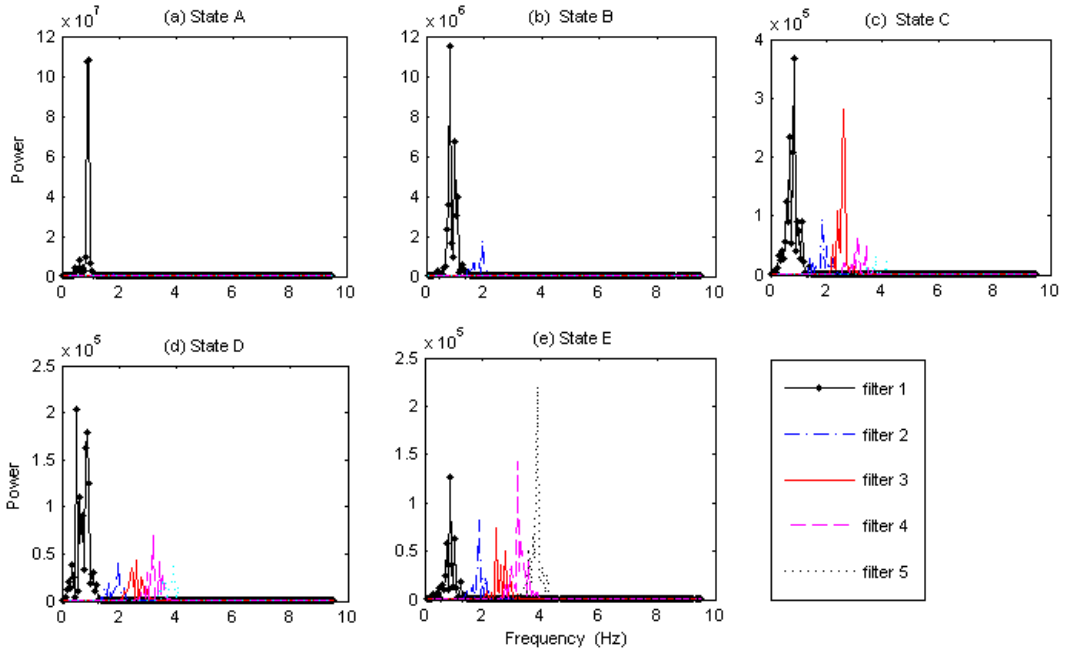

Figure 5.9: The power spectrum of EEG signal after crossing 5 band-pass filters, $Ps_0 = 600x10^5$ is the threshold.

(a) State A: Ps_1=1,083x10^5> Ps_0 = 600x10^5;

(b) State B: $Ps_0 > Ps_1 > Ps_2 > Ps_3 > Ps_4 > Ps_5$;

(c) State C: $Ps_0 > Ps_1 > Ps_3 > Ps_2 > Ps_4 > Ps_5$;

(d) State D: $Ps_0 > Ps_1 > Ps_4 > Ps_2 > Ps_3 > Ps_5$;

(e) State E: $Ps_0 > Ps_5 > Ps_4 > Ps_1 > Ps_2 > Ps_3$.

5.5.3 Identify the states of anaesthesia

To identify these states, we use the diagram in Figure 5.10 with four blocks: input, filter bank, FFT and identified states. In input block, the input EEG signals with different states are fed into the system. The filter bank block has five band-pass filters with a frequency range from 1.5 Hz to 8.5 Hz. After crossing the filter bank, the characteristic magnitude and frequency are detected in the FFT block. In

identified state block, the power spectrums of five FFT blocks are compared. The maximum of power spectrums (MaPS) is selected and presented in Table 5.1. Let us define Ps_1, Ps_2, Ps_3, Ps_4 and Ps_5 as the MaPS of EEG signal after crossing five FFT blocks: FFT_1, FFT_2, FFT_3, FFT_4 *and* FFT_5. $Ps_0 = 600x10^5$ is the threshold.

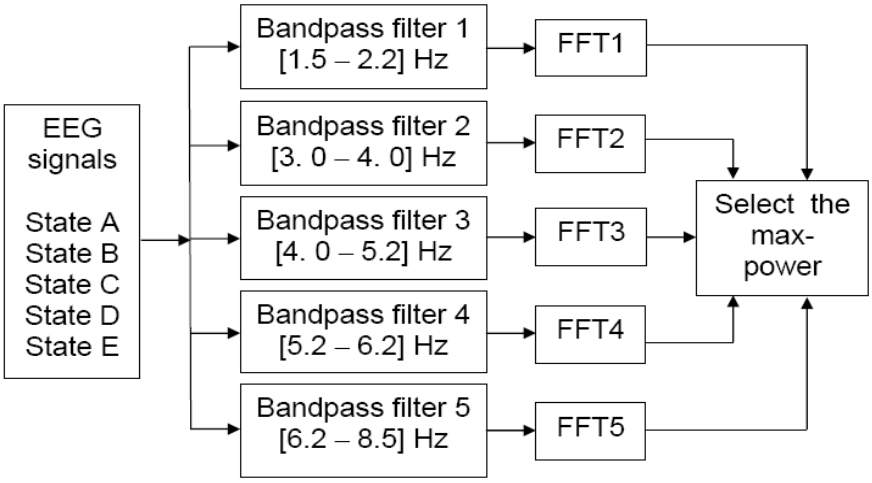

Figure 5.10: Diagram for identifying states of anaesthesia. In input block, the input EEG signals with different states are fed into the system. The filter bank block has five band-pass filters with a frequency range from 1.5 Hz to 8.5 Hz. After crossing the filter bank, the characteristic magnitude and frequency are detected in the FFT block. In identified state block, the power spectrums of five FFT blocks are compared. The maximum of power spectrums is selected.

We identify five states using the five band-pass filters by comparing the MaPS of states *A, B, C, D* and *E*. In Table 5.1, we can see that after crossing the filter bank, MaPS values of different states have the rule as the foloowing:

- State A: $Ps_1 > Ps_0 > Ps_2 > Ps_3 > Ps_4 > Ps_5$;
- State B: $Ps_0 > Ps_1 > Ps_2 > Ps_3 > Ps_4 > Ps_5$;
- State C: $Ps_0 > Ps_1 > Ps_3 > Ps_2 > Ps_4 > Ps_5$;
- State D: $Ps_0 > Ps_1 > Ps_4 > Ps_2 > Ps_3 > Ps_5$;
- State E: $Ps_0 > Ps_5 > Ps_4 > Ps_1 > Ps_2 > Ps_3$.

Table 5.1: The FFT max-power values of filter bank outputs

Bandpass filter	State *A*	State *B*	State *C*	State *D*	State *E*
Ps_1 (Filter 1)	**$1{,}083x10^5$**	$115.1x10^5$	$3.680x10^5$	$2.040x10^5$	$1.271x10^5$
Ps_2 (Filter 2)	$11.40x10^5$	**$18.20x10^5$**	$0.950x10^5$	$0.438x10^5$	$0.820x10^5$
Ps_3 (Filter 3)	$2.130x10^5$	$1.252x10^5$	**$2.800x10^5$**	$0.430x10^5$	$0.734x10^5$
Ps_4 (Filter 4)	$0.932x10^5$	$0.708x10^5$	$0.658x10^5$	**$0.695x10^5$**	$1.427x10^5$
Ps_5 (Filter 5)	$0.420x10^5$	$0.371x10^5$	$0.320x10^5$	$0.373x10^5$	**$2.212x10^5$**

From the results in Table 5.1 and Figure 5.9, we have an algorithm to define the states as follows:

Algorithm 5.1: Defining the states

- *If* $Ps_1 > Ps_0$, *the state* $\equiv$ *state A,*
- *If* $Ps_1 < Ps_0$ & $Ps_2 > \{Ps_3, Ps_4, Ps_5\}$, *the state* $\equiv$ *state B,*
- *If* $Ps_1 < Ps_0$ & $Ps_3 > \{Ps_2, Ps_4, Ps_5\}$, *the state* $\equiv$ *state C,*
- *If* $Ps_1 < Ps_0$ & $Ps_4 > \{Ps_2, Ps_3, Ps_5\}$, *the state* $\equiv$ *state D,*
- *If* $Ps_1 < Ps_0$ & $Ps_5 > \{Ps_1, Ps_2, Ps_3, Ps_4\}$, *the state* $\equiv$ *state E.*

5.6 MODIFIED DFA METHOD FOR MONITORING THE DEPTH OF ANAESTHESIA USING DIFFERENT BOX SIZE

5.6.1 Modified DFA method using different box size

We propose to apply a different technique in the third step of DFA method to distinguish states C and D. For the modified DFA method, we compute the de-trending time series $Y_s(i)$ in (5.3) for states *A*, *B* and *C* as follows:

$$Y_s(i) = Y(i) - \sum_{k=1}^{m} \frac{1}{s(k)} \sum_{\mu=1}^{L_s} f(\nu) \tag{5.7}$$

with $m=length(s)$ and $f(v)=\sum_{i=1}^{s} Y[i+(v-1)s]$, $Y(i)$ is defined in (5.1).

In (5.3), $Y_s(i)=Y(i)-p_v(i)$, with $p_v(i)$ is the fitting line in the vth segment. In fact, the fitting line $p_v(i)$ crosses $Y(i)$. Therefore, $Y_s(i)$ usually has the smallest values at these points which are nearly crossing point when $Y(i)\approx p_v(i)$. When two signals having the fluctuation are not quite difference, the overlap of their $F(s)$ will happen in DFA method. This is the reason why $F(s)$ of the states *C* and *D* are overlapped. In order to separate them, equation (5.3) was modified into equation (5.7).

In equation (5.7), the averaging of $F(v)$ was computed over all data points *i* in the vth segment. By this way, there is not a crossing point. In our method, equation (5.7) was used for states *A, B* and *C*. Equation (5.3) was used for states *D* and *E*. The fluctuations $F(s)$ of states *C* and *D* are separated in Figure 5.11. The limitation of this method is that the state must be identified before selecting equations (5.3) or (5.7). Therefore, a method to identify the states of anaesthesia is proposed in the previous section.. The results of modified DFA method are compared with DFA method in Figure 5.11. In this Figure, the curve (3) is the fluctuation of state *C* in DFA method and the curve (5) is the fluctuation of state *D* in modified DFA method. We can see that they are clearly separated. With modified DFA method, we discriminate four states: deep anaesthesia (states *A* and *B*), moderate anaesthesia (state *C*), light anaesthesia (state *D*) and awake (state *E*). The results also show the region of the best box size for fluctuation analysis.

In Figure 5.6, the $Y(i)$ in state *A* has the fluctuation higher than those in states *B, C, D* and *E*. Similarly, $Y(i)$ in state *B* has the highest fluctuation among those in states *C, D* and *E*; $Y(i)$ in state *C* has the highest fluctuation among those in states *D* and *E*; and $Y(i)$ in state *D* has the fluctuation higher than that in state *E*. Therefore,

with the *Y(i)* value having the higher fluctuation, we choose the small box size and vice versa. The different box sizes were chosen for each state.

We define s_A, s_B, s_C, s_D and s_E as box sizes for the states *A, B, C, D* and *E*. We choose box sizes using the following rules: $s_A \leq s_B \leq s_C \leq s_D \leq s_E$. As shown in Figure 5.11, states *A, B, C, D* and *E* have the linear diagrams in the ranges $3 \leq s_A \leq 12$, $3 \leq s_B \leq 12$, $3 \leq s_C \leq 19$, $3 \leq s_D \leq 35$ and $3 \leq s_E \leq 55$. Table 5.2 shows the relationship among different box sizes, and the fluctuation values *F* in every state, *A, B, C, D* or *E*.

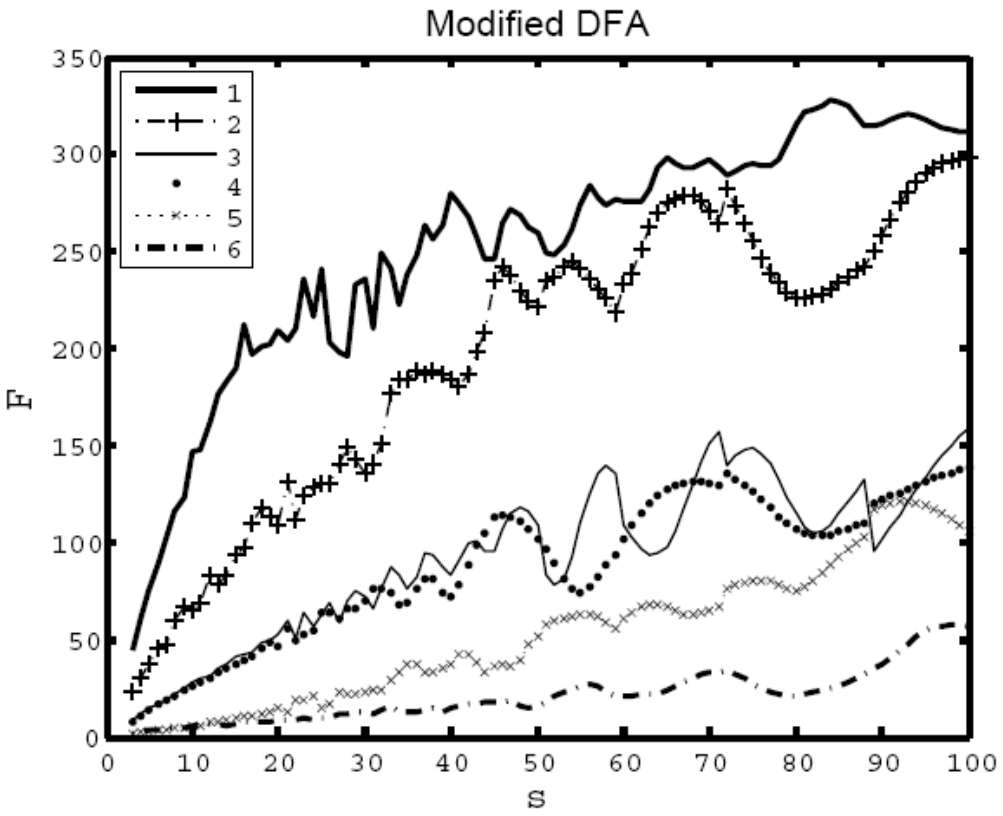

Figure 5.11: The fluctuation function *F* versus *s*

a) The curve (1), (2), (3), (4) are the fluctuation of states *A*, *B*, *C*, and *D* in modified DFA method, respectively.

b) The curve (5) and (6) are the fluctuation of state *D* and *E* in DFA method, respectively.

5.6.2 Monitor the Depth of Anaesthesia

We tried ten options for choosing the box sizes corresponding to T values (T = 1, 2,…, 10). We found that the results in Table 5.2 have the relationship with the BIS value as follows:

$$F_{jDoA} = \frac{K_T}{F_j} \approx BIS^{\,j} \tag{5.8}$$

with BIS^j is the BIS value of state j and K_T is the correlative parameter between BIS and DFA.

With the results in Table 5.2, we calculate the DoA value as follows:

a) *Step 1*: Choose the value of a box size in Table 5.2. The box size in the deep anaesthesia state (states *A* and *B*) is less than those in the moderate anaesthesia (state *C*), light anaesthesia (state *D*) and awake state (state *E*).

b) *Step 2*: Apply DFA algorithm to compute the fluctuation function F_j value using box size chosen in step 1 (j = *A, B, C, D and E*). We note that (5.3) is used for states C and D and (5.7) for states A, B and C.

c) *Step 3*: Compute the DoA value F_{jDoA} in (5.8), where K_T *(T=1, 2,..., 10)* is the our experiments values in Table 5.2.

Comparing with the most popular BIS method, our modified DFA method extends the deep anaesthesia and very deep anaesthesia ranges to provide more information about these states as they need more attention. F_j *(j = A, B, C, D and E)* has a relation with BIS values as follows: $F_{jDoA} = K_T / F_j \approx BIS^j$, with BIS^j is the BIS value of state j. For example, we can choose one of ten cases in Table 5.2: $s_A = s_B = 7$, $s_C = 12$, $s_D = 22$, $s_E = 41$. In this case, we have $T=5$ *and* $K_T = 1500$; and compute the DoA values F_{jDoA}. The results are $F_{A\text{-}DoA} = 14.6$, $F_{B\text{-}DoA} = 31.77$, $F_{C\text{-}DoA} = 48.73$,

$F_{D\text{-}DoA}$ *= 79.83, and* $F_{E\text{-}DoA}$ *= 95*. In Figure 5.12, we found that the DoA values are close to the BIS values: $BIS^A = 15$, $BIS^B = 30$, $BIS^C = 50$, $BIS^D = 80$, and $BIS^E = 97$.*

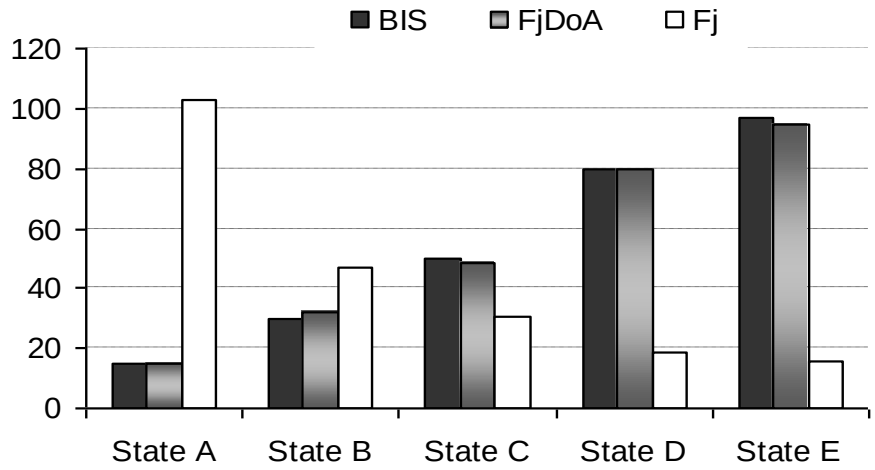

Figure 5.12: Comparison of the values of BIS, F_{jDoA} and F_j index

Table 5.2: Ten options for choosing the box sizes

s_A	s_B	s_C	s_D	s_E	F_A $(BIS^A=15)$	F_B $(BIS^B=30)$	F_C $(BIS^C=50)$	F_D $(BIS^D=80)$	F_E $(BIS^E=97)$	K_T	T
3	3	5	13	17	44.64	22.53	14.35	8.15	7.22	670	1
4	4	7	18	23	60.42	30.57	19.24	11.46	9.74	906	2
5	5	8	20	28	75.36	37.00	22.40	14.74	11.57	1130	3
6	6	10	22	32	89.30	45.14	27.89	18.79	13.40	1340	4
7	7	12	22	41	102.7	47.21	30.78	18.79	15.79	1500	5
8	8	13	28	44	115.8	59.84	35.53	22.05	18.17	1737	6
9	9	15	31	52	123.0	67.30	41.10	24.40	20.70	2000	7
10	10	17	33	53	147.2	65.31	43.38	29.40	22.77	2200	8
11	11	17	33	53	147.8	68.80	43.38	29.40	22.77	2217	9
12	12	19	34	55	161.7	83.50	49.35	33.00	25.82	2500	10

5.7 DISCUSSION

Comparing our method with BIS Index, we observed that:

BIS Index is calculated from following four sub-parameters: Burst Suppression Ratio (*BSR*), *Quazi* suppression, Relative β ratio and *SynchFastSlow* (see Section 2.6.4).

- Relative β ratio ($logP_{30\text{-}47Hz}/P_{11\text{-}20Hz}$) by power spectral analysis, with $P_{30\text{-}47Hz}$ is the sum of the spectral power in the band extending from frequency *30 Hz* to *47 Hz*. $P_{11\text{-}20Hz}$ is the *sum of the spectral power* in the band extending from frequency *11 Hz* to *20 Hz*.
- *SynchFastSlow* ($logB_{0.5\text{-}47Hz}/B_{40\text{-}47Hz}$) by bispectral analysis, with $B_{0.5\text{-}47Hz}$ is the sum of the bispectrum activity in the area subtended from frequency 0.5 Hz to 47 Hz. $B_{40\text{-}47Hz}$ is *the sum of the bispectrum activity* in the area subtended from frequency 40 to 47 Hz

Comparing with our method, we found that the computation of BIS value is very complex and requires more time than our method.

EEG signal is essentially a non-stationary time series. The DFA method has been established as an important fractal analysis technique for the detection of long-range temporal correlations in non-stationary time series. The BIS Index is only calculated focusing on the frequency domain (β ratio and *SynchFastSlow*). The analyses of the EEG signals in frequency domain are restricted because it only captures the information relevant to frequency without any reference to time. Although BIS Index computes *BSR* and *Quazi* in time domain, they are used for the detection of epochs that represent electrical suppression of EEG signal. This only happens in the case of very deep of anaesthesia. Therefore, these analyses can not be used for light anaesthesia detecting.

Chapter 6

Monitoring DoA using Modified De-trended Fluctuation Analysis (MDFA II) Method II.

This chapter presents another modified detrended fluctuation analysis method (MDFA II) to improve the accuracy of depth of anaesthesia monitoring. MDFA II is applied to classify anaesthesia state levels into awake, light, moderate, deep and very deep states. Then five zones are built up using linear regression method from very deep anaesthesia state to awake state, corresponding to different box sizes. Finally, the Lagrange method is applied to compute the DoA.

Comparing with the most popular Bispectral index (BIS) method, this new modified MDFA II method extends the ranges of the moderate anaesthesia, deep anaesthesia and very deep anaesthesia. This extension is significant in the clinical perspective as these states are within the ranges for operations and need more attentions. Simulation results demonstrate that the new technique monitors the DoA in all anaesthesia states accurately.

6.1 MODIFIED DETRENDED FLUCTUATION ALGORITHM II (MDFA II)

The detail of DFA method is presented in Chapter 5. *F(s)* values in DFA results are overlapped in states *C* and *D* (see Figure 5.7) and are also overlapped in log-log representation. Therefore, modified detrended fluctuation analysis method MDFA II is proposed to detect and separate light anaesthesia (states *C*) and moderate anaesthesia (state *D*).

6.1.1 Classify five anaesthesia states

We propose to apply modified DFA to classify five states *A, B, C, D* and *E*. When calculating the variance for each of the $2L_s$ segments of the detrended time series $Y_s(i)$, we modify (5.4) as:

$$F_s^*(\nu) = \left\langle Y_s^2(i) \right\rangle = \frac{1}{(L_s - s)} \sum_{i=1}^{s} Y_s^2[(\nu - 1)s + i], \tag{6.1}$$

and compute the value $F^*(s)$ over all segments by defining

$$F^*(s) = \exp\left[\frac{1}{(L_s - s)} \sum_{\nu=1}^{2L_s} \log F_s^*(\nu) \right]. \tag{6.2}$$

We define:

$$P_j = \log \frac{F^*(s)}{s}, \; j = 1, 2, 3, 4, 5. \tag{6.3}$$

Figure 6.1 presents the values of P_j (with $j = 1, 2, 3, 4, 5$) for five states *A, B, C, D* and *E*, respectively. We have P_A = 114.47, P_B = 92.3175, P_C = 67.9175, P_D = 64.3995 and P_E = 59.9935. We can classify the five states of anaesthesia using the above P_j. values.

6.1.2 Separate fluctuation function *F(s)* in moderate and light anaesthesia states

The purpose of equation (6.1) to (6.3) is to find the characters of five states. Based on these characters, these states were classified. After classification, $F_{MDFA}(s)$ was computed based on these equations (6.4) and (6.5) below. We redefine (5.5) as:

$$F_{MDFA}(s) = \left[\frac{1}{q_j L_s} \sum_{s=3}^{L} F^2(s) \right]^{\frac{1}{2}}, \quad q_j > 0, \; j = 1, 2, 3, 4, 5; \qquad (6.4)$$

where parameter q_j is introduced to change the amplitude of $F_{MDFA}(s)$. We denote q_j as:

$$q_j = \begin{cases} 14 & if \quad P_j \le P_O \\ 2 & if \quad P_j > P_O \end{cases}, \qquad P_O = 66. \qquad (6.5)$$

The values of q_i are determined by several facts below.

Firstly, states *C* and *D* have P_C = 67.9175, and P_D = 64.3995. These values are symmetrical through value 66. We choose $P_O = 66$ as the break point to separate states *C* and *D*.

Secondly, in Figure 5.3, the fluctuation functions of *F(s)* in states *A*, *B* and *C* already separate the range of $s \le 40$, and the values of P_j in states *A*, *B* and *C* are higher than P_O. We, therefore, choose $q_A = q_B = q_C = 2$ as the original values in (5.5) of DFA method.

Thirdly, the amplitudes of $F_{MDFA}(s)$ decrease when the values of q_j increase in (6.4). We choose $q_D = q_E = 14$ to provide the best for selecting box sizes and the range of $F_{MDFA}(s)$ as discussed in the section 6.2. They are, therefore, the optimal results based on our experiments.

In this section, we define (6.1), (6.2) and (6.3) to classify the five states of the DoA in Figure 6.1.

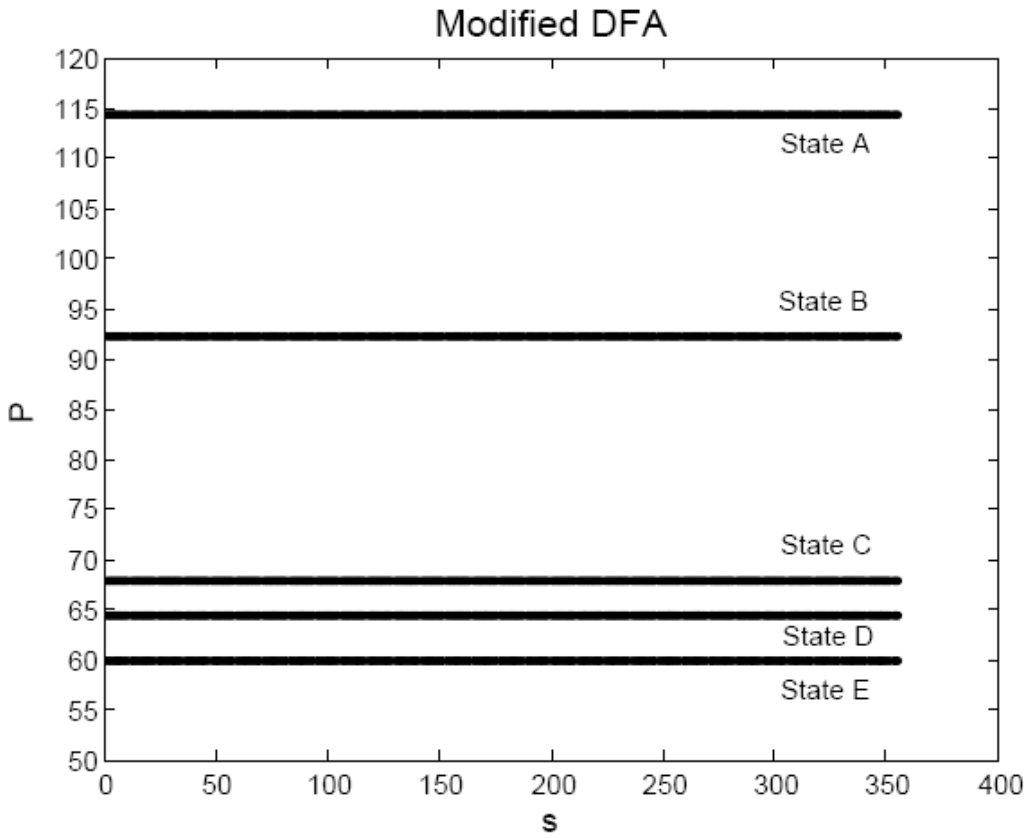

Figure 6.1: Using modified DFA2, we have:

P_A = 114.47, P_B = 92.3175, P_C = 67.9175, P_D = 64.3995 and P_E = 59.9935.

Five states of anaesthesia can be classified using the above values from P_j.

6.2 STATE IDENTIFICATION

From the result in Figure 6.1, five states of DoA were distinguished. The fluctuation *F(s)* of five states were shown in Figure 6.2. In figure 6.2, the curve *F(s)* of states *C* and *D* were distinguished. The curve *F(s)* of states *D* and *E* closed because they have the BIS values 80 and 97, respectively. In the range BIS form 80 to 100, the patient's states are the same because this is awake state. We can see that *F(s)* has an almost linear relationship with states *A, B, C, D* and *E* in the ranges of the box size *s* such as:

$3 \le s_A \le 20$, $3 \le s_B \le 25$, $3 \le s_C \le 35$, $3 \le s_D \le 45$ and $3 \le s_E \le 55$, respectively, and their slope increases from the state *E* to the state *A*. These characteristics are used for the purpose of setting up the ranges of F_{MDFA} and box size values. We assume that *F(s)* are lines in small ranges of s ($3 \le s \le 60$). In figure 6.3, the linear regression method is used to draw the line $\hat{F}(s)$ from F(s) values. These lines are used to divide five zones corresponding with five states from very deep anaesthesia to awake state. These results are used in the next step when we develop the depth of anaesthesia index using the Lagrange method.

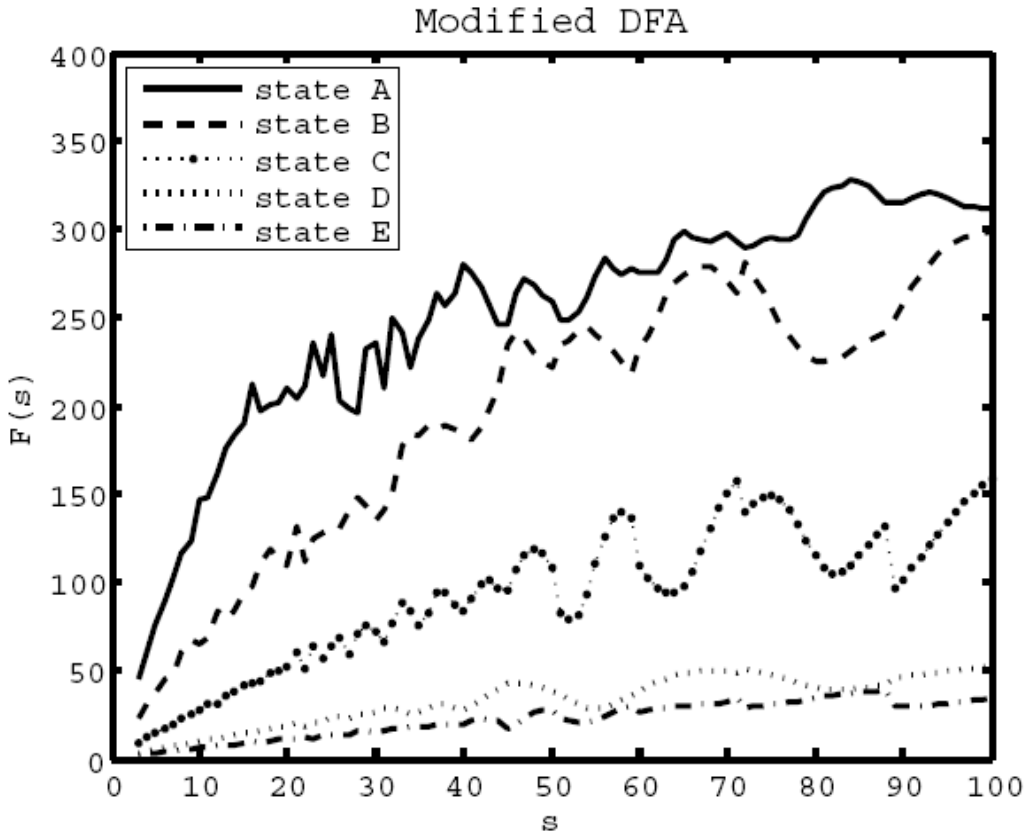

Figure 6.2: Using modified DFA to separate states *C* and *D*, *F(s)* has an almost linear relationship with states *A, B, C, D* and *E* in the ranges of: $3 \le s_A \le 20$, $3 \le s_B \le 25$, $3 \le s_C \le 35$, $3 \le s_D \le 45$ and $3 \le s_E \le 55$, respectively; and their slope increases from the state *E* to the state *A*.

6.2.1 The Depth of Anaesthesia range

Linear regression is a technique that determines the best fit linear equation to a set of data points in terms of minimizing the sum of the squared distances between the $\hat{F}(s)$ lines and the data points $F(s)$ (Levin, 1998). The distance from each point to its linear estimate is defined as

$$e = F(s) - \hat{F}(s). \tag{6.6}$$

The value of the best fit linear estimate is the sum of the squared distances. The linear equation can be written as

$$\hat{F}(s) = a \times s + b, \tag{6.7-a}$$

where, a is the slope of the line and b is called the $F(s)$-intercept. To find the derivatives of (6.7-a) with respect to a and b, we let the derivatives equal to zero, and obtain:

$$a = \frac{\sum sF(s) - n\bar{s}\bar{F}(s)}{\sum s^2 - n\bar{s}^2},\ b = \bar{F}(s) - a\bar{s}. \tag{6.7-b}$$

$\bar{F}(s)$ and $\bar{s}$ are means of $F(s)$ and s respectively. The values of a and b represent the straight line with the minimum sum of the squared distances.

The line *Z(s)* was chosen based on the chosen ranges of $F_{MDFA}(s)$ and s such as $0 \le F_{MDFA}(s) \le 200$ and $0 \le s \le 50$. From this choice, the ranges are expanded in moderate anaesthesia, deep anaesthesia and very deep anaesthesia states. A comparison between $F_{MDFA}(s)$ and BIS ranges was presented in Table 6.1. The expanded ranges will help clinicians having more detailed DoA values during surgery. To set the range of $F_{MDFA}(s)$ from 0 to 200 and the range of the box size values from 0 to 50, the equation of the line *Z(s)* is: $Z(s) = -4s + 200$ (Figure 6.3). This line is used to divide the zones of five states from very deep anaesthesia to

awake state, corresponding to the DoA and box sizes. When the line Z is crossing all $\hat{F}_{MDFA}(s)$ lines (BIS=20, BIS=40, BIS=60, BIS=80), we have five zones as follows:

- *Zone 1* has the space formed by lines $s=42$, $F(s)=0$ and $Z(s)$,
- *Zone 2* has the space formed by lines $s=35$, $F(s)=30$ and $Z(s)$,
- *Zone 3* has the space formed by lines $s=25$, $F(s)=60$ and $Z(s)$,
- *Zone 4* has the space formed by lines $s=12$, $F(s)=100$ and $Z(s)$,
- *Zone 5* has the space formed by lines $s=0$, $F(s)=150$ and $Z(s)$.

In zone 1, line Z has $F_{MDFA}(s)$ values from 0 to 30 when s values decrease from 50 to 42. We define the range of $F_{MDFA}(s)$ (0-30) as range 1 to monitor the awake state.

In zone 2, line Z has $F_{MDFA}(s)$ values from 30 to 60 when s values decrease from 42 to 35. We define the range of $F_{MDFA}(s)$ (30-60) as range 2 to monitor the light anaesthesia state.

In zone 3, the line Z has the $F_{MDFA}(s)$ values from 60 to 100 when s values decrease from 35 to 25. We define the range of $F_{MDFA}(s)$ (60-100) as range 3 to monitor the moderate anaesthesia state.

In zone 4, the line Z has $F_{MDFA}(s)$ values from 100 to 150 when s values decrease from 25 to 12. We define the range of $F_{MDFA}(s)$ (100-150) as range 4 to monitor the deep anaesthesia state.

Finally in zone 5, the line Z has $F_{MDFA}(s)$ values from 150 to 200 when s values decrease from 12 to 0. We define the range of $F_{MDFA}(s)$ (150-200) as range 5

to monitor the very deep anaesthesia state in Figure 6.3. We chose *Z(s)* depending on two parameters: box size values and F_{MDFA} ranges.

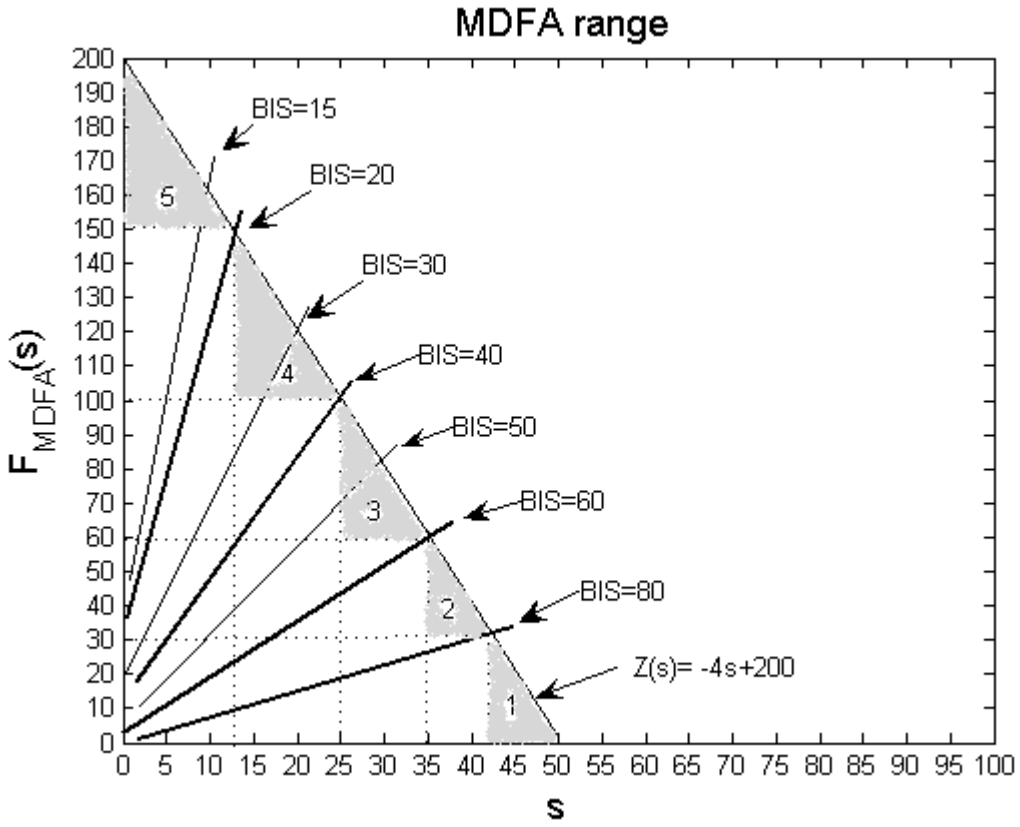

Figure 6.3: The Depth of Anaesthesia range. Based on five states of DoA (very deep anaesthesia, deep anaesthesia, moderate anaesthesia, light anaesthesia and awake), five zones of MDFA range was chosen in the five shading zones as follows:

- *Zone 1*: awake state;
- *Zone 2*: light anaesthesia state;
- *Zone 3*: moderate anaesthesia state;
- *Zone 4*: deep anaesthesia state;
- *Zone 5*: very deep anaesthesia state.

6.2.2 Box size values

As shown in Figure 5.6, the *Y(i)* in five states have different fluctuations. *Y(i)* in state *A* has the fluctuation higher than those in states *B, C, D* and *E*. Similarly, *Y(i)*

in state *B* has the highest fluctuation among those in states *C, D* and *E*; *Y(i)* in state *C* has the highest fluctuation among those in states *D* and *E*; and *Y(i)* in state *D* has the fluctuation higher than that in state *E*. We chose the small box size for *Y(i)* with the higher fluctuation, and vice versa.

We choose box sizes using the following rules: $s_A \leq s_B \leq s_C \leq s_D \leq s_E$, with s_A, s_B, s_C, s_D and s_E as box sizes for the states *A, B, C, D* and *E*. In Figure 6.2, we can see that *F(s)* has an almost linear relationship with states *A, B, C, D* and *E* in the ranges of: $3 \leq s_A \leq 20$, $3 \leq s_B \leq 25$, $3 \leq s_C \leq 35$, $3 \leq s_D \leq 45$ and $3 \leq s_E \leq 55$, respectively, and their slope increases from the state *E* to the state *A*. This characteristic is used for the purpose of setting up the ranges of F_{MDFA} and box size values.

6.2.3 Depth of Anaesthesia range

With a BIS Index value of less than 60, a patient has an extremely low probability of consciousness. BIS Index values lower than 40 signify a greater effect of the anaesthetic on the EEG. With low BIS values, the degree of EEG suppression is the primary determinant of the BIS value. Prospective clinical trials have demonstrated that maintaining BIS Index values in the range of 40-60 ensures adequate hypnotic effect during general anaesthesia while improving the recovery process. During this case, clinicians adjust the dose of medication to keep BIS values in the range of 40-60 (Kelley). Therefore, the DoA values in this range are very important.

In order to expand the ranges of anaesthesia states in MDFA II method, the ranges of F_{MDFA} are chosen as below: awake state (0-30), light anaesthesia (30-60), moderate anaesthesia (60-100), deep anaesthesia (100-150) and very deep anaesthesia (150-200). We finally obtain a relationship of range s and range of F_{MDFA} as *Z(s)* = -4s+200 as shown in Table 6.1 for the five zones.

In the case of expanded range, lost of consciousness (LOC) was clinically assessed by lack of response to verbal and tactile stimulus. Loss of the lash reflex was used in case of doubt. These clinical signals are used to estimate the new range. The expanded ranges will help clinicians having more anaesthesia information of the patient during surgery. These results are very significant for monitoring the DoA accurately as the clinical perspective needs more attention and information about the DoA in these states.

6.3 MONITOR THE DEPTH OF ANAESTHESIA USING LAGRANGE METHOD

Let $s_{\max T}$ and $s_{\min T}$ be the maximum and minimum box sizes in zone T ($T = 1,2,3,4,5$), $F_{\max T}$ and $F_{\min T}$ be the maximum and minimum of F_{MDFA}, and s_T be the value of the box size in the range of $s_{\min T} < s_T \le s_{\max T}$. We have F_{MDFA} value in the range of $F_{\min T} \le F_{MDFA} < F_{\max T}$.

We compute the smallest distance from data point $F(s)$ to the $Z(s) = -4s + 200$ line using Lagrange method. We take $F_{MDFA}(s)$ of EEG signals in state C (BIS=50) in Figure 6.4 as an example. In this case, we have $T = 3$. In the range of ($s_{\min 3}, s_{\max 3}$), we have ten corresponding values for $F_{MDFA}(s)$ in the range ($F_{\min T}, F_{\max T}$). We need to find out the best value of $F_{MDFA}(s)$ for DoA. That is, the value which has the shortest distance from line Z.

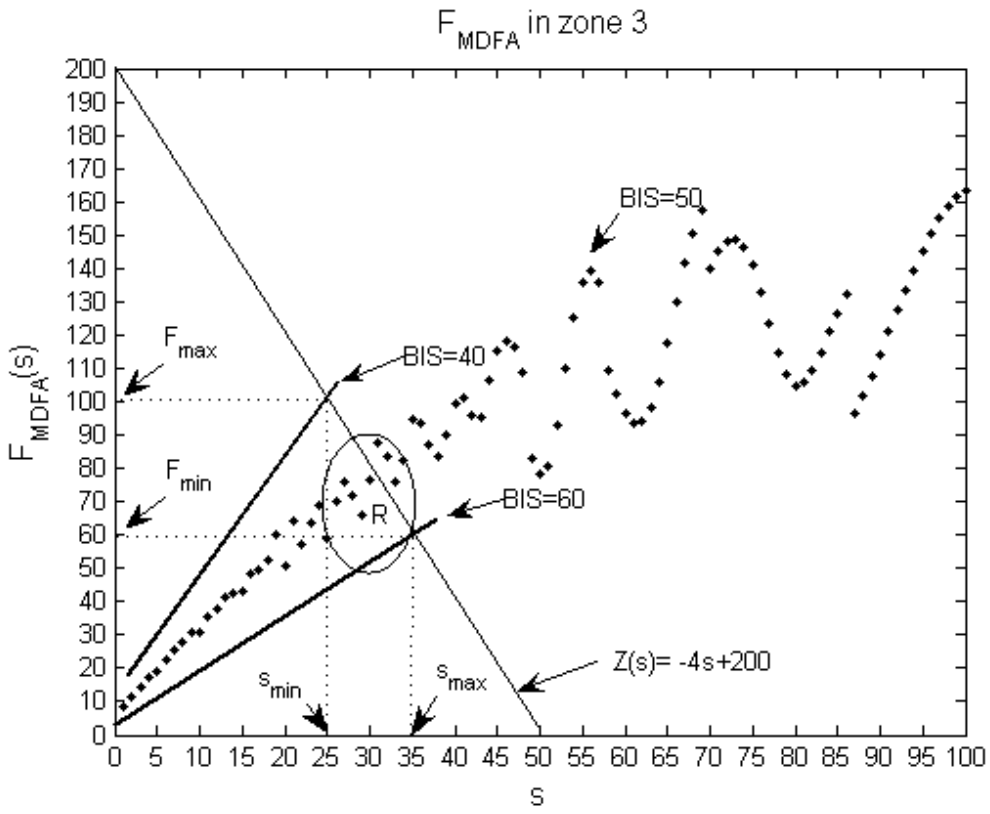

Figure 6.4: The $F_{MDFA}(s)$ of EEG signal (BIS=50) in zone 3. In the range of ($s_{\min 3}, s_{\max 3}$), we have ten corresponding values for $F_{MDFA}(s)$ in the range ($F_{\min T}, F_{\max T}$).

6.3.1 Lagrange method and application

In Figure 6.4, we choose one random point $R(s_K, F_K)$ in the ellipse and compute the distance d from point R to line Z. The minimum d value is:

$$\begin{aligned} &\textit{minimize} \quad d(s_K) \\ &\textit{Subject to} \quad s_{\min T} < s_K \le s_{\max T}, \quad K = 1,2,...,50 \\ &\qquad\qquad F_{\min T} \le F_K < F_{\max T}. \end{aligned} \tag{6.8}$$

Let $e(s_K) = \Delta F = |F_K - Z(s_K)|$ be the deviation of F_K and θ be the angle between d and ΔF. We can see that θ equals the angle between line Z and line $s = 0$ (Figure 6.5).

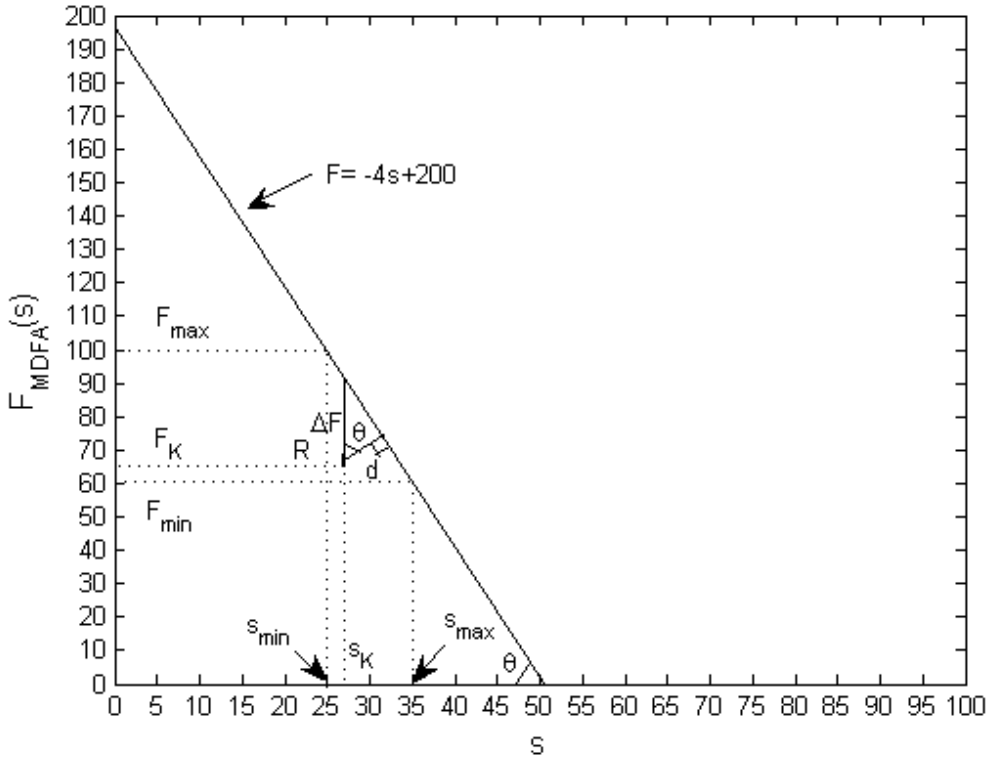

Figure 6.5: Choosing the optimum box size s. The distance d is computed by $d = \Delta F \cos\theta$, with $0 \le \theta \le 90$ and $\theta = const$. With $e(s_K) = \Delta F = |F_K - Z(s_K)|$ be the deviation of F_K and θ be the angle between d and ΔF.

The distance d is computed by $d = \Delta F \cos\theta$, with $0 \le \theta \le 90$ and $\theta = const$.

The optimization problem in (6.8) becomes:

$$\begin{aligned} &\textit{minimize} \quad e(s_K) \\ &\textit{Subject to} \quad s_{\min T} < s_K \le s_{\max T}, \\ &\qquad Z(s_K) \le F_{\max T}, \; K = 1,2,...,50. \end{aligned} \tag{6.9}$$

The Lagrange of the problem in (6.9) is defined as

$$L(s_K, \lambda) = e(s_K) + \sum_{K=1}^{50} \lambda_K [Z(s_K) - F_{\max T}], \tag{6.10}$$

where λ_K is the Lagrange multiplier associated with the Kth inequality constraint $Z(s_K) \le F_{\max T}$ (Boyd, 2004).

The optimization variable s_K is called the *primal variable*. $g(\lambda_K)$ is defined as the minimum value of the Lagrange over s_K:

$$g(\lambda_K) = \inf_{s_K} L(s_K, \lambda). \tag{6.11}$$

The result is given by the optimality Karush-Kuhn-Tucker conditions that require any primal-dual solution to satisfy the followings (Boyd, 2004):

$$\begin{aligned} &\frac{\partial L}{\partial s_K} = 0 \\ &\lambda_K [Z(s_K) - F_{\max T}] = 0, \quad \lambda_K \ge 0; \quad F_{\max T} \le Z(s_K) \end{aligned} \quad . \tag{6.12}$$

6.3.2 Monitor the depth of anaesthesia

The above procedure is implemented in four steps in the algorithm:

Algorithm 6.1: *Monitoring the DoA*

- *Define the state using modified DFA. Select zone T and range s in Table 6.1.*
- *Use modified DFA to classify the states, select zone T and range s_K.*
- *Use Lagrange method to F_K value with the box size s_K, adjust the box size s_K to the optimum value.*
- *Output F_K as the DoA.*

The diagram of the algorithm is shown in Figure 6.6. The states of input EEG signals are defined in section 6.1. After identifying the states (from very deep anaesthesia to awake), we select zone T and range s in Table 6.1. We use the Lagrange method to compute the box size s. With box size s, we apply the MDFA II algorithm to compute the F_K. The feedback error between the F_K and $Z(s)$ is used to adjust the box size s to the optimum value. With the optimum value s, we have the DoA value equal to the F_K value. Table 6.2 shows the best values for states A, B, C, D and E based on our results.

In zone $T=1$, we compute the minimum of $e(s_K)$ in the range of $s=(42-50)$ of state E. The DoA in state E is $F_K=21.514$, corresponding with $s_K=44$. Similarly, in zones $T=2,3,4,5$, we compute the minimum of $e(s_K)$ in the ranges of $s=(35-41)$ of state D, $s=(25-34)$ of state C, $s=(13-24)$ of state B and $s=(1-12)$ of state A. We have the DoA in state D ($F_K=33.356$), corresponding with $s_K=42$; state C ($F_K=76.747$), corresponding with $s_K=32$; state B ($F_K=111.598$), corresponding with $s_K=22$; and state A ($F_K=147.848$), corresponding with $s_K=11$.

Figure 6.7 shows the values of BIS and F_K. In this Figure, we can see that the range of F_K is extended in the states of moderate anaesthesia, deep anaesthesia and very deep anaesthesia.

Prospective clinical trials have demonstrated that maintaining BIS Index values in the range of 40-60 ensures adequate hypnotic effect during general anaesthesia while improving the recovery process. Comparing the range in our method and BIS Index, we can see that the ranges in our method (MDFA) are expanded in the states of moderate anaesthesia ($60<F_{MDFA}<100$, $40<BIS<60$), deep

anaesthesia ($100<F_{MDFA}<150$, $20<\text{BIS}<40$) and very deep anaesthesia ($150<F_{MDFA}<200$, $0<\text{BIS}<20$) in Table 6.1. The expanded ranges will help clinicians having more detailed DoA values during surgery.

Table 6.1: Define the state using modified DFA by selecting zone T and range s.

	Awake	Light anaesthesia	Moderate anaesthesia	Deep anaesthesia	Very deep anaesthesia
Zone T	1	2	3	4	5
Range s	50-42	42-35	35-25	25-12	12-0
Range $Z(s)$	0-30	30-60	60-100	100-150	150-200
BIS values	80-100	80-60	60-40	40-20	20-10

Table 6.2: The best values s_K, F_K of states A, B, C, D and E based on simulation results.

	State E	State D	State C	State B	State A
s_K	44	42	32	22	11
$Z(s_K)$	24	32	72	112	156
F_K	21.514	33.356	76.747	111.598	147.848

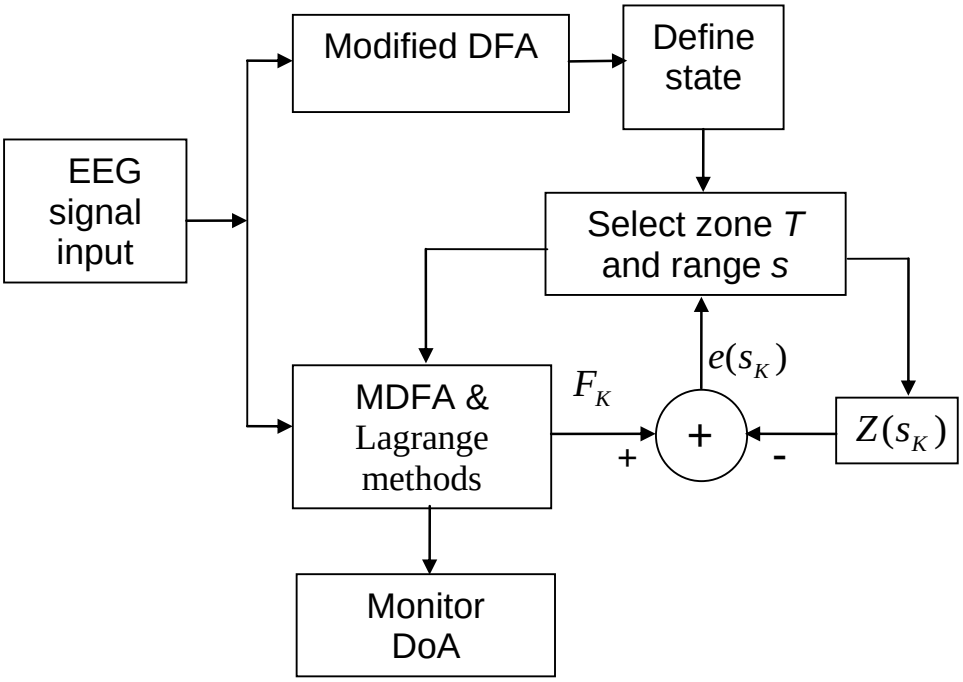

Figure 6.6: Diagram for monitoring the DoA. The states of input EEG signals are defined by the modified DFA in section 5.1. After identifying the states (from very deep anaesthesia to awake), we select zone T and range s in Table 6.1. We use the MDFA algorithm to compute the box size value s. With value s, we use the Lagrange method to compute the F_K. The error feedback between the F_K and $Z(s)$ is used to adjust the box size s to the optimum value. With the optimum value s, we have the DoA value to equal the F_K value.

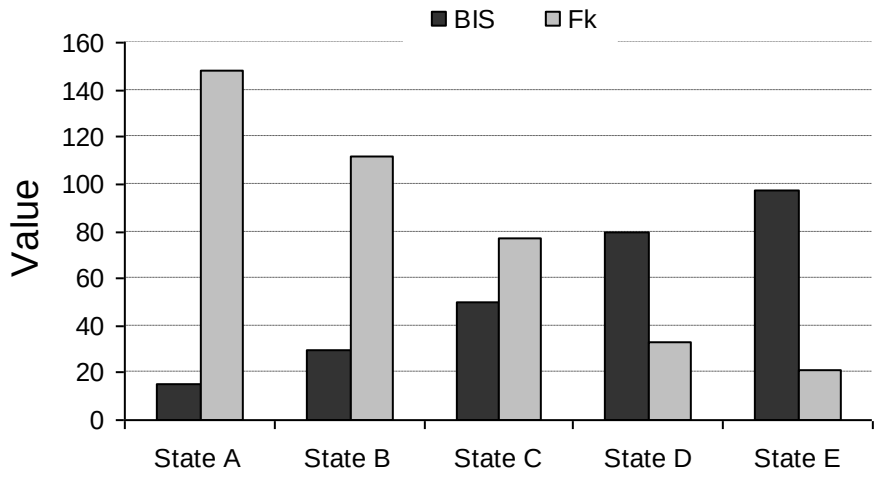

Figure 6.7: Comparison between BIS and F_k. Opposite with BIS range, F_k value decreases from very deep anaesthesia state to awake state. The range of F_K is extended in the states of moderate anaesthesia ($60<F_{MDFA}<100$, $40<BIS<60$), deep anaesthesia ($100<F_{MDFA}<150$, $20<BIS<40$) and very deep anaesthesia ($150<F_{MDFA}<200$, $0<BIS<20$) (see Table 6.1).

Chapter 7

An Improved De-trended Moving Average Method for Monitoring the DoA

The de-trended moving average (DMA) method is a new approach to quantify correlation properties in non-stationary signals with underlying trends. This method provides a power law relation between the fluctuation function $F_{MDMA}(s)$ and the scale s: $F_{MDMA}(s) \; \alpha \; s^{\alpha}$, where α is the slope of $F_{MDMA}(s)$ in the logarithm scale. We modify and apply DMA method to monitor the depth of anaesthesia through computing the scaling exponent F_{α} and F_{min} values. These new indices (F_{α}, F_{min}) are responsive to anaesthetic agent and can estimate a patient's hypnotic state in case of poor signal quality. This new method also reduces the time delay during which the patient's hypnotic state changes from consciousness state to unconsciousness state, and vice versa. Three special cases were analysed in comparison with BIS. The results of our methods are better correlation with the patient's hypnotic state in clinical observation.

7.1 DE-TRENDED MOVING AVERAGE METHOD

The DFA and DMA algorithms are widely used techniques to quantify the long-term correlations of non-stationary time series and the long-range correlations of fractal surfaces. The striking difference between the DMA and DFA methods is that the DMA algorithm does not need a division of the series in boxes. The scaling property is obtained by using a simple continuous function: the moving average (Carbone, 2009; Arianos, 2007; Chen 2006; 2002).

The first step of the DMA method is to detect trends in data by employing a moving average. The moving average assigns equal weight to each data point in a window of size *s*. The time series x_i of EEG sample has the length *L*. For a window of size *s*, the simple backward moving average is defined as:

$$\hat{Y}_s(i) = \frac{1}{s}\sum_{k=0}^{s-1} Y(i-k), \tag{7.1}$$

where *Y(i)* is the integrated signal defined in:

$$Y(i) = \sum_{k=1}^{i}[x_k - \langle x \rangle], \qquad i = 1,...,L, \tag{7.2}$$

with EEG sample length *L*, and the average of the time series <x> is:

$$\langle x \rangle = \frac{1}{L}\sum_{k=1}^{L} x_k \ . \tag{7.3}$$

Here, the average of the signal data points within the window refers to the last data point covered by the window. Thus, the average value at each data point *i* depends only on the past *n-1* values of the signal.

In the second step**,** we de-trended the signal by subtracting the trend $\hat{Y}_s$ from the integrated profile *Y(i)*:

$$C_s(i) = Y(i) - \hat{Y}_s(i). \tag{7.4}$$

For the backward moving average, we then calculated the fluctuation for a window of size *s* as

$$F^2(s) = \frac{1}{(L-s)} \sum_{i=3}^{L} [C_s(i)]^2 , \tag{7.5}$$

$$F_{DMA}(s) = \left[\frac{1}{L} \sum_{s=3}^{L} F^2(s) \right]^{\frac{1}{2}} . \tag{7.6}$$

Repeating the calculation for different *s*, we obtained the fluctuation function $F_{DMA}(s)$. A power law relation between the fluctuation function $F_{DMA}(s)$ and the scale *s* indicates a self-similar behaviour. Equation (7.4) defines a generalized variance of the random part $Y(i)$ with respect to the moving average $\hat{Y}_s(i)$. The moving average $\hat{Y}_s(i)$ was calculated for different values of the window *s*, with *s* ranging from 3 to a maximum value s_{max} depending on the size of the series. $F_{DMA}(s)$, defined by (7.6), was calculated for all the windows of size *s* over the interval [*s*, *L*]. For each $\hat{Y}_s(i)$, the value of $F_{DMA}(s)$ corresponding to each $\hat{Y}_s(i)$ was plotted as a function of logarithmic axes.

7.2 MONITORING THE DoA USING DMA METHOD

The most remarkable property of the log-log plot is to demonstrate a power-law dependence on *s*: $F_{DMA}(s) \propto s^{\alpha}$, where α is the slope of the line observed in the log-log representation of F_{DMA} in the function of *s*. The fluctuations in a signal can be characterized by the scaling exponent α. If $\alpha = 0.5$, there is no correlation and the signals are uncorrelated (white noise). If $\alpha < 0.5$, the signal is anti-correlated. If $\alpha > 0.5$, the signal is correlated (Ferree, 2003; Bardet, 2008). The exponent α provides a measure of the dynamics across a range of *s*.

The linear regions in plots of $ln(F_{DMA})$ versus $ln(s)$ indicate power-law behavior, with the slope of the line given by the exponent α. Figure 7.1(a) shows the fluctuations versus box sizes in the logarithmic scale of $ln(F_{DMA})$ and $ln(s)$ of patient 3 when the patient's BIS value reduced from 97 to 22 in range 0-250 seconds of the recorded time. There are two scaling regions with a discernible bend when the slopes in the two regions were distinctly different. This feature was found from all patients.

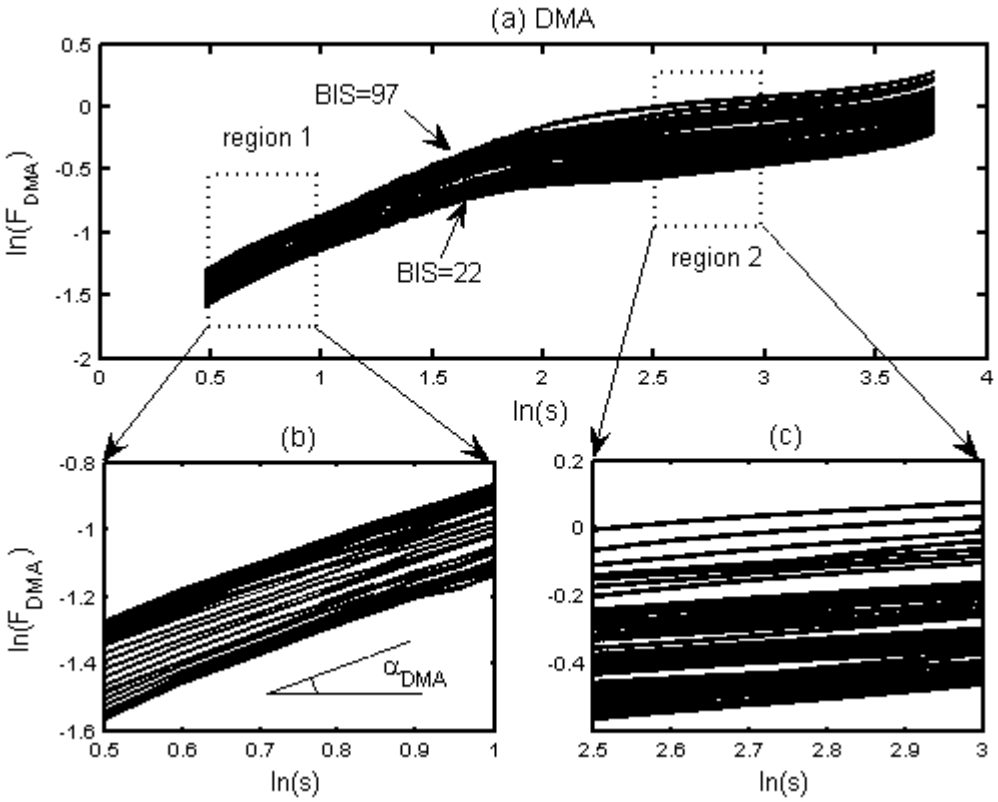

Figure 7.1: The DMA trends of patient 3.

(a) The curves $ln(F_{DMA})$ moved up when the BIS values increased from 22 to 97.

(b) Scaling exponent α_{DMA} of $\ln(F_{DMA})$ *i*In region 1 with $ln(s)$ from 0.5 to 1.

(c) The curves $ln(F_{DMA})$ in region 2 at large scales of $ln(s)$ from 2.5 to 3.

In Figure 7.1(a), when the patient's BIS value reduced from 97 to 22, the curves $ln(F_{DMA})$ moved down. In region 1 of low $ln(s)$ from 0.5 to 1, $ln(F_{DMA})$ exhibited an approximate power-law behavior characterized by a scaling exponent α_{DMA}, as shown in Figure 7.1(b). At large scales of $ln(s)$ in region 2 from 2.5 to 3, $ln(F_{DMA})$ was approximately flat in Figure 7.1(c). In (Jospin, 2007), different scaling exponent indexes were considered for monitoring the DoA using DFA method.

To quantify the scaling behaviour, we computed scaling exponent α_{DMA} in region 1 with $1 \geq ln(s) \geq 0.5$ and $ln(F_{DMA})$ value in region 2 with $3 \geq ln(s) \geq 2.5$. This choice was consistent with the two slopes found in (Ferree, 2002; 2003) to analyze the EEG using DFA method.

A sliding window with a fixed length (m) was used for reading and processing the EEG data. By using this window, F_{α}^{DMA} and $F_{\min}^{DMA}$ were computed from the mean value of the previous and present values. Let B_l be a window of length m, with $l = 1, 2, \ldots, N\text{-}m\text{-}1$. The window B_l slides along the raw EEG signals. In this window, F_{α}^{DMA} and $F_{\min}^{DMA}$ were computed and updated every second in regions 1 and 2. The window length was also an important parameter affecting the correctness of the values of F_{α}^{DMA} and $F_{\min}^{DMA}$. If a small window was chosen, the F_{α}^{DMA} and $F_{\min}^{DMA}$ values were more sensitive and were subject to fluctuation. If a large window was chosen, the updated results were affected more by previous data and may not be in real time. In accordance with experimental results, the length of a sliding window was 30 seconds. F_{α}^{DMA} and $F_{\min}^{DMA}$ are set:

$$F_{\alpha}^{DMA}(s) = K_{DMA1}\alpha_{DMA}(s) \tag{7.7}$$

which is the correlation exponent of $ln(F_{DMA})$ in zone 1, and:

$$F_{\min}^{DMA} = K_{DMA2}\min(\ln F_{DMA}) \tag{7.8}$$

as the minimum of $ln(F_{DMA})$ in zone 2, with $K_{DMA1}=7700$ and $K_{DMA2}=150$ being the gain parameters. These constant values were merely estimates for a unit of measure, to fix F_{α}, F_{min} values in the range of 0-100.

In order to estimate our results on anaesthesia states of the patients, F_{α}^{DMA} and $F_{\min}^{DMA}$ trends were compared with BIS trends, covering the whole scale from 100 to 0 with a full recording time. Figure 7.2 shows the comparison of F_{α}^{DMA}, $F_{\min}^{DMA}$ trends and BIS trend of patient 3 in the 2500 second recording time.

Patient 3 was a 55 year old, 87 kg, male. Surgery was undertaken from 10:10:58 PM to 10:55:30 PM. Drug administration consisted of midazolam (4 mg) as a sedative drug at 10:10:58 PM. At 10:11:20 PM, alfentanil (1000 μg) was used as strong pain relief given only once during the operation. Propofol (160 mg) at 10:12:29 PM was the main drug used to induce sleep.

The patient fell asleep within 30 seconds of injection, eyes closed, and the effect wore off in about 3 minutes. At 10:12:46 PM, desflurane and nitrous oxide (N_2O) were started. Desflurane is a gaseous anaesthesic agent, breathed continuously during anaesthesia to keep a patient asleep. N_2O is a gaseous anaesthesic agent, breathed continuously for short-acting pain relief. Parecoxib (40 mg) was used at 10:19:24 PM for moderate pain relief.

In Figures 7.2(a) and 7.2(b), when the patient's state have changed from consciousness to unconsciousness, F_{α}^{DMA} and $F_{\min}^{DMA}$ values reduced from 60 to 22, corresponding to BIS values reducing from 97 to 20. During the deep anaesthesia time, F_{α}^{DMA} and $F_{\min}^{DMA}$ have values between 20 and 40. F_{α}^{DMA} and $F_{\min}^{DMA}$ trends are close to BIS trend in this time range.

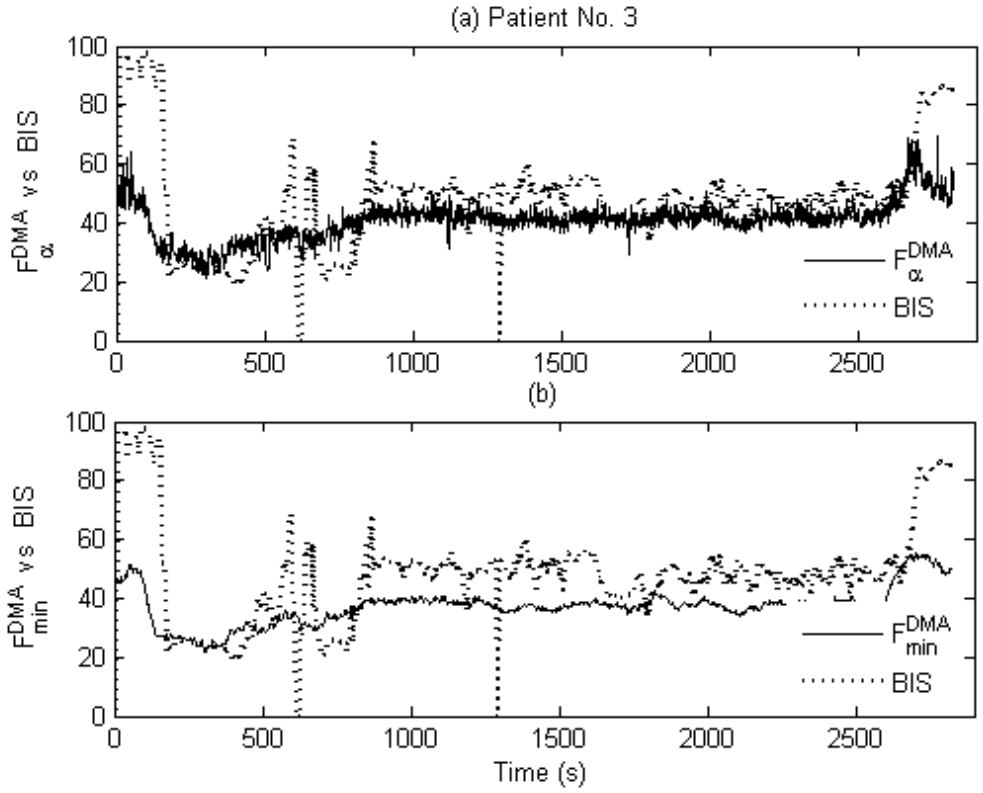

Figure 7.2: F_{α}^{DMA} and $F_{\min}^{DMA}$ trends were compared with BIS trends of patient 3. When the patient's state have changed from consciousness to unconsciousness, F_{α}^{DMA} and $F_{\min}^{DMA}$ values reduced from 60 to 22, corresponding to BIS values reducing from 97 to 20. During the deep anaesthesia time, F_{α}^{DMA} and $F_{\min}^{DMA}$ have values between 20 and 40. F_{α}^{DMA} and $F_{\min}^{DMA}$ trends are close to BIS trend in this time range. However, the ranges are small between maximum and minimum of F_{α}^{DMA} and $F_{\min}^{DMA}$.

With this result, the DMA method can be used to estimate the depth of anaesthesia. However, the ranges are small between maximum and minimum of F_{α}^{DMA} and $F_{\min}^{DMA}$. The curves $ln(F_{DMA})$ were very close, as shown in Figures 7.1(b) and 7.1(c). Therefore, in Figure 7.2, it was difficult to distinguish the awake and deep

anaesthesia states by F_{α}^{DMA} and $F_{\min}^{DMA}$ values. To solve this problem, the modified de-trended moving average (MDMA) is proposed to identify and separate the states.

7.3 MODIFIED DETRENDED MOVING AVERAGE METHOD AND THE DEPTH OF ANAESTHESIA MONITORING

The curves $ln(F_{DMA})$ of the patient's states were close to each other in Figure 7.1. In the modified DMA method, we changed (7.5) as:

$$F_M^2(s) = \frac{1}{(L_s - s)} \sum_{i=3}^{L_s} C_s(i)^2 [(\nu - 1)s + i], \tag{7.9}$$

where $L_s = [L/s]$, $\nu = 1, \ldots, 2L_s$ and $C_s(i)$ is as in (7.4).

Finally, we averaged all the ν^{th} segments and took the square root to obtain the fluctuation function. For reliable and accurate estimation of the depth of anaesthesia, we needed to separate the curves $ln(F_{DMA})$ in Figure 7.1 by modifying (7.6) as follows:

$$F_{MDMA}(s) = \left[\frac{E_m}{L} \sum_{s=3}^{L} F_M^2(s) \right]^{\frac{1}{2}}, \tag{7.10}$$

where E_m is the wavelet entropy which is computed in (4.20) (Chapter 4, page 50).

In (7.10), E_m is considered as the gain parameter. The relation between E_m and the patient's state is presented in Figure 7.3 when comparing $log_{10}E_m$ with BIS trends. In this Figure, when the patient's state changed from awake state (BIS=97) to deep anaesthesia (BIS =25), the $log_{10}E_m$ values decreased from 6.9 to 6.2. During general anaesthesia, BIS values were in the range of 45 to 55, and $log_{10}E_m$ values were in the range of 6.4 to 6.55.

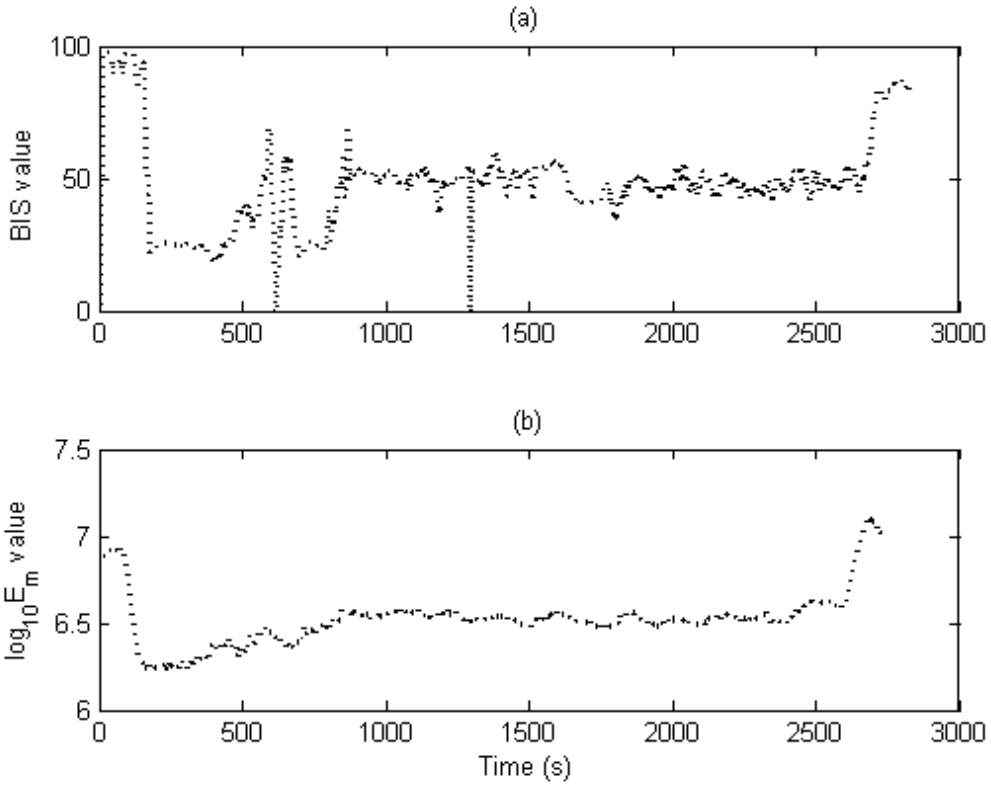

Figure 7.3: The relation between E_m and the patient's state is presented when comparing $log_{10}E_m$ (Figure 7.3(b)) with BIS trends (Figure 7.3(a)). In these Figures, when the patient's state changed from awake state (BIS=97) to deep anaesthesia (BIS =25), the $log_{10}E_m$ values decreased from 6.9 to 6.2. During general anaesthesia, BIS values were in the range of 45 to 55, and $log_{10}E_m$ values were in the range of 6.4 to 6.55.

Using (7.9) and (7.10), $ln(F_{MDMA})$ is plotted versus $ln(s)$ of patient 3 in Figure 7.4. The curve $ln(F_{MDMA})$ moved down when E_m decreased and vice versa. With this result, the curves $F_{MDMA}(s)$ can be separated in different states as shown in Figure 7.4. The curves $ln(F_{MDMA})$ in Figures 7.4(b) and 7.4(c) were separated into three groups. Group 1 represented the awake state with BIS values ranging from 80 to 97. Group 2 represented the light anaesthesia state with BIS values ranging from 60 to

80. This state occurred during the short time when the BIS trend fell. Therefore in this group, only a few curves of $ln(F_{MDMA})$ are seen. Group 3 showed deep anaesthesia states with BIS values ranging from 20 to 40, and moderate anaesthesia state in the range of 40 to 60.

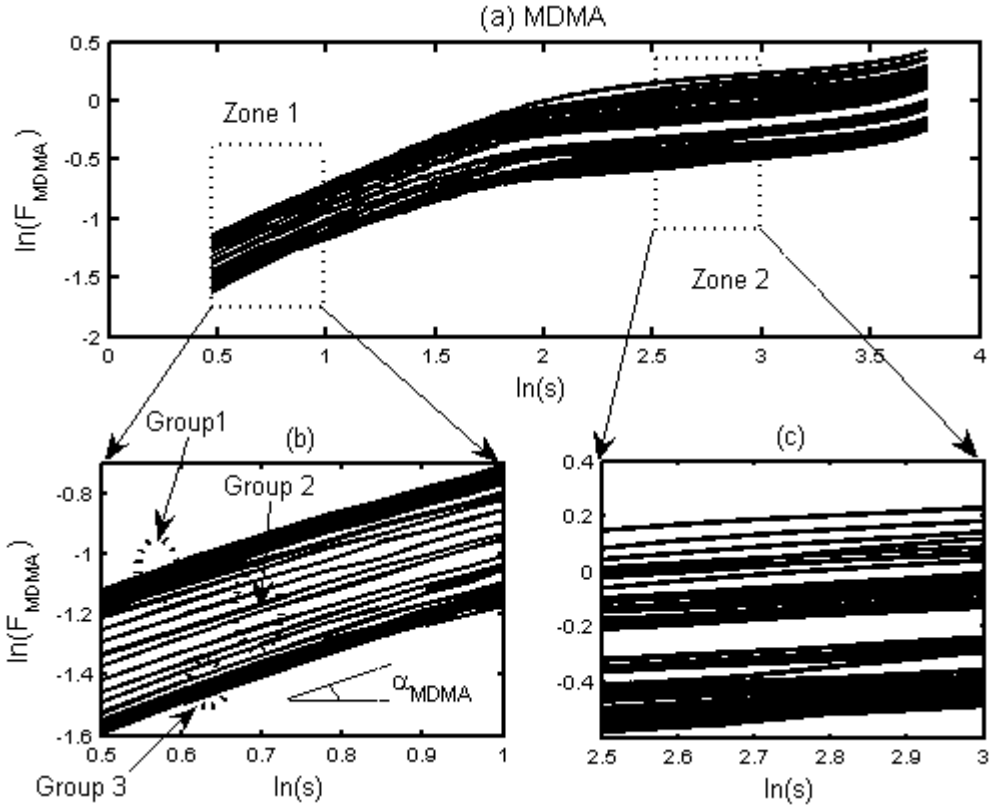

Figure 7.4: (a) The curves $ln(F_{MDMA})$ in MDMA method.

(b) The curves $ln(F_{MDMA})$ are separated in zone 1.

(c) The curves $ln(F_{MDMA})$ are separated in zone 2.

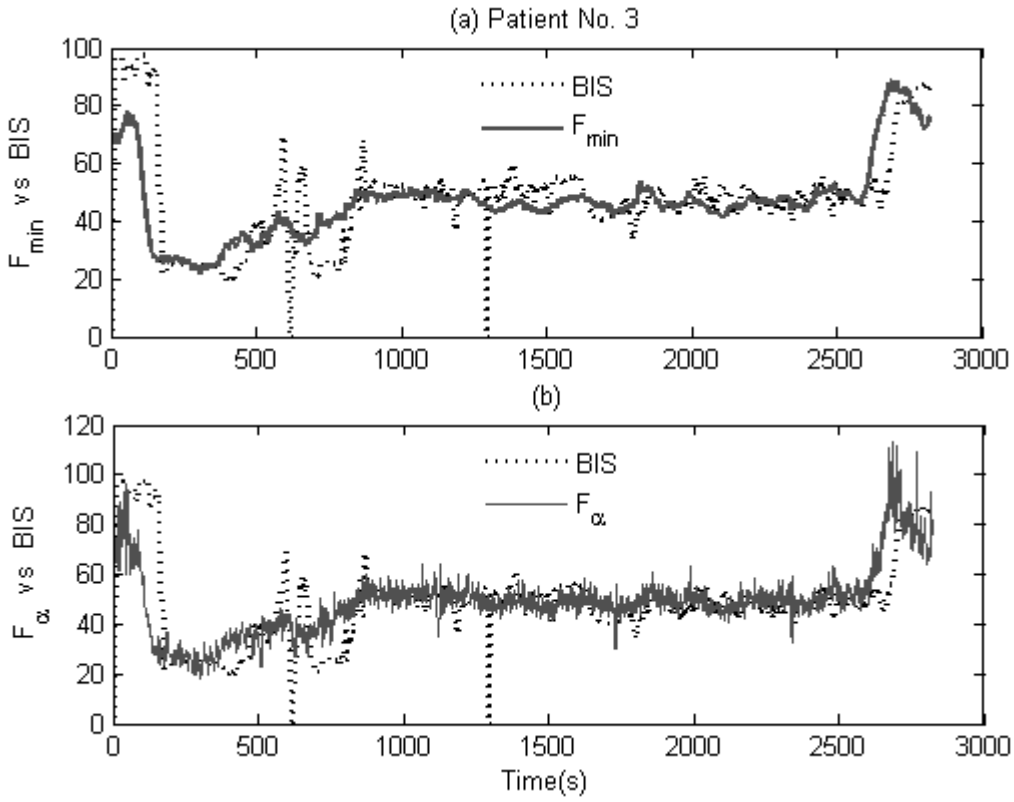

Figure 7.5: F_α and F_{min} trends are compared with BIS trend. F_α (Figure 7.5 a) and F_{min} (Figure 7.5b) ranges are expanded. Comparing DMA and MDMA methods, F_α and F_{min} trends in the MDMA method are closer to the BIS trends than F_α^{DMA} and $F_{\min}^{DMA}$ in the DMA method (see Figure 7.2).

Two new indices for monitoring DoA are proposed as:

$$F_\alpha(s) = K_\alpha^{Modify}\alpha(s), \tag{7.11}$$

$$F_{\min}(s) = K_{\min}^{Modify}\min(\ln F_{MDMA}) \tag{7.12}$$

with $K_\alpha^{Modify} = 250$ and $K_{\min}^{Modify} = 5$ as the gain parameters.

These constant values are merely estimates of a unit of measure, to fix the F_α and F_{min} values in the range of 0-100. F_α and F_{min} trends are compared with BIS trend in Figure 7.5. Figures 7.5(a) and 7.5(b) present the corresponding relation between F_α, F_{min} and BIS trends. In this result, F_α and F_{min} ranges are expanded.

Comparing DMA and MDMA methods, F_α and F_{min} trends in the MDMA method are closer to the BIS trends than F_α^{DMA} and $F_{\min}^{DMA}$ in the DMA method.

7.4 DETECTION OF BURST SUPPRESSION IN THE EEG SIGNAL

During deep anaesthesia, the EEG voltage may change from high activity to low or even isoelectricity. This pattern is known as burst suppression. The burst suppression ratio (BSR) is a time domain EEG parameter developed to quantify this phenomenon (flat EEG or no significant electrical activity in the brain). The burst suppression is recognized as those periods longer than 0.50 s, during which the EEG voltage does not exceed approximately +/- 5.0 μV (Rampil, 1998).

Figure 7.6 presents EEG signal during the burst suppression of patient 2. The F_{Min}, F_α and BIS trends are shown in Figure 7.6(a). In one case of our study, the burst suppression lasted 1.5 seconds. From 715.5 to 717 seconds, BIS have low values from 5.7 to 7.7. The EEG signal is shown in Figure 7.6(b) with a full recording time and during the burst suppression in Figure 7.6(c). During the burst suppression time, the EEG signal has an amplitude value lower than +/- 5.0 μV. Our method can show DoA values during burst suppression by F_α and F_{min} values in Figure 7.6(a), with the ranges of F_{min} value from 16.3 to 19.7, and F_α value from 12 to 25. As this is a single example of burst suppression, future research is needed to further assess the behaviour of our new index over varying degrees of burst suppression.

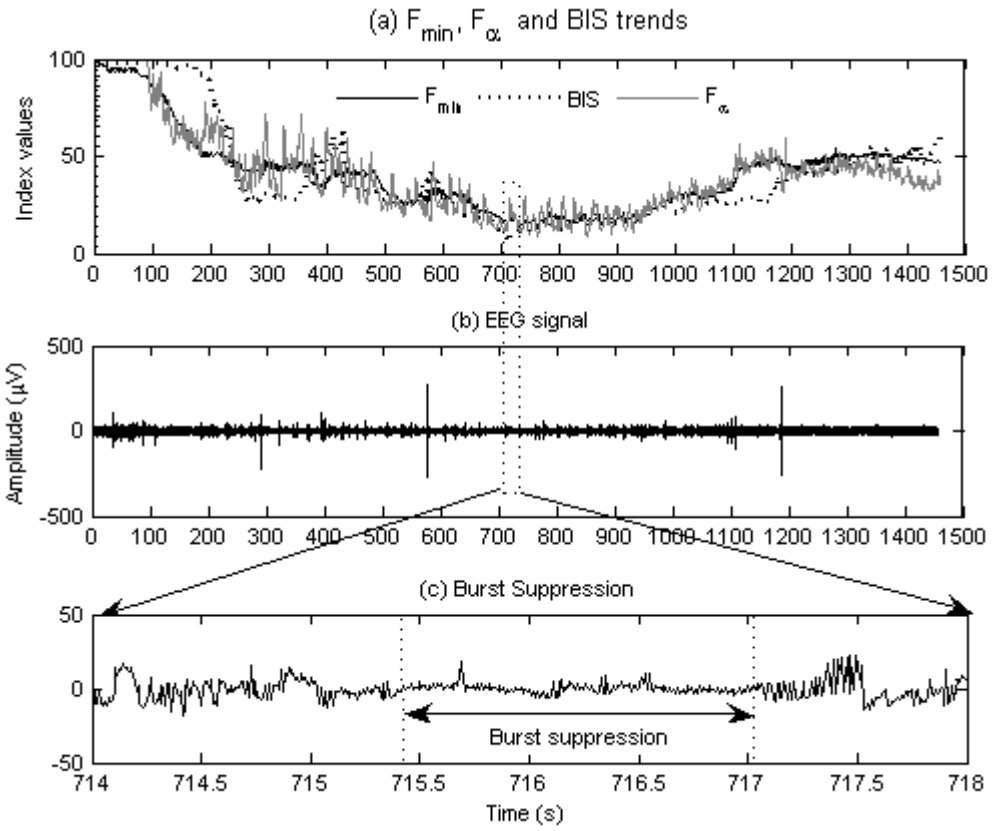

Figure 7.6: The burst suppression happens from 715.5 second to 717 second. F_{Min} and F_{α} can show the DoA values during this time.

7.5 TIME DELAY FROM CONSCIOUSNESS TO UNCONSCIOUSNESS

Let t_{delay} be the time delay between F_{min} trend and BIS trend at BIS=80. We observed a delay time between F_{min} and BIS trends in Figure 7.7 and Table 7.1. The minimum of time delay is 12 seconds (patient 8) and the maximum is 178 seconds (patient 16) at BIS=80. The patients had loss of consciousness when BIS is less than 80.

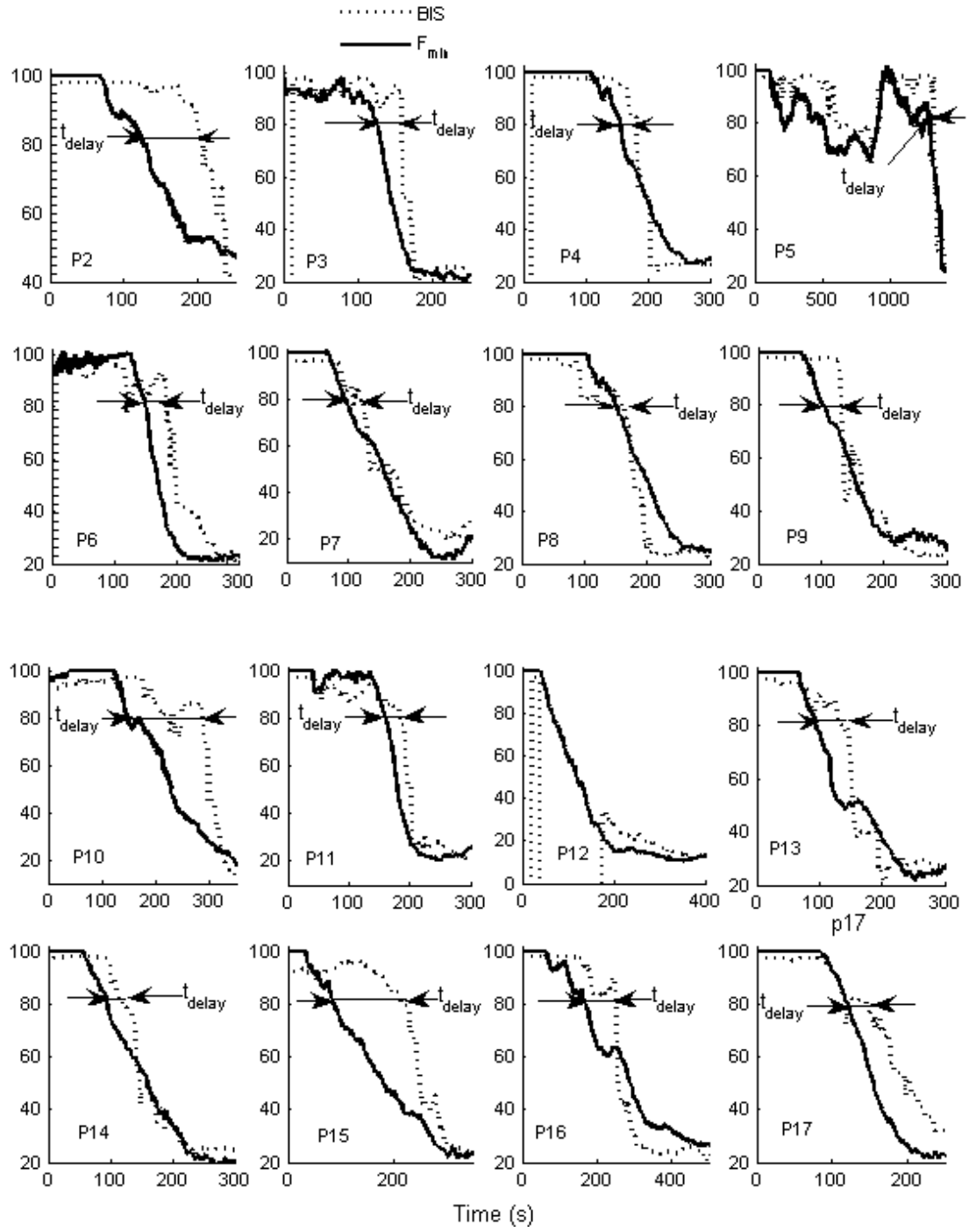

Figure 7.7: Time delay between BIS and F_{min} trends. P2,…, P17 are labelled as patients 2 to 17. The minimum of time delay is 12 seconds (patient 8) and the maximum is 178 seconds (patient 16) at BIS=80.

Table 7.1: Time delay between F_{min} and BIS trends at BIS=80.

Patient	1	2	3	4	5	6	7	8
t_{delay} (s)	36	81	31	36	37	34	32	12
Patient	9	10	11	13	14	15	16	17
t_{delay} (s)	28	127	22	42	24	133	178	27

7.6 TESTING THE DE-NOISING RESULT USING MDMA

In chapter 4, we presented the relation between raw EEG signal and noise in the equation (4.1) as: $y_i=x_i+ e_i$. To estimate the efficiency of our de-noising method, we propose F_{min} in (7.12) to analyze y_i and e_i by MDMA method. $F_{min}(y_i)$ and $F_{min}(e_i)$ are the values in MDMA method of y_i and e_i respectively. If e_i has a clinical meaning, $F_{min}(e_i)$ will present it. $F_{min}(y_i)$ and $F_{min}(e_i)$ are shown in Figure 7.8(a) and Figure 7.8(b), respectively.

The difference between $F_{min}(y_i)$ and $F_{min}(e_i)$ is presented by $\delta = F_{\min}(y_i) - F_{\min}(e_i)$. In Figures 7.8(a) and 7.8(b), $F_{min}(y_i)$ and $F_{min}(e_i)$ clearly show the change of patient's state from awake state to deep anaesthesia, and from general anaesthesia to awake. However, the trends of $F_{min}(y_i)$ and $F_{min}(e_i)$ are almost flat during general anaesthesia time. Moreover, δ has a small value. This means that $F_{min}(y_i)$ and $F_{min}(e_i)$ do not present a clinical meaning better than F_{min} and F_{α}. The results of F_{min} test are presented in Table 7.2.

From Table 7.2, we found that:

- MDMA method can be used to distinguish the change of patient's state from raw EEG signal directly when the patient's state changes from awake state to deep anaesthesia state.
- Our de-noising algorithm did not remove much of the true EEG signal.

Table 7.2: The results of F_{min} test for EEG signal.

$y_i = x_i + e_i$	**Distinguish the patient's state**
$y_i \rightarrow F_{\min}(y_i)$	Two states: awake, deep anaesthesia
$e_i \rightarrow F_{\min}(e_i)$	Two states: awake, deep anaesthesia
$x_i \rightarrow F_{\min}(x_i)$	From awake to deep anaesthesia

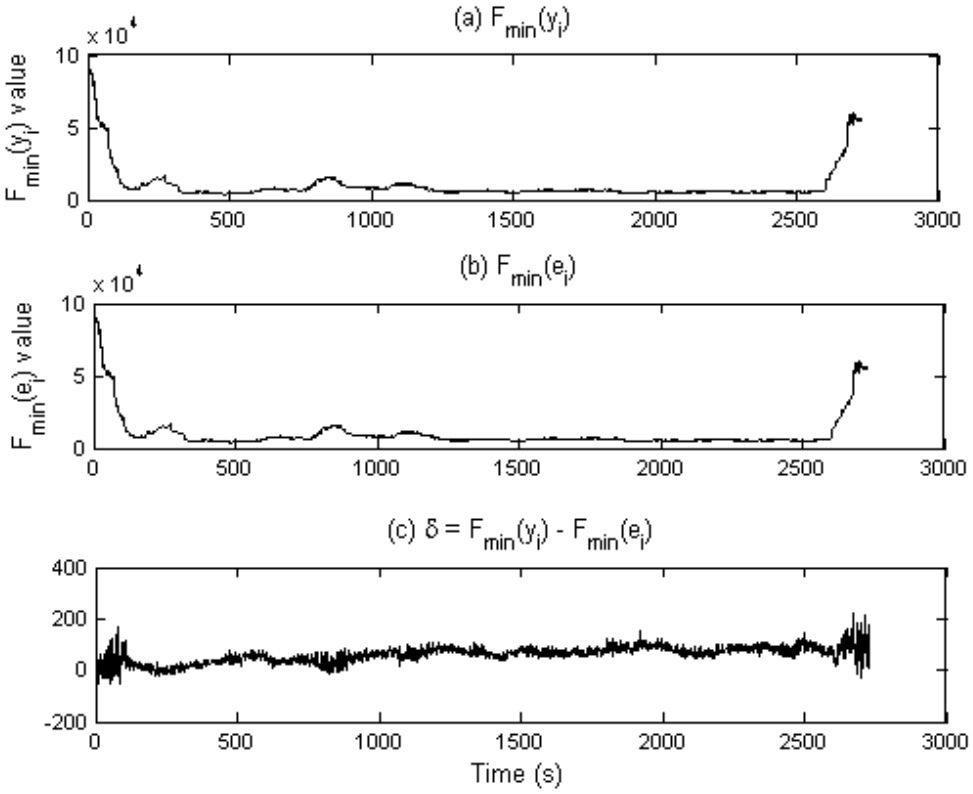

Figure 7.8: The comparison of $F_{min}(y_i)$ and $F_{min}(e_i)$.

7.7 STATISTIC TEST

Linear regression method was used to find the best-fit values of the slopes and intercepts of F_α, F_{min} and BIS. Figures 7.9(a) and 7.10(a) represent the correlation density plot of F_{min} versus BIS and F_α versus BIS, respectively. These plots have 42,972 data points of 17 patients. The best-fit line is solid, and the 95% confidence boundaries are shown by the two dashed lines surrounding the best-fit line. The 95% confidence interval of the slope is 9.496. There is a range of values corresponding to the 95% confidence interval of the intercept. The r-squared values $r^2(F_{min}) = 0.9183$ and $r^2(F_\alpha) = 0.8855$ show a strong correlation between F_{min}, F_α and BIS. Statistical significance was assumed at probability levels of $p<0.0005$.

Figures 7.9(b) and 7.10(b) show the sample residual plots. A residual is the distance of a point from the best-fit line. A residual is positive when the point is above the best-fit line. A residual is negative when the point is below the best-fit line. In Figures 7.9(b) and 7.10(b), the data points are scattered above and below the X-axis in the range of [-10, 10], indicating a very good agreement between F_{min}, F_α and BIS (Chernik, 2003).

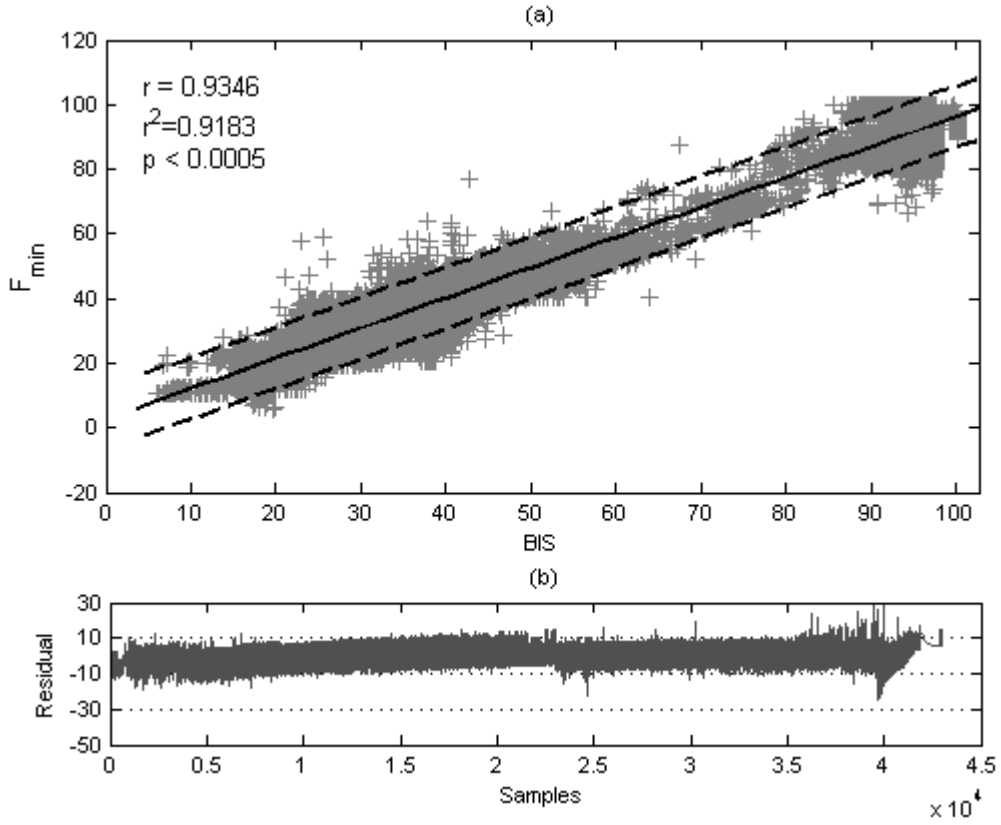

Figure 7.9: (a) Correlation between F_{min} and BIS calculated from 17 patients with 42,972 data points. The best-fit line is solid, and the 95% confidence boundaries are shown by the two dashed lines surrounding the best-fit line. The 95% confidence interval of the slope is 9.496. There is a range of values corresponding to the 95% confidence interval of the intercept. The r-squared value $r^2(F_{min})$ = 0.9183 shows a strong correlation between F_{min}, F_α and BIS. Statistical significance was assumed at probability levels of $p<0.0005$.

(b) A sample residual plot. The data points are scattered above and below the X-axis in the range of [-10, 10], indicating a very good agreement between F_{min} and BIS.

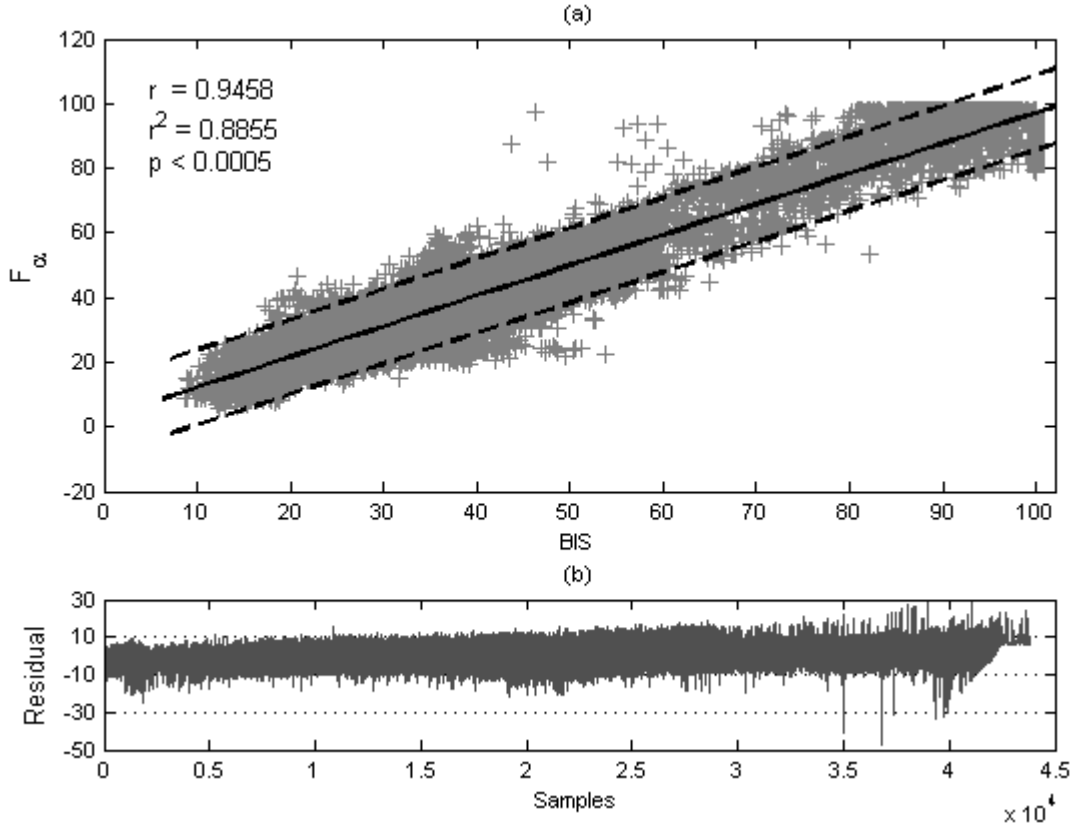

Figure 7.10:

(a) Correlation between F_α and BIS calculated from 17 patients with 42,972 data points. The best-fit line is solid, and the 95% confidence boundaries are shown by the two dashed lines surrounding the best-fit line. The 95% confidence interval of the slope is 9.496. There is a range of values corresponding to the 95% confidence interval of the intercept. The r-squared value $r^2(F_\alpha)$ = 0.8855 shows a strong correlation between F_α and BIS. Statistical significance was assumed at probability levels of $p<0.0005$.

(b) A sample residual plot. The data points are scattered above and below the X-axis in the range of [-10, 10], indicating a very good agreement between F_α and BIS.

7.8 CASE STUDIES

Three special cases were reported based on our study of recorded EEG data from 25 adult patients. These cases demonstrate some of the limitations of the current BIS index and the advantages of our proposed methods.

- *The first case* demonstrates artefactually high BIS values. Indices greater than 70 were recorded whilst the patient was clinically unconscious.
- *The second case* is of recorded negative BIS values. Whilst these outputs are a monitor function advising inadequate signal, they provide no information as to the underlying EEG and are unhelpful in diagnosing anaesthesia depth.
- *The third case* demonstrates the problem of time delay. Recorded BIS values changed into the appropriate sense long after the observed change in state of consciousness.

7.8.1 The first case

7.8.1.1 BIS trend

Patient 19 was a 74 years old, 100 kg male. BIS values were recorded between 09:21:36 am and 10:33:44 am. Anaesthesia induction was with intravenous midazolam 3mg at 09:22:00, alfentanil 1000μg at 09:22:03 and propofol 120mg at 09:25:53. At 09:25:55, inhaled sevoflurane and nitrous oxide were introduced. Sevoflurane is a volatile maintenance anaesthesic agent and nitrous oxide is a short-lived gaseous analgesic agent.

The attending anaesthetist noted BIS values higher than 70 between 09:40:17 and 09:53:19. During this period, the patient was not paralyzed and did not move. The systemic blood pressure and pulse were stable. Sevoflurane concentration in excess of one monitored anaesthesia care (MAC) was confirmed using end-tidal inhaled agent monitoring. Morphine was used at 09:30:00 and again at 09:44:50.

Supplemental propofol 60 mg was used at 09:43:00. There was liberal use of diathermy during this period. The patient denied recall of intraoperative events at postoperative interview. The BIS index trend for this case presented in Figure 7.11.

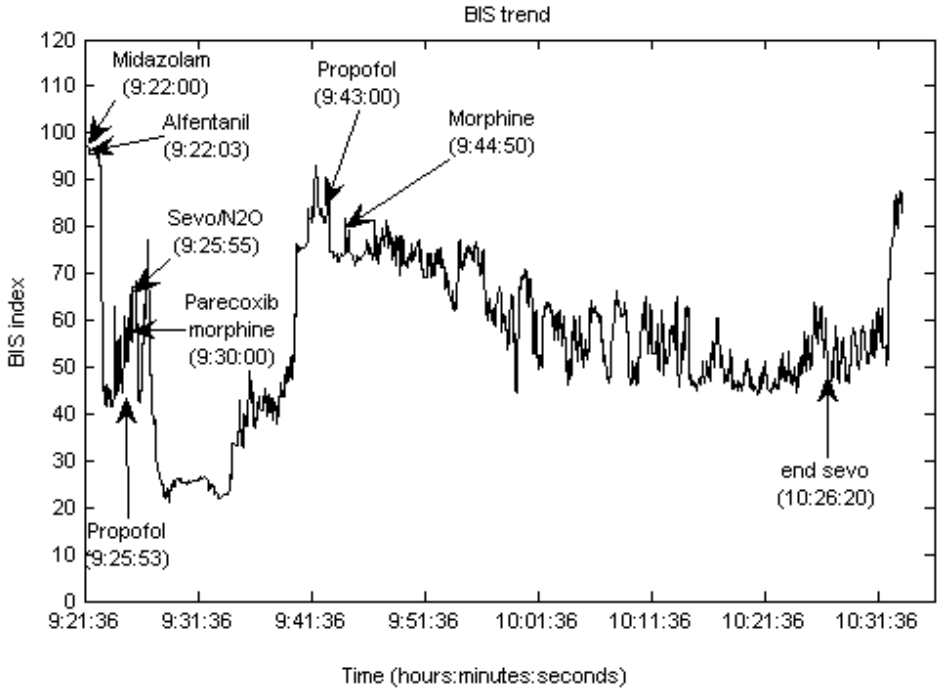

Figure 7.11: The BIS trend of patient 19 during surgery.

7.8.1.2 EEG signal analysis

Figure 7.12 presents the raw EEG signal of patient 19. Spike noise is clearly demonstrated in the raw EEG trace presented in Figure 7.12(a). The attending anesthetist reported artefactually high BIS values between 09:40:10 and 09:57:06. From 09:40:10 to 09:42:02, the BIS value was increasing from 59 to 91.8. From 09:42:02 to 09:57:06, the BIS value was steeply decreasing from 91.8 to 61.2. During these periods, the raw EEG signal has three spikes. The first is a positive spike lasting 0.3 seconds with maximum amplitude of 350 μV in Figure 7.12(b). The second is a negative spike lasting 0.03 seconds with maximum amplitude of -

658.1μV in Figure 7.12(c). The third is a positive spike lasting 0.025 seconds with maximum amplitude of 729μV in Figure 7.12(c).

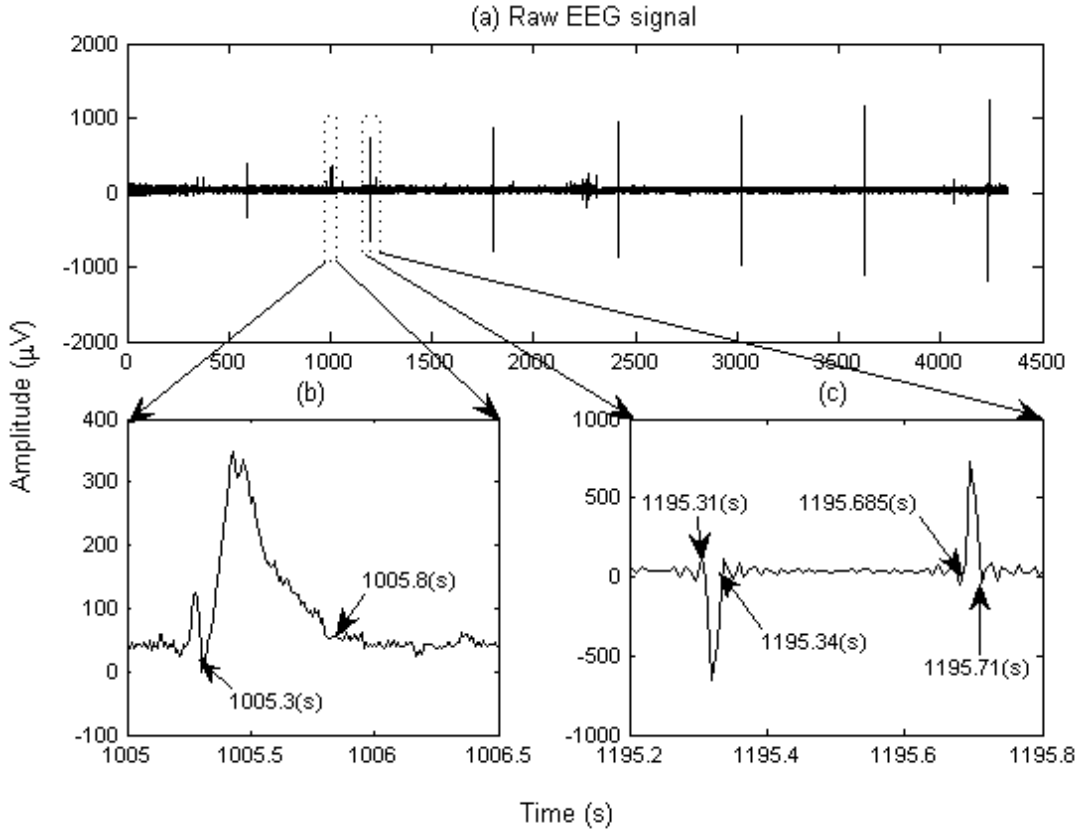

Figure 7.12: (a) The raw EEG signal of patient 19, corresponding to the BIS trend in Figure 1;

(b) Positive spike noise happened for 0.5 seconds, from 1005.3 to 1005.8 seconds;

(c) Negative spike noise happened for 0.03 seconds, from 1195.31 to 1195.34 seconds; and positive spike noise happened for 0.025 seconds, from 1195.685 to 1195.71 seconds.

7.8.1.3 Comparison between F_{min} and BIS index

A comparison between the F_{min} and BIS trends for patient 19 is presented in Figure 7.13. The F_{min} trend briefly moves into a high range from 9:40:17 to 9:42:08 and thereafter recovers to a range of 45 to 50 during surgery. This F_{min} trend more

accurately reflects clinical observation than does the coincident BIS index. The patient was not paralyzed and did not move. The systemic blood pressure and pulse were stable.

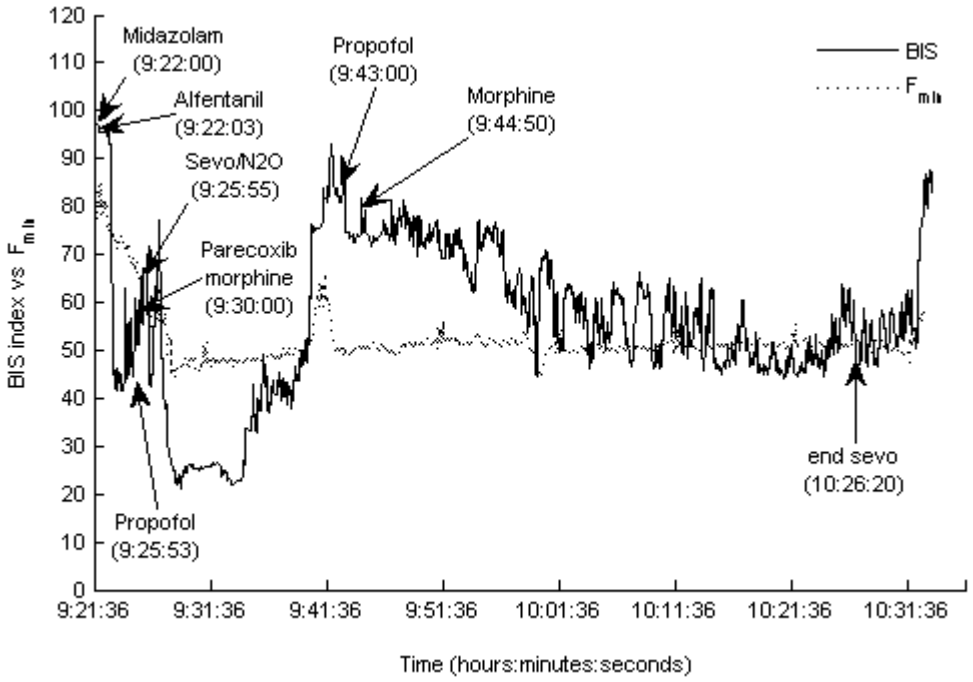

Figure 7.13: Comparison of the F_{min} and the BIS trends of patient 19.

7.8.2 The second case

7.8.2.1 BIS trend

A BIS index of -3276.8 was recorded in the trend file on several occasions during otherwise uneventful anaesthesia of three patients (patients 3 and 4 in Figure 7.14 and patient 12 in Figure 7.15). In the BIS monitor, the Signal Quality Indicator (SQI) is a measure of the EEG signal quality and is calculated based on impedance data, artefact, and other variables. When signal quality is too low to accurately calculate a valid BIS value, the BIS value and other trend variables that are adversely

affected by artefact will not be displayed on the screen. As with any monitored parameters, artefacts and poor signal quality may lead to inappropriate BIS values.

The value of -3276.8 is presented as a "non-valid value" or a "non-supported parameter" by the BIS monitor. Only "valid" BIS values when SQI is above 15 are displayed on the monitor screen. In the case of patient 12, the clinically important transition from the awake state (BIS=100) to deep anaesthesia (BIS=33.6) is masked by this phenomenon (see Figure 7.15). In this case, the anaesthetist could not use the BIS index to estimate the state of the patient.

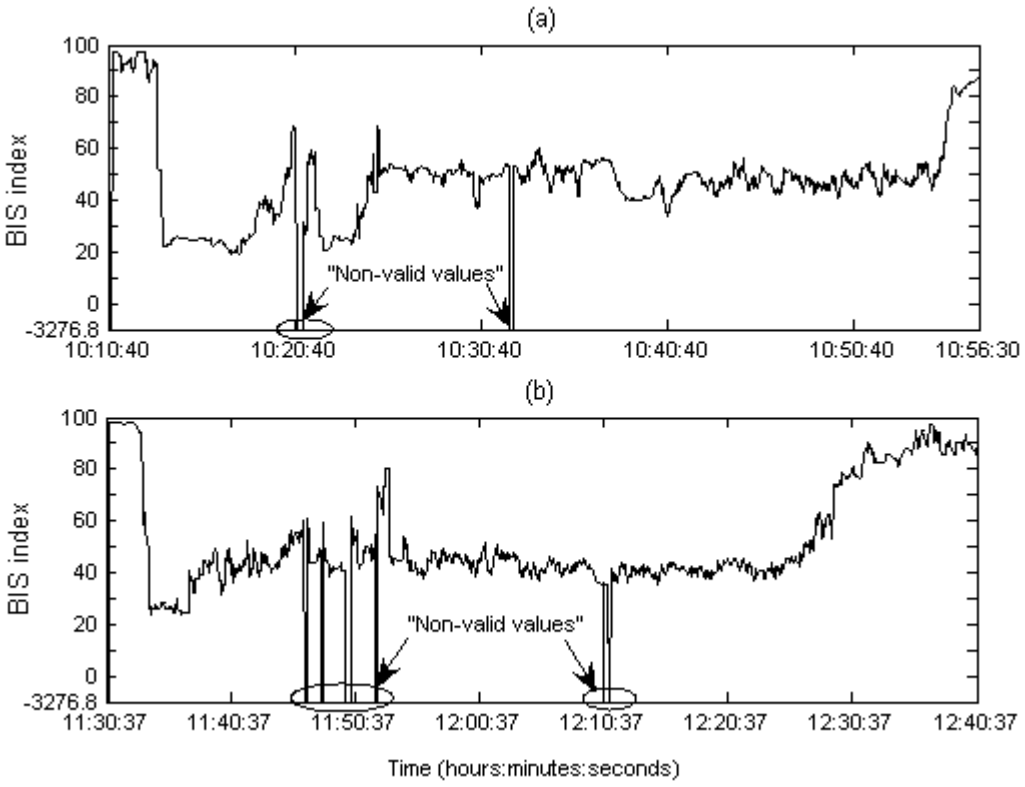

Figure 7.14: "Non-valid values" of BIS in the case of patient 3 in Figure 7.14(a) and patient 4 in Figure 7.14(b).

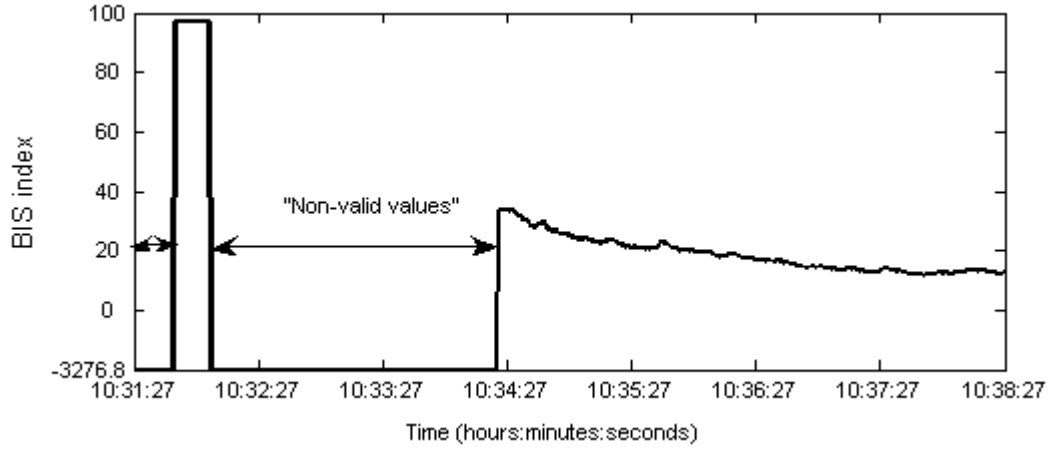

Figure 7.15: "Non-valid values" of BIS in the case of patient 12. The BIS value changes to -3276.8 within a few seconds and persists during two distinct time periods: 10:31:27-10:31:44 AM and 10:32:02-10:34:20 AM.

7.8.2.2 EEG signal analysis

The raw EEG signal during periods when a negative BIS index was recorded is shown in Figure 7.16 as (b), (c), (d) and (e). Figure 7.17 presents the raw EEG signal of patient 12 including the window of 240 seconds from 10:31:27 to 10:34:27 corresponding with **"**non-valid" BIS values.

The EEG signals in Figs 7.16 and 7.17 are not affected by ECG signals or other artefacts and no strictly isoelectric. If the SQI is less than 15, that means too many epochs of data contain artefacts, and the BIS value cannot be reliably calculated. Electrical interference could be the cause, but it would be regarded as EMG and artefacts, not EEG, by the algorithm.

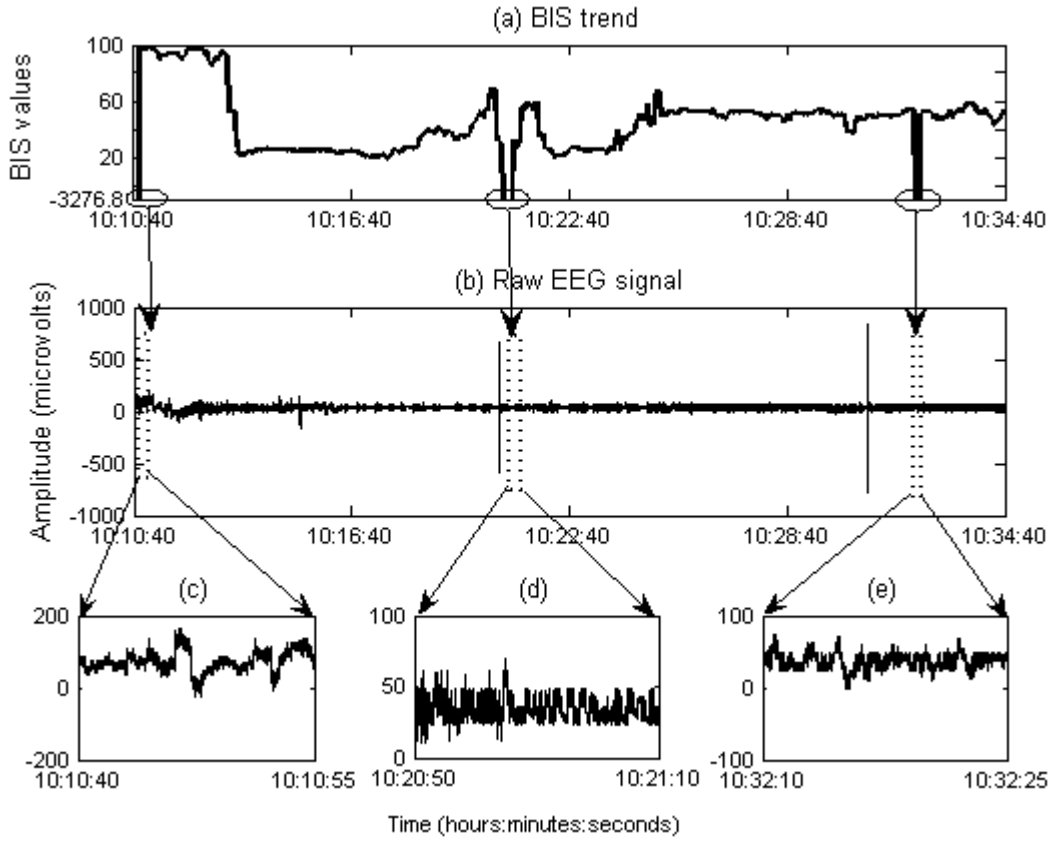

Figure 7.16: A comparison of the BIS trend and the EEG signal of patient 3:

(a) BIS trend;

(b) raw EEG signal;

(c), (d) and (e) The scope of raw EEG signals during periods when the negative BIS index were recorded.

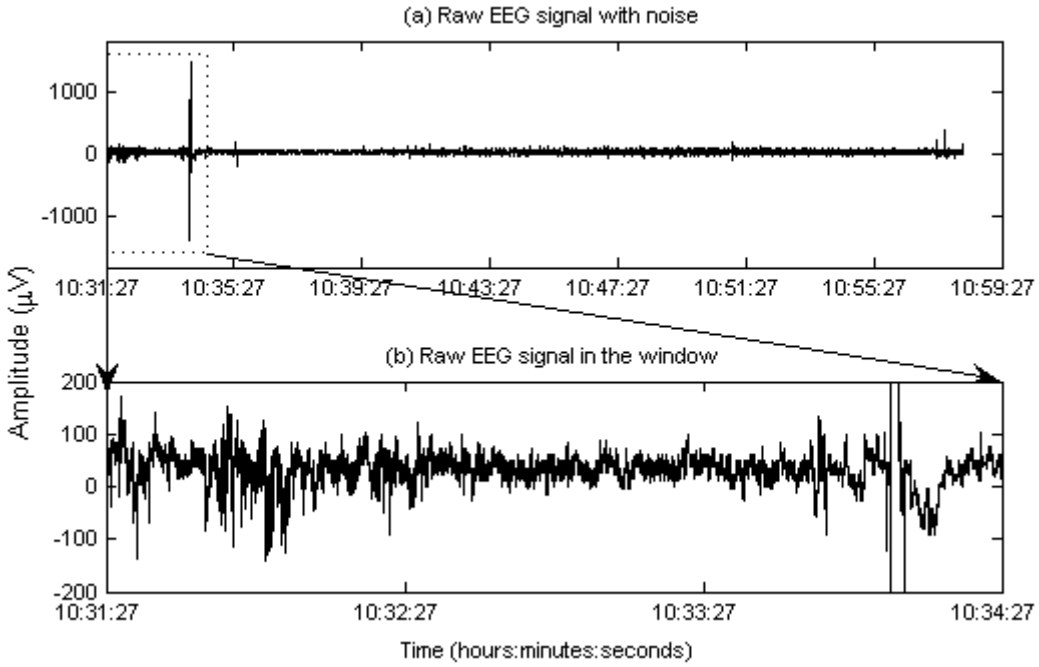

Figure 7.17: (a) The raw EEG signal of patient 12;

(b) The scope of EEG signal in 240 seconds corresponding with **"**non-valid" BIS values. (The corresponding BIS trend is in Figure 7.15)

7.8.2.3 Comparison between F_α and F_{min} and BIS index

Our method can compute (and display) the DoA index at times when the BIS monitor produces the -3276 value representing "non-valid values" and "non supported parameters" (see Figures 7.5 and 7.18). F_α and F_{min} do not produce negative values and outputs remain stable when the BIS monitor output defaults to the -3276 value.

It must be emphasized that the BIS monitor could not analyse EEG signals in this case and the invalid BIS value (-3276.8) did not display on the monitor screen. In contrast, our method can display DoA values as shown in Figure 7.18 by F_α and F_{min} trends. The comparison of BIS with F_α and F_{min} values is presented in Table 7.3.

In this table, we compare BIS values before, during and after changes with F_α and F_{min} at the same time. During this interval, F_α and F_{min} have stable values. Compared with BIS in these cases, during periods of poor signal quality, our results better correlate to clinical observation.

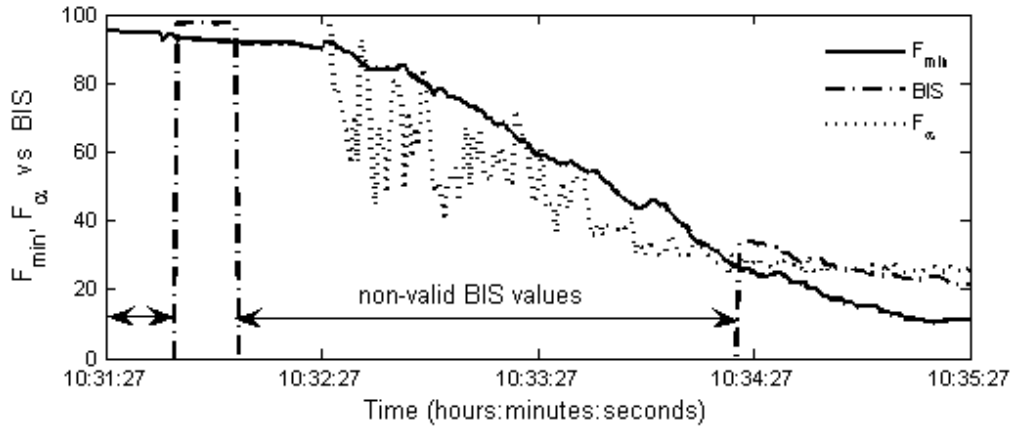

Figure 7.18: DoA values in the case of poor signal quality of patient 12: a comparison between F_α, F_{min} and BIS trends.

Table 7.3: Comparisons of BIS values with F_α and F_{min} values during BIS value changes with patient 12 during two time zones

Time (s)	Index	Before change	During change	After change
1 - 19	BIS	0	-3276.8	97.2
	F_{min}	95.4	93.7 to 95.4	92.2
	F_α	100	100	100
36-175	BIS	97.1	-3276.8	33.6
	F_{min}	91.9	91.9 to 26.8	26.8
	F_α	100	100 to 31.1	31.1

7.8.3 The third case

7.8.3.1 BIS trend

BIS recordings during anaesthesia for patient 1 were made between 15:36:52 and 16:58:48. Patient 1 was a 66 years old, 106 kg female. Intravenous midazolam 4mg was given at 15:37:15. Intravenous alfentanil 1000μg was given at 15:37:30 and propofol 150mg was given at 15:38:47. At 15:38:48, desflurane and nitrous oxide (N_2O) were started. Our observations of the example BIS trend (Figure 7.19) were that:

- The BIS trend did not reflect the administration of midazolam and alfentanil in real-time. The initial response to these drugs was an increase in BIS (89 to 97) over 30 seconds (15:37:30 to 15:38:00). The expected fall in BIS index (97 to 55) was delayed and took 34 seconds (15:38:04 to 15:38:38).
- The BIS trend did not fall immediately after propofol administration at 15:38:47. The BIS value increased rapidly from 54 to 84 in a short time period from the 15:38:48 (point A) to 15:38:57 (point B). The BIS index then decreased rapidly from 84 (point B) to 54 (point C) in 14 seconds. It continued decreasing to 43 (point D) in 7 seconds before steeply decreasing.

There is clearly a time "lag" between clinical events and changes to the BIS index, even allowing for pharmaceutical circulation time in elderly patients. The described lag is not an isolated event and is commonly observed clinically.

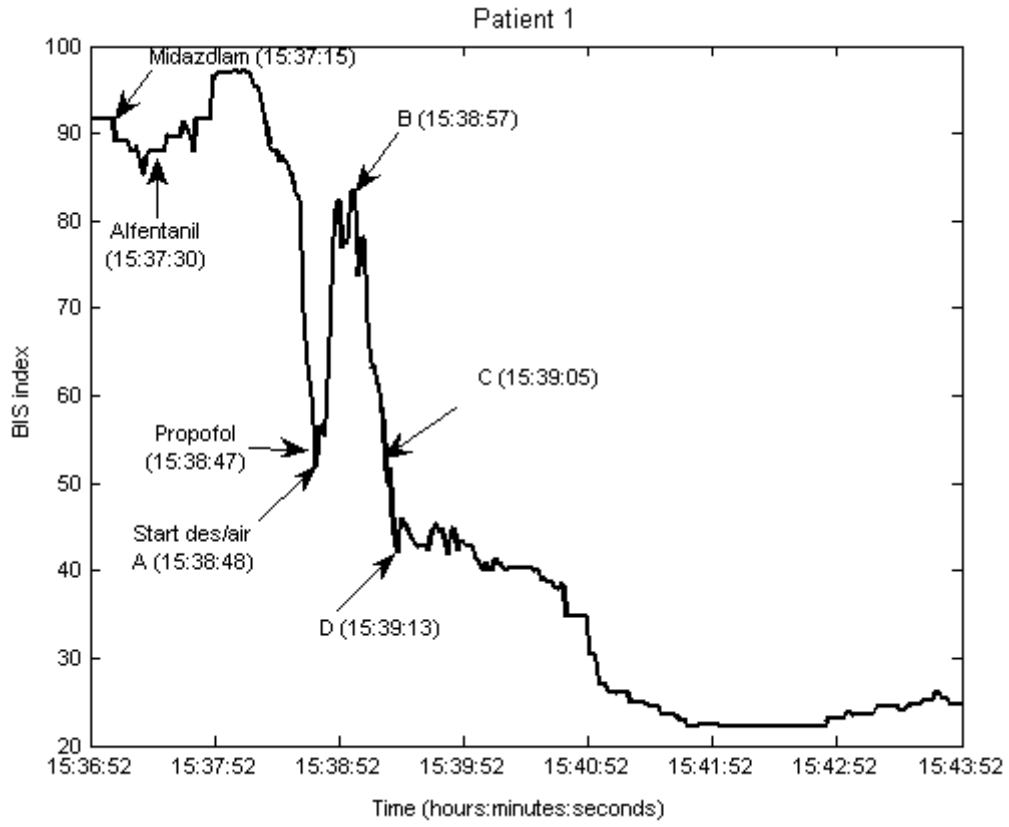

Figure 7.19: The BIS trend of patient 1 after an altered state of consciousness. There is clearly a time "lag" between clinical events and changes to the BIS index, even allowing for pharmaceutical circulation time in elderly patients. The described lag is not an isolated event and is commonly observed clinically.

7.8.3.2 EEG signal analysis

The raw EEG signal of patient 1 is presented in Figure 7.20, including the scope of EEG signal from 15:36:52 to 15:40:52. Reasons for sudden changes of the BIS value were presented in (Koitabashi, 2004) when low levels of suppression were detected. Other explanations for this case were shown in (Scott) as:

- high frequency artifacts may contaminate the EEG signal and cause bias towards a higher value.

- changes in vaporizer setting, fresh-gas flow rate, intravenous infusion pump settings and intravenous delivery routes may account for a sudden change in the level of anaesthetic effect and the resulting BIS value.
- abrupt changes in BIS may reflect a new cortical state relative to anaesthetic dosing and current surgical conditions. BIS may show a transient increase in response to an increase in noxious stimulation.

However, none of these suggestions are helpful to the above case. There are no high frequency artifacts or low levels of suppression in the raw EEG signal and the sequence of drug administration was routine. In this case, the BIS algorithm did not reflect exactly the clinical state of the patient.

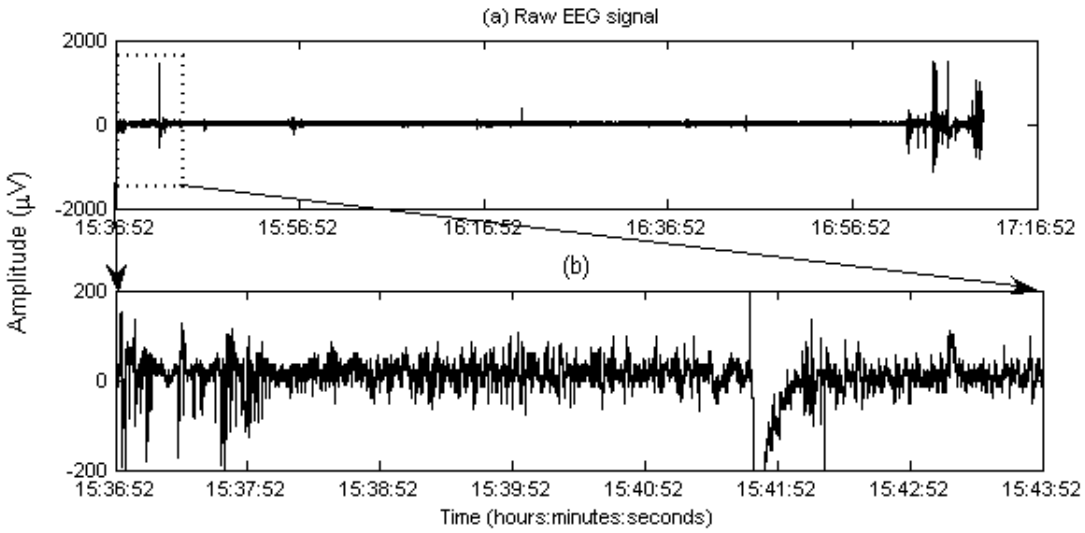

Figure 7.20: (a) The raw EEG signal of patient 1;

(b) EEG signal from 15:36:52 to 15:40:52 (The corresponding BIS trend is in Figure 7.19).

7.8.3.3 Comparison between F_{min} and BIS index

A significant criticism of the BIS index is its inherent “time lag". We often see the BIS index change long after an altered state of consciousness is observed. A major aim of this study is to define a method which reflects conscious state changes in “real time” - so as to prevent unintentional lightening of anaesthesia relative to surgical stimulus. Figure 7.21 demonstrates the superiority of F_{min} over BIS index in this regard in one of the 25 patients. The F_{min} trend moves intuitively following pharmaceutical administration and appears to track clinically observed changes in conscious state. The patient lost consciousness. Patient was lack of response to verbal and tactile stimulus, loss of the lash reflex.

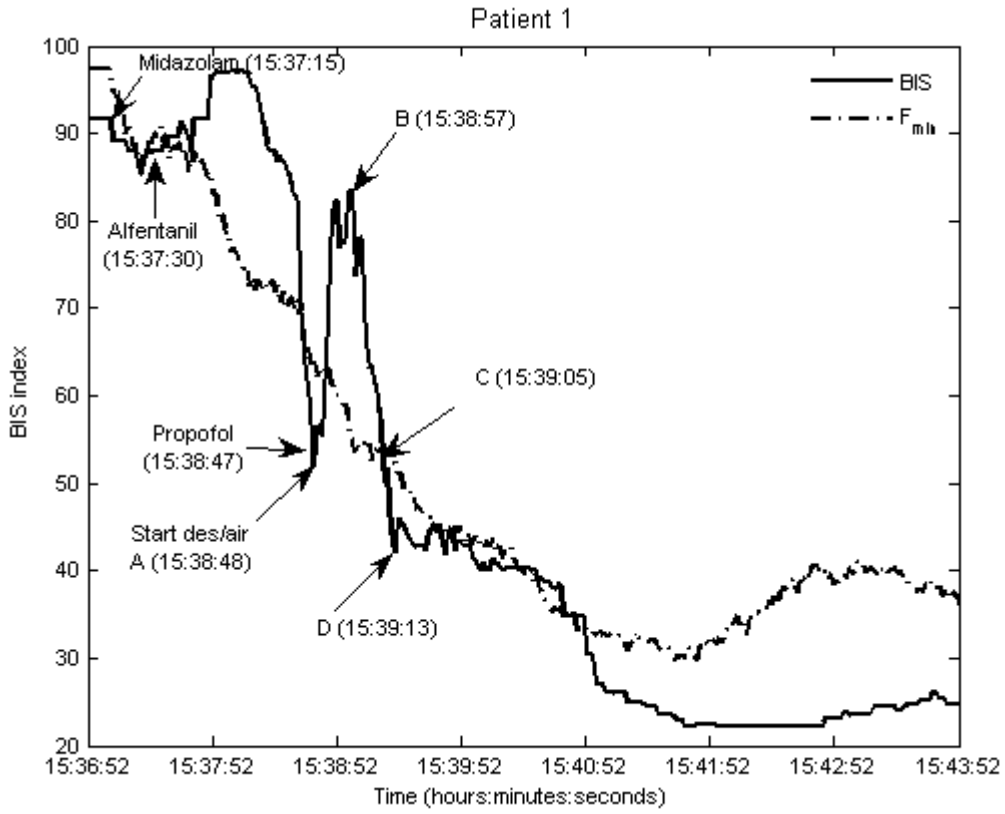

Figure 7.21: A comparison between F_{min} and BIS trends of patient 1 from consciousness to unconsciousness. BIS index often change long after an altered state

of consciousness is observed. The BIS trend did not reflect the administration of midazolam and alfentanil in real-time and did not fall immediately after propofol administration in the 108th second. The F_{min} trend moves intuitively following pharmaceutical administration and appear to track clinically observed changes in conscious state.

7.9 CONCLUSION REMARKS

In this chapter, a modified DMA method was proposed to assess the DoA. The results demonstrated that the MDMA method can distinguish the patient's clinical states from awake to deep anaesthesia more accurately than the original DMA method. To evaluate the MDMA method, data from 17 patients was collected and processed the DoA.

The accuracy and reliability of the MDMA method were investigated by computing the scaling exponent α (F_{α}) and minimum $\ln F_{MDMA}$ value (F_{Min}). A close correlation was found between our results (F_{Min}, F_{α}) and BIS Index with $r(F_{Min})$ = 0.9346, $r(F_{\alpha})$ = 0.9458 and $r^2(F_{Min})$ = 0.9183, $r^2(F_{\alpha})$ = 0.8855. The MDMA method reflects the consciousness of a patient undergoing general anaesthesia faster than BIS as observed clinically. The minimum time delay between the BIS and F_{Min} trends is 12 seconds and the maximum is 178 seconds. F_{α} and F_{Min} are responsive and their movement seem similar to the changes in the clinical state of the patients. Furthermore, the results can also accurately estimate a patient's hypnotic state in the case of poor signal quality. The proposed new MDMA method provides more accurate and reliable indicators for DoA monitoring in real-time.

Chapter 8

Measuring DoA using Wavelet and Power Spectral Density Techniques

In this chapter, a new method is proposed for constructing a wavelet-based depth of anaesthesia (*WDoA*) index. This method is based on discrete wavelet transform (DWT) and power spectral density (PSD) function. DWT is applied to pre-process EEG data. The PSD with eigenvector method is chosen as a feature function for six levels of the coefficients in DWT. The adaptive threshold is used to de-noise the low frequency and spike noise. During computation, an adaptive window length (AWL) is applied to reduce the time delay. AWL is a function of the wavelet energy entropy and adapts to the clinical state of the patient. *WDoA* and BIS indices are compared through the whole scale from 100 to 0 with full recording time on 25 patients.

8.1 WAVELET AND POWER SPECTRAL DENSITY TECHNIQUES

EEG signals have a broad frequency spectrum and complex dynamics. Wavelet transform (WT) can be applied to decompose an EEG signal into different scaling components (see Section 3.2.3, page 36).

8.1.1 Decomposition of EEG signals using wavelet method

In order to select a basis function that matches the frequency characteristics of a spike, EEG signals are decomposed into six sub-bands to obtain the desired frequency resolution. The corresponding frequency sub-bands of a decomposed signal are presented in Table 4.1. The components D_6 and D_5 are within the δ-band whilst D_4, D_3, D_2 and D_1 are within the θ-band, α-band, β-band, and γ-band, respectively (Daubechies, 1992; Vetterli, 1992).

8.1.2 Estimate the pseudospectrum of wavelet coefficients using the Eigenvector method

We apply the Eigenvector method to compute the pseudospectrum from an autocorrelation matrix estimation of the wavelet coefficient (Eriksson, 1994; Karhunen, 1992). The data matrix from autocorrelation matrix estimation is used as the input of the pseudospectrum using MUSIC algorithm. The signal x with the length n and the input argument m have the autocorrelation matrix in (8.1).

The eigenvector approximation of the pseudospectrum from a correlation matrix A_j is presented in Figure 8.1. We label *EAj* as pseudospectrum of correlation matrix A_j. High magnitude specified peaks (HMSPs) *EAj* are observed in different frequency bands. HMSPs of the given raw EEG data reveals six principal frequency zones: *EA6* (0< frequency ≤ 2 Hz), *EA5* (0≤ frequency ≤ 4 Hz), *EA4* (0 ≤ frequency ≤ 8 Hz), *EA3* (0 ≤ frequency ≤ 16 Hz), *EA2* (0 ≤ frequency ≤ 32 Hz), and *EA1* (0 ≤

frequency ≤ 64 Hz) (see Figure 8.1). These results are used to identify EEG signals in different anaesthesia states.

$$X = \begin{bmatrix} x(1) & \cdots & 0 \\ \vdots & \ddots & \vdots \\ x(m+1) & \cdots & x(1) \\ \vdots & \ddots & \vdots \\ x(n-m) & \cdots & x(m+1) \\ \vdots & \ddots & \vdots \\ x(n) & \cdots & x(n-m) \\ \vdots & \ddots & \vdots \\ 0 & \cdots & x(n) \end{bmatrix} \tag{8.1}$$

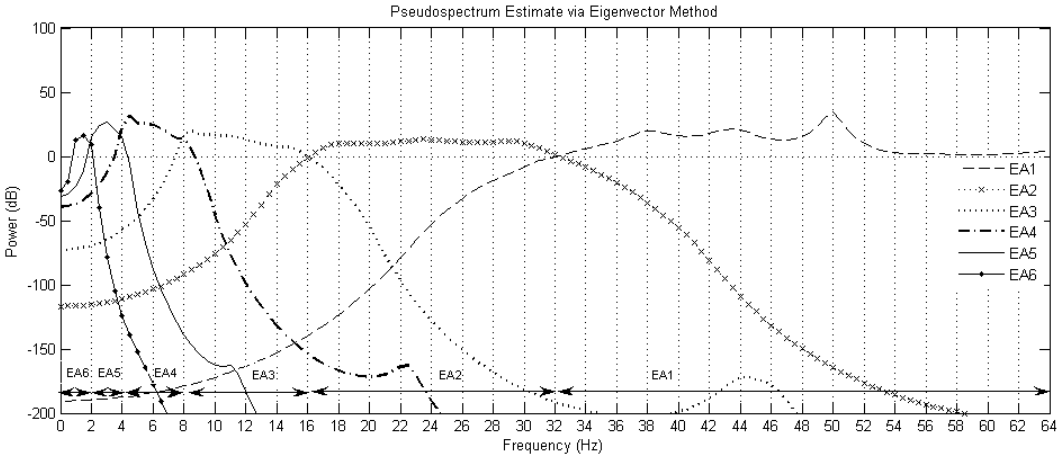

Figure 8.1: The difference of pseudospectrum estimate of correlation matrix of wavelet coefficients from A_1 to A_6. *EAj* is labelled as pseudospectrum of correlation matrix of A_j. High magnitude specified peaks (HMSPs) of *EAj* are observed in different frequency bands. HMSPs of the given raw EEG data reveals six principal frequency zones: *EA6* (0< frequency ≤ 2 Hz), *EA5* (2 ≤ frequency ≤ 4 Hz), *EA4* (4 ≤ frequency ≤ 8 Hz), *EA3* (8 ≤ frequency ≤ 16 Hz), *EA2* (16 ≤ frequency ≤ 32 Hz), and *EA1* (32 ≤ frequency ≤ 64 Hz).

8.2 MONITOR THE DEPTH OF ANAESTHESIA

8.2.1 Feature function selection

In order to extract information pertinent to the depth of anaesthesia from the EEG signal, the power spectral density (PSD) of the wavelet coefficients is chosen as a feature function. A_j and D_j are used as input signals for the eigenvector method. The function Φ_{PSD} is denoted as:

$$\Phi_{PSD}:\begin{cases} D_j \rightarrow \Phi_{PSD}(D_j) = EDj \\ A_j \rightarrow \Phi_{PSD}(A_j) = EAj \end{cases}, \tag{8.2}$$

where j is the decomposition level, wavelet filter is *db16* and the principal eigenvector $p=6$. The following statistical features are defined to characterize the time-frequency distribution of the EEG signals:

1. Mean of *EAj* and *EDj* are:

$$\begin{aligned} M(EDj) &= \frac{1}{l_{D_j}} \sum_{s_D=1}^{l_{D_j}} EDj, \quad s_D = 1,2,...,l_{D_j} \\ M(EAj) &= \frac{1}{l_{A_j}} \sum_{s_A=1}^{l_{A_j}} EAj, \quad s_A = 1,2,...,l_{A_j} \end{aligned}, \tag{8.3}$$

where l_{A_j} and l_{D_j} are the length of *EAj* and *EDj*.

2. Standard deviation (STD) of *EAj* and *EDj* are

$$\begin{aligned} S(EDj) &= \left(\frac{1}{l_{D_j}} \sum_{s_D=1}^{l_{D_j}} \left(EDj - M(EDj)\right)^2 \right)^{1/2} \\ S(EAj) &= \left(\frac{1}{l_{A_j}} \sum_{s_A=1}^{l_{A_j}} \left(EAj - M(EAj)\right)^2 \right)^{1/2} \end{aligned}. \tag{8.4}$$

Zikov *et al* only used the γ-band (32-64 Hz) and the information in other bands is lost (Zikov, 2006; Bibian, 2008). In contrast, all six levels of decompositions are used in our method.

8.2.2 DoA index

Figure 8.2(a) and Figure 8.3(a) show the mean *M(EAj)* and the standard deviation *S(EAj)* of *EAj*, respectively. Figure 8.2(b) and Figure 8.3(b) show the mean *M(EDj)* and the standard deviation *S(EDj)* of *EDj*, respectively. The means and the standard deviations move from high values to low values when the patient state moves from consciousness to unconsciousness and vice versa. Therefore, a new function is proposed as follows:

$$V_{MAD} = \frac{1}{2}\left(\log(\frac{1}{J}\sum_{j=1}^{J} M(EAj)) + \log(\frac{1}{J}\sum_{j=1}^{J} M(EDj)) \right), \tag{8.5}$$

$$V_{SAD} = \frac{1}{2}\left(\log(\frac{1}{J}\sum_{j=1}^{J} S(EAj)) + \log(\frac{1}{J}\sum_{j=1}^{J} S(EDj)) \right). \tag{8.6}$$

And the algorithm for computing the DoA index is designed below:

Algorithm 8.1: New DoA index computing

- *Select the number of decompositions J=6*
- *Compute WDoA:*

$$WDoA = f(V_{MAD}, V_{SAD}) = \frac{(k_1 V_{MAD} + k_2 V_{SAD} + V_{offset})}{k_3} \tag{8.7}$$

- *If WDoA > 100*

  WDoA = 100

  else WDoA = WDoA, end.

k_1, k_2, k_3 and V_{offset} are the values calculated in the offline analysis. Empirically, values like $k_1=35$, $k_2=100$, $k_3=2$ and $V_{offset}=85$ were chosen. This choice based on experiments and practical experience from the analysed data. These constant values are merely estimates of a unit of measure, to fix the WDoA value in the range of 0-100.

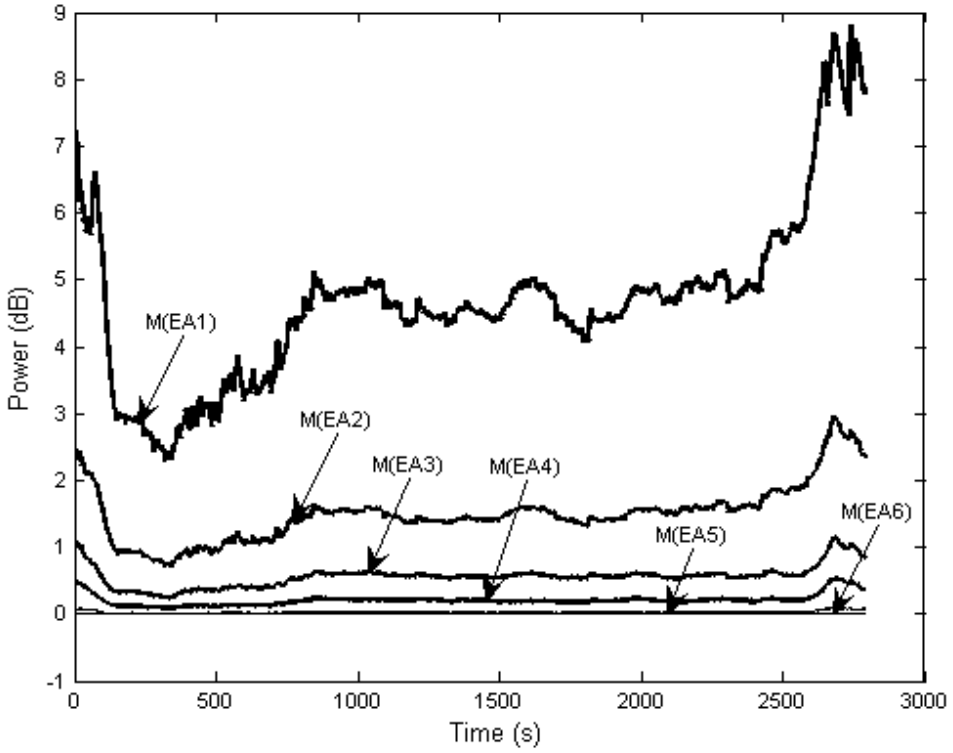

Figure 8.2(a): *M(EAj)* of patient 3. There are some correlation between patient clinical state and *M(EAj)* in the time domain. These values are high during wakefulness and decrease as the patient moves into anaesthesia. *M(EAj)* correlates with the DoA and BIS values. *M(EA1)> M(EA2)> M(EA3)> M(EA4)> M(EA5)> M(EA6).*

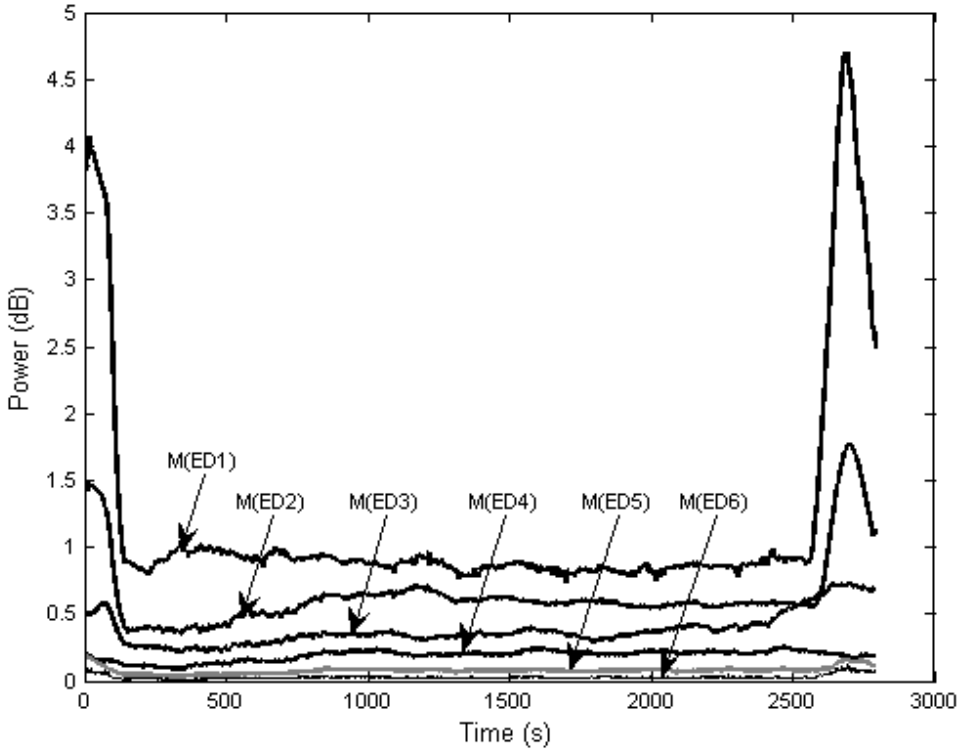

Figure 8.2(b): *M(EDj)* of patient 3. There are some correlation between patient clinical state and *M(EDj)* in the time domain. These values are high during wakefulness and decrease as the patient moves into anaesthesia. *M(EDj)* and correlates with the DoA and BIS values. *M(ED1)> M(ED2)> M(ED3)> M(ED4)> M(ED5)> M(ED6).*

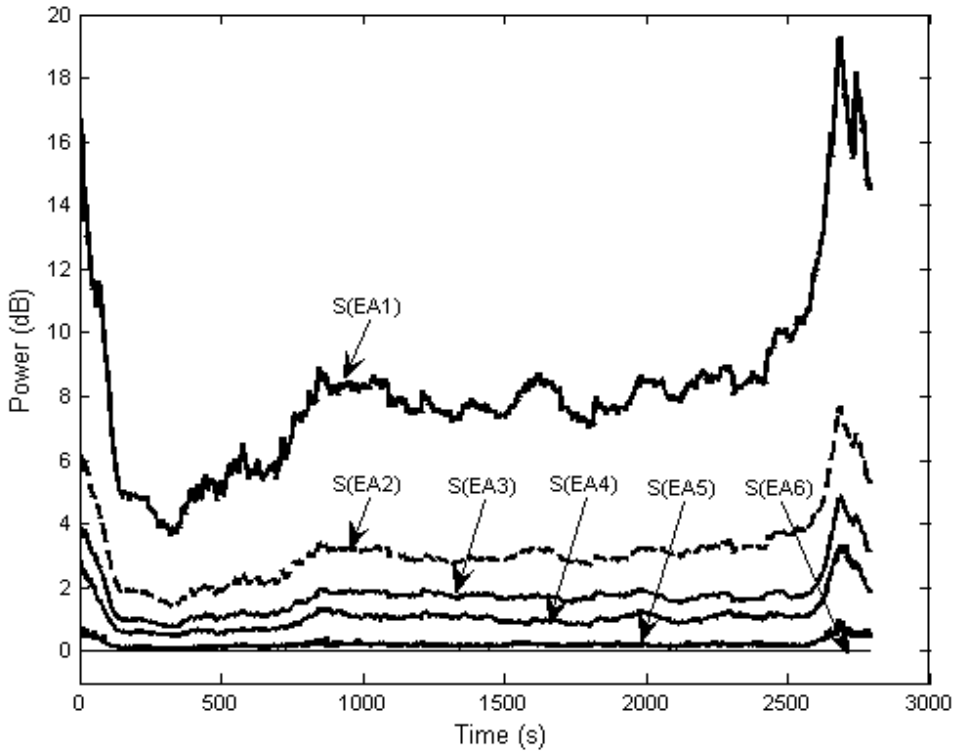

Figure 8.3(a): *S(EAj)* of patient 3. There are some correlation between patient clinical state and *S(EAj)* in the time domain. These values are high during wakefulness and decrease as the patient moves into anaesthesia. *S(EAj)* correlates with the DoA and BIS values. *S(EA1)*> *S(EA2)*> *S(EA3)*> *S(EA4)*> *S(EA5)*> *S(EA6).*

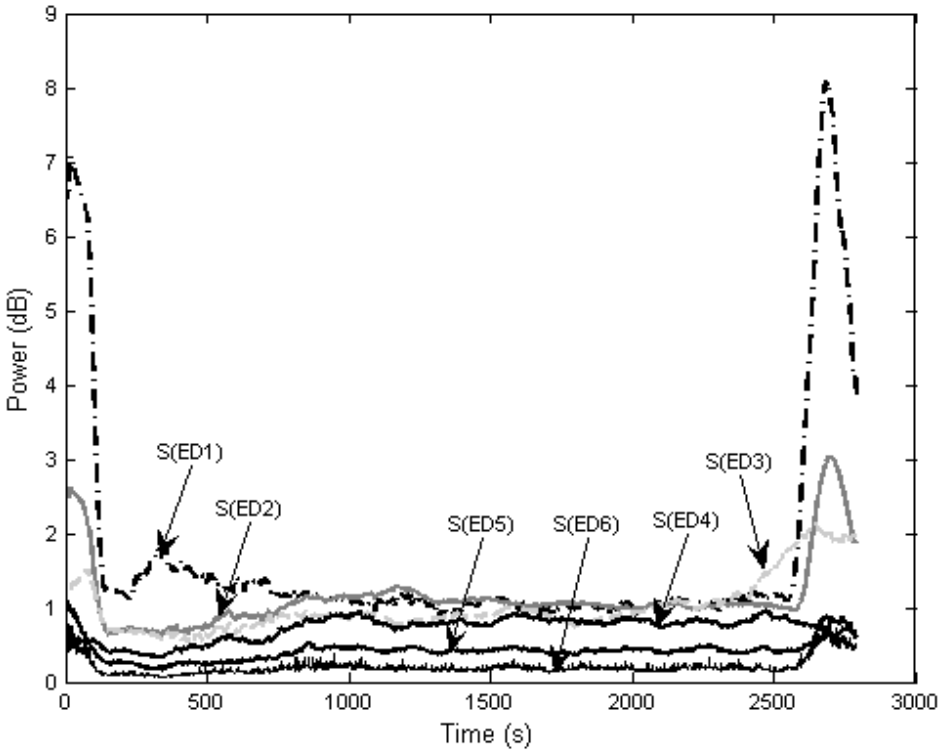

Figure 8.3(b): *S(EDj)* of patient 3. There are some correlation between patient clinical state and *S(EDj)* in the time domain. These values are high during wakefulness and decrease as the patient moves into anaesthesia. *S(EDj)* correlates with the DoA and BIS values.

S(ED1)≥ S(ED2)> S(ED3)> S(ED4)> S(ED5)> S(ED6).

8.3 TESTING AND VERIFICATION

8.3.1 Select a mother wavelet and the principal eigenvector

There is no standard method for choosing the best wavelet. Daubechies (DB) orthogonal wavelets DB2, DB4,…, DB20 are commonly used, where the index number refers to the number of coefficients. Each wavelet has a number of vanishing moments which is equal to half the number of coefficients. For example, DB2 (the Haar wavelet) has one vanishing moment, DB4 has two, etc. A vanishing moment limits the wavelet's ability to represent polynomial behaviour or information in a signal (Daubechies, 1992).The *db* value is increased from 4 to 6, 8,…, 20 when the *p* principal eigenvector changes from *p = 1, 2,..., 11*. The maximum *p* value is *11* as it is the smallest size of Toeplitz autocorrelation matrix which provides meaningful results and takes less computing time. In our results, the Daubechies wavelet (*db* = 16) and the rank *p* (*p*=6) in eigenvector method are selected for identifying the different states of anaesthesia. With *db* = 16 and *p*=6, we can distinguish more clearly the different states of anaesthesia. The details are shown in Figs. 8.4(a) and 8.4(b).

- In Figure 8.4(a), at *db*=16, we have:

  $mean(S(EDj))_{BIS97} > mean(S(EDj))_{BIS94} > mean(S(EDj))_{BIS80} > mean(S(EDj))_{BIS60} >$
  $mean(S(EDj))_{BIS50} > mean(S(EDj))_{BIS40} > mean(S(EDj))_{BIS30} > mean(S(EDj))_{BIS15}.$

- In Figure 8.4(b), at *p*=5, 6, 7, 8, 9, we have:

  $mean(S(EDj))_{BIS97} > mean(S(EDj))_{BIS94} > mean(S(EDj))_{BIS80} > mean(S(EDj))_{BIS60} >$
  $mean(S(EDj))_{BIS50} > mean(S(EDj))_{BIS40} > mean(S(EDj))_{BIS30} > mean(S(EDj))_{BIS15}.$

Therefore, *db* = 16 and *p*=6 were chosen as the input parameters in this study.

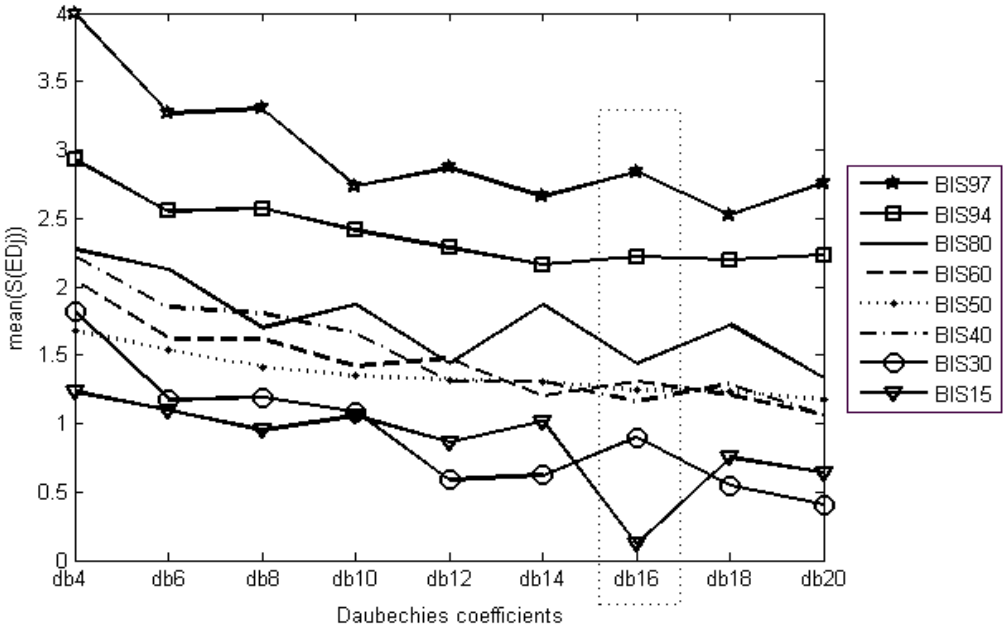

Figure 8.4(a): The relationship between *mean*(*S*(*EDj*)) and orthogonal Daubechies coefficients with *p*=6. At *db=16*, we have:

$$mean(S(EDj))_{BIS97} > mean(S(EDj))_{BIS94} > mean(S(EDj))_{BIS80} > mean(S(EDj))_{BIS60} > mean(S(EDj))_{BIS50} > mean(S(EDj))_{BIS40} > mean(S(EDj))_{BIS30} > mean(S(EDj))_{BIS15}.$$

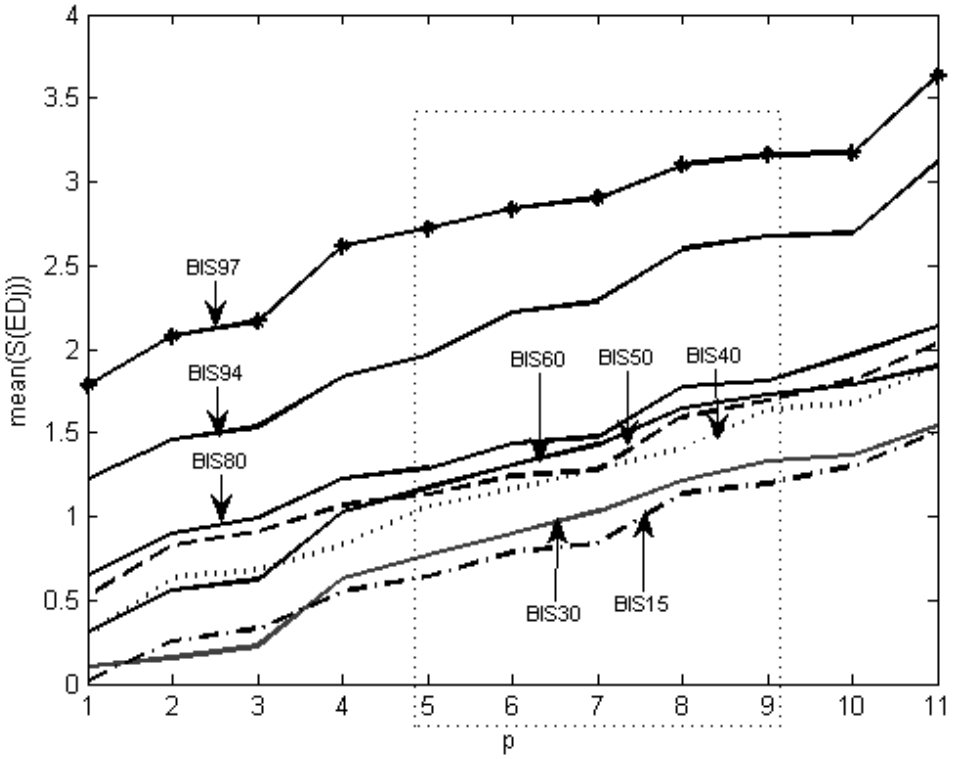

Figure 8.4(b): The relationship between *mean*(*S*(*EDj*)) and the principal eigenvector *p* with Daubechies coefficients *db*=16. With *p*=5, 6, 7, 8, 9, we have:

$mean(S(EDj))_{BIS97} > mean(S(EDj))_{BIS94} > mean(S(EDj))_{BIS80} > mean(S(EDj))_{BIS60} > mean(S(EDj))_{BIS50} > mean(S(EDj))_{BIS40} > mean(S(EDj))_{BIS30} > mean(S(EDj))_{BIS15}$.

8.3.2 Select the level of decompositions

In order to select the level of decompositions in the DWT method, we compute *M(EAj)*, *M(EDj)*, *S(EAj)* and *S(EDj)* using (8.3) and (8.4) with *J* values changing from 1 to 6. Figs. 8.5 and 8.6 depict the correlation of mean of *M(EAj)*, *M(EDj)*, *S(EAj)* and *S(EDj)* with BIS values for 25 patients. With *J*=6, there is a good correlation between patient clinical state and mean of *M(EAj)*, *M(EDj)*, *S(EAj)* and *S(EDj)*. These values are high during conscious period and decrease as the patient moves into anaesthesia. Therefore, we chose the level of decomposition as *J* = 6, which correspond to the δ-band; θ-band; α-band; β-band and γ-band.

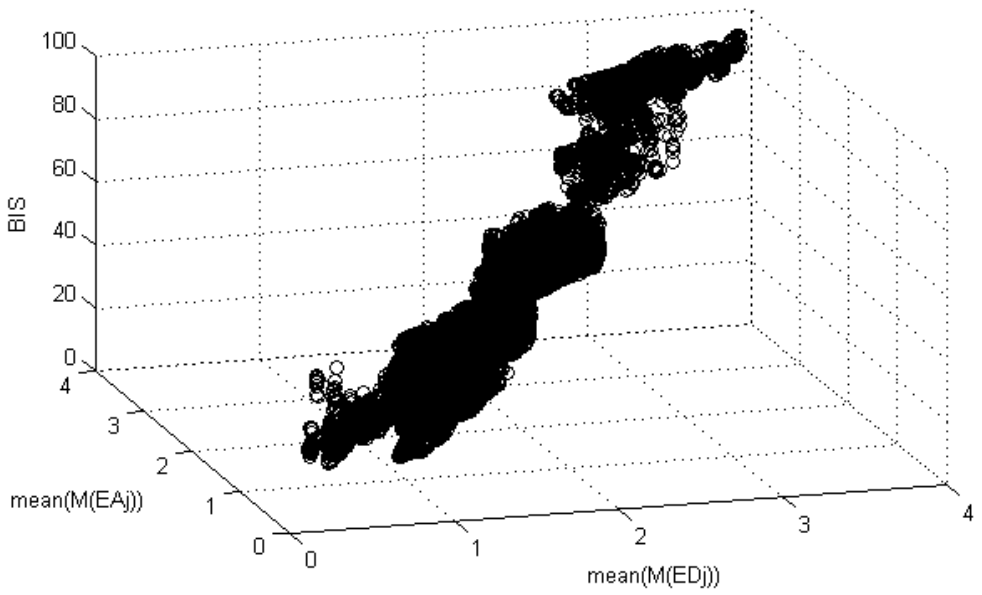

Figure 8.5: The correlation of mean of *M(EAj)* and *M(EDj)* with BIS values for 25 patients in 3D plot with *J*=6. Mean of *M(EAj)* and *M(EDj)* are high during conscious period and decrease as the patient moves into anaesthesia.

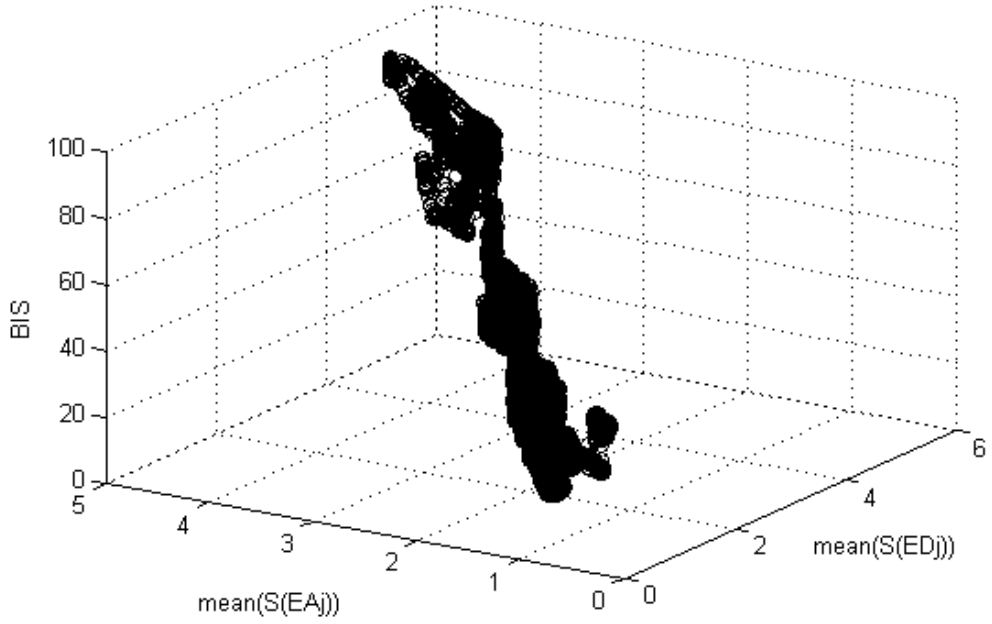

Figure 8.6: The correlation of mean of *S(EAj)* and *S(EDj)* with BIS values for 25 patients in 3D plot with *J*=6. Mean of *S(EAj)* and *S(EDj)* are high during conscious period and decrease as the patient moves into anaesthesia.

8.3.3 Length of a sliding window

In this method, a sliding window with fixed length is used for reading and processing EEG data. The *DoA* value is computed from the mean value of the previous and presented values. Let B_l be a window of length *L*, with $l = 1, 2, \ldots, (M-L-1)$. We slide the window B_l along the raw EEG signal. If we choose too small a window, the *DoA* values fluctuate and are more sensitive to noise. If we choose too large a window, the updated result is affected more by previous data and may be less useful in real-time.

In *WDoA* value calculation, the length of a sliding window was considered in two cases with *L*=10 and *L*=30.

- With the window length set at 10 seconds, the *WDoA* trend fluctuates widely from negative to positive in Figure 8.7(a).
- With the window length set at 30 seconds, the *WDoA* trend closes to the BIS trend covering the whole scale range from 100 to 0 in Figure 8.7(b).

The BIS monitor and the WAV_{CNS} indices (Zikov, 2006) both use a window of 30 seconds without an explanation of why this window size is chosen. Zikov *et al.* (Zikov, 2006) chose a window of 30 seconds for a comparison with the BIS method. As the computation starts, both the BIS index and the WAV_{CNS} index suffer a 30 second delay until the window is filled up.

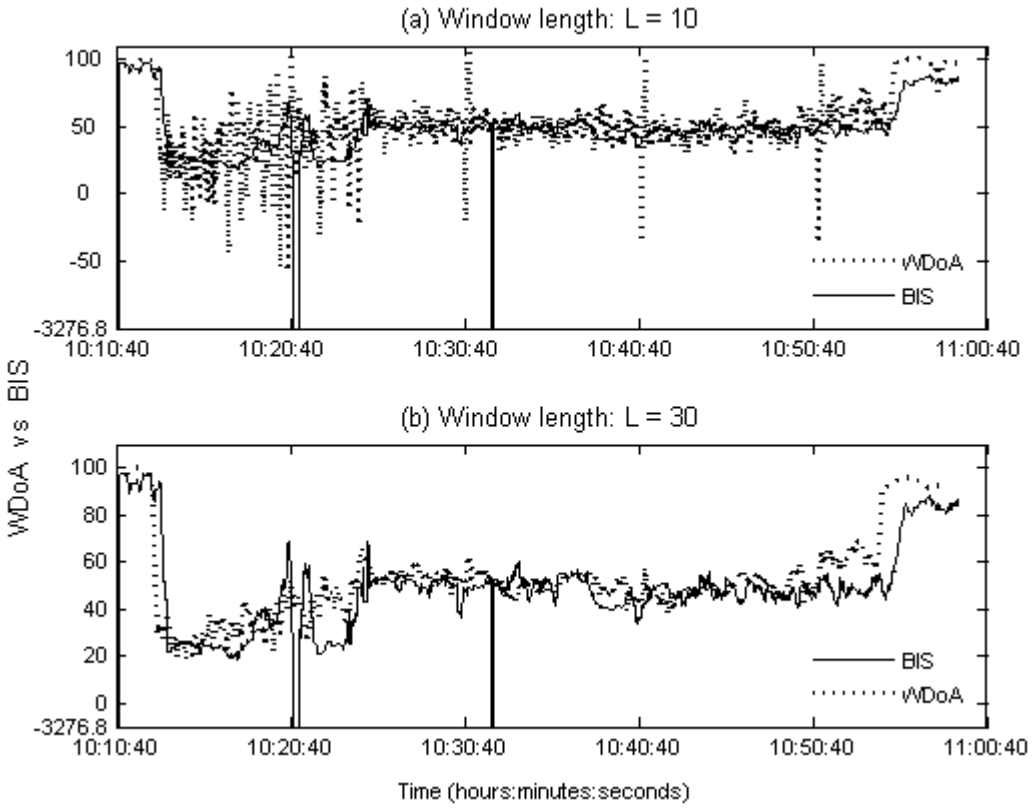

Figure 8.7: Comparison of *WDoA* and BIS values of patient 3;

(a) length $L = 10$; (b) length $L = 30$.

8.3.4 Adaptive window length

To reduce the time delay, we propose an adaptive window length (*AWL*) technique to compute the length of the sliding window. *AWL* is designed as a function of wavelet energy entropy E_m, where E_m is computed in (4.20) (Chapter 4, page 50). We start to compute the DoA value with the window length $L=2$, increasing this value for every subsequent window until $L = AWL$. The length of an adaptive window is presented in the following Algorithm 8.2.

Algorithm 8.2: Length of a sliding window

- *Set* $L_O = 2,\ L = L_O + 1$
- $AWL = f(\log(E_m))$
- *If* $L < [AWL]$

  $L = L+1$

  else $L = [AWL];$ *end.*

Figure 8.8 presents the window length of patient 19 in the time domain. Using this method, the window length adapts to the wavelet energy entropy and is continually appropriate.

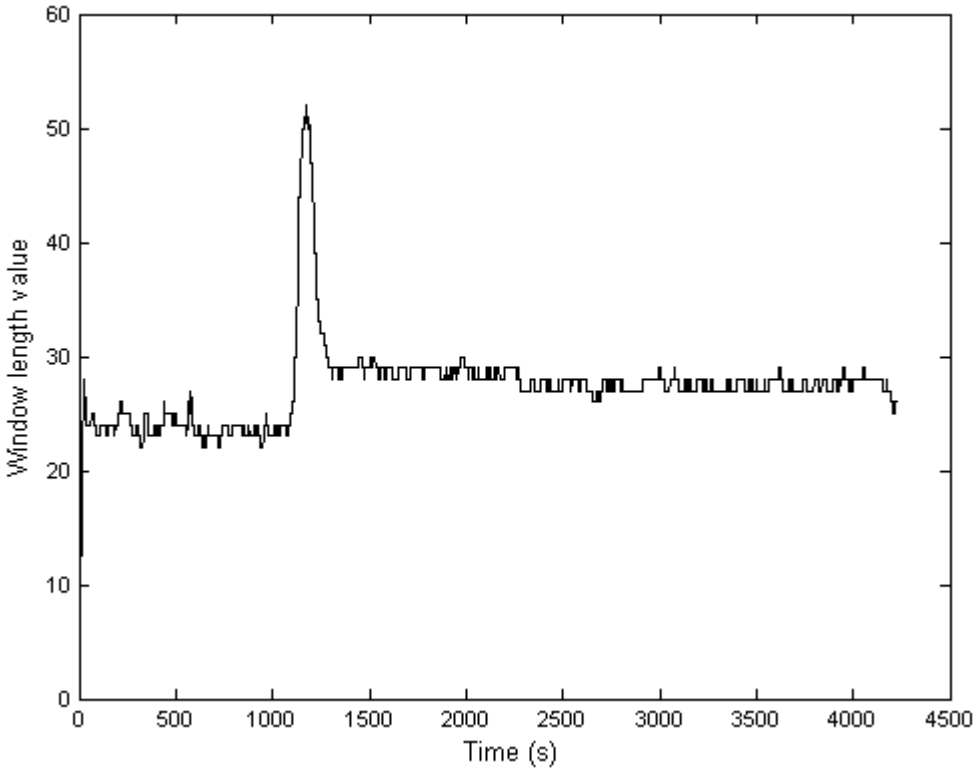

Figure 8.8: Adaptive length of sliding window for patient 19.

8.3.5 Detection of Burst Suppression in the EEG signal

The introduction about burst suppression ratio (BSR) was presented in section 7.4. In this section, *WDoA* index is used to monitor the DoA during burst suppression time.

Figure 8.9 presents EEG signal during the burst suppression of patient 2 with *WDoA* and BIS trends in Figure 8.9(a). Figure 8.9(b) shows the EEG signal of a full recording time and Figure 8.9(c).shows the EEG signal during the burst suppression. In one case of our study, the burst suppression lasted 1.9 seconds. From 715.1 to 717 seconds, BIS has low value from 5.7 to 7.7. During the burst suppression time, the EEG signal has an amplitude value lower than 5.0 μV. Our method shows DoA values during burst suppression by *WDoA* value in Figure 8.9(a), with the ranges of value from 16.0 to 17.9. As this is a single example of burst suppression, future

research is needed to further assess the behavior of our new index over varying degrees of burst suppression.

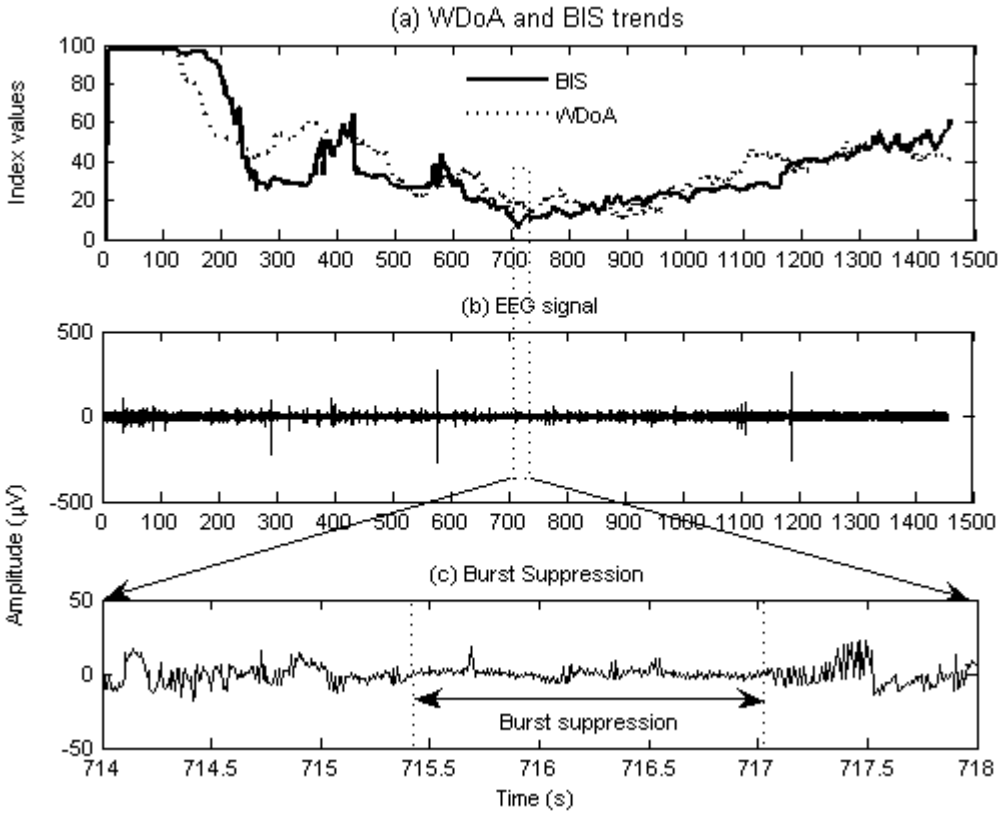

Figure 8.9: The burst suppression happens from 715.1 to 717 seconds. *WDoA* index can show the DoA values during this time.

8.3.6 Time delay from consciousness to unconsciousness

A time delay between BIS and *WDoA* is observed from consciousness to unconsciousness with the induction of anaesthesia. Figure 8.10 presents comparable data and Table 9.2 presents the anaesthetizing time line for patient 7. The conscious state as measured by *WDoA* falls precipitously around the time of propofol injection and rises steeply after the desflurane is discontinued. This more closely reflects the observed conscious state changes for a patient undergoing otherwise routine general anaesthesia. During this time, patient was lack of response to verbal and tactile

stimulus, loss of the lash reflex. WDoA index decreased steeply from 97 to 10 in the first 160 seconds as shown in Figure 8.10.

Zikov showed that the WAV_{CNS} preceded the BIS by an average of 15 seconds at BIS = 80. Indices such as Cerebral State Index; BIS Index and the Narcotrend Index invariably suffer from some degree of time delay between the patient's hypnotic state and index calculation (Pilge, 2006). Our method addresses this time delay by means of the adaptive window length method described above.

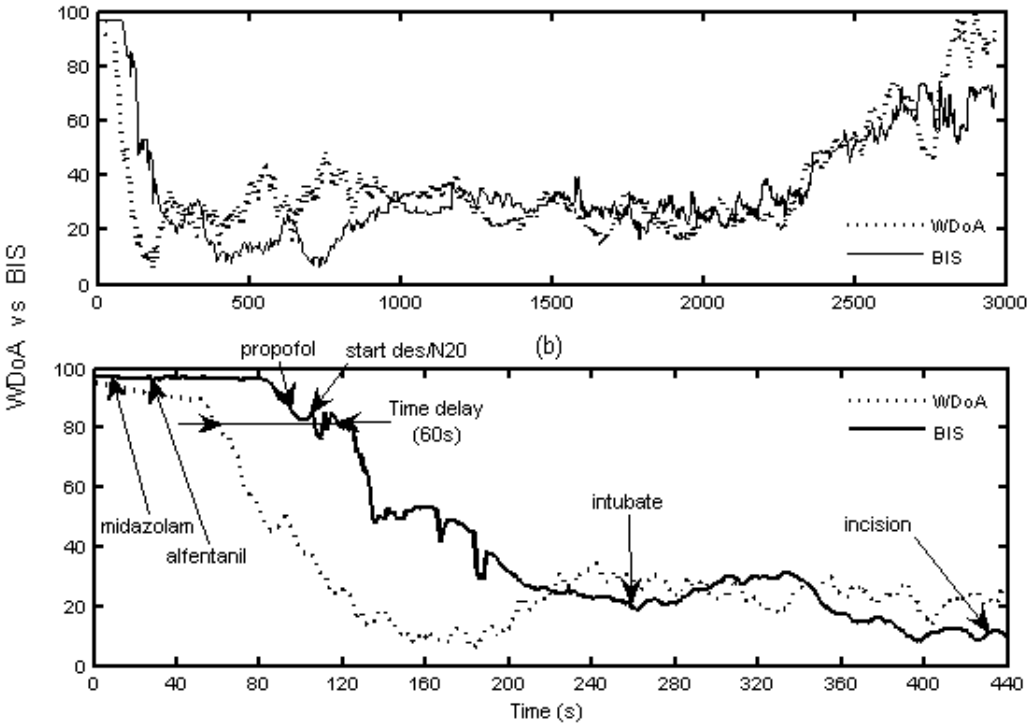

Figure 8.10: Patient 7

(a) *WDoA* and BIS trends for the entire recording period;

(b) *WDoA* and BIS during induction pharmaceutical administration and airway manipulation.

Table 8.1: Anaesthetizing time line of patient 7

Time (s)	**Day: 22/06/09**	**Patient No. 7**	
on axis	Time record	Drugs and progress	Drug dosage
0	09:03:49	start record	
11	09:04:00	midazolam	4 mg
26	09:04:15	alfentanil	1000 μg
100	09:05:29	propofol	110 mg
106	09:05:35	start des/N2O	
256	09:08:05	intubate	
431	09:11:00	incision	
2192	09:40:21	end des/N2O	
3013	09:54:02	End record	
	09:54:10	extubate	

8.4 TESTING THE DE-NOISING RESULT USING WDoA

In the section 7.6, we have proposed the testing denoising using MDMA method. In this section, *WDoA* is used an estimate from the error estimation. To estimate the efficiency of our de-noising method, we propose to analyze y_i and e_i by *WDoA* value in (8.7). Two parameters *WDoA*(y_i) and *WDoA*(e_i) are computed from the values of y_i and e_i. In the case e_i still brings a clinical meaning of the patien, *WDoA*(e_i) will present it. If not, the de-noisng algorithm does not remove the information of the EEG signal. The plots of *WDoA*(y_i), *WDoA*(e_i) and *WDoA*(x_i) are shown in Figures 8.11(a), 8.11(b) and 8.11(c), respectively. In these two figures, *WDoA*(y_i) and *WDoA*(e_i) did not show the change of patient's state from awake state to deep anaesthesia, and from general anaesthesia to awake. The trends of *WDoA*(y_i) and *WDoA*(e_i) are almost flat during general anaesthesia time, except four spikes.

This means that *WDoA*(y_i) and *WDoA*(e_i) do not present a clinical meaning better than *WDoA*(x_i). The results of *WDoA* test are presented in Table 8.2.

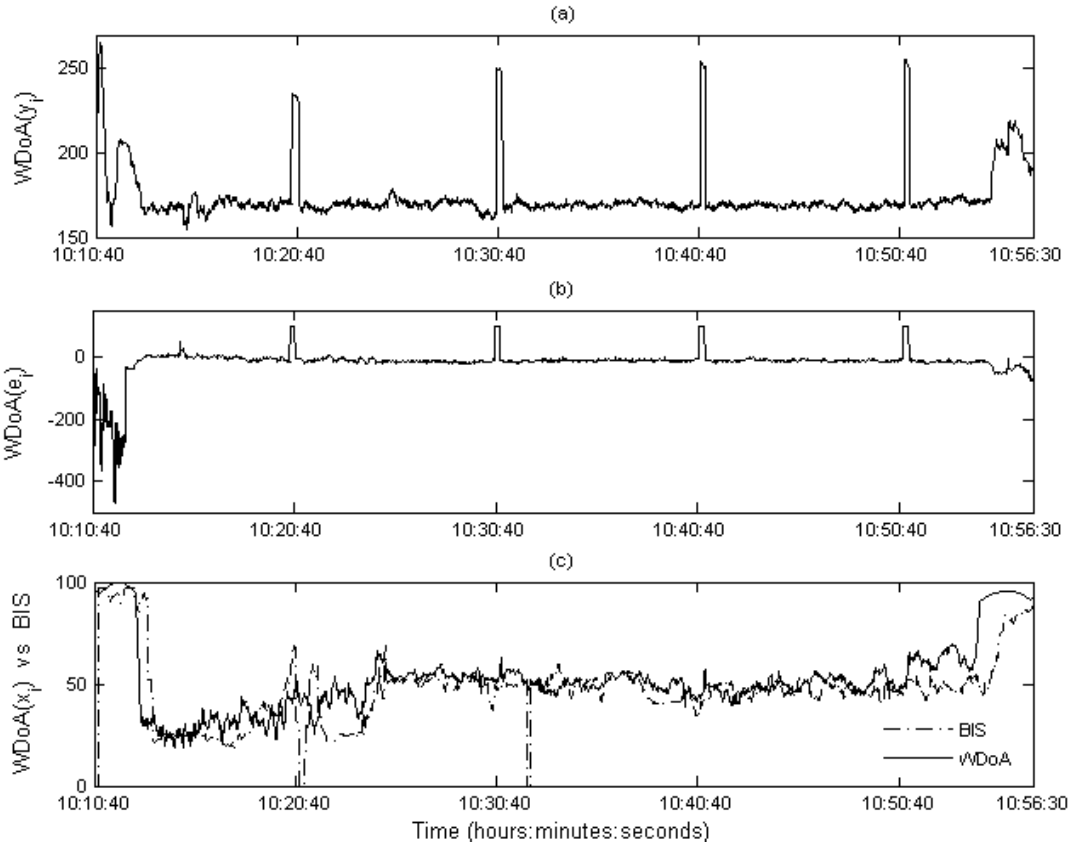

Figure 8.11: (a) *WDoA*(y_i) trend;

(b) The *WDoA*(e_i) trend;

(c) *WDoA*(x_i) trend verse BIS trend of patient 3. *WDoA*(y_i) and *WDoA*(e_i) trends do not present a clinical meaning better than *WDoA*(x_i) trend.

Table 8.2: The results of *WDoA* test for EEG signal.

$y_i = x_i + e_i$	Distinguish the patient's state
$y_i \rightarrow WDoA(y_i)$	No
$e_i \rightarrow WDoA(e_i)$	No
$x_i \rightarrow WDoA(x_i)$	From awake $\leftrightarrow$ deep anaesthesia

Using WDoA test, we found that:

- The raw EEG signal (yi) can not use directly to distinguish the change of patient's state from awake state to deep anaesthesia state and vice verse.
- The low frequency noise (ei) is indeed noise and do not have an useful part of the signal.
- Our de-noising algorithm only removes a very small portion of the true EEG signal.

8.5 RESULTS

There are five states of anaesthesia. Very deep anaesthesia and deep anaesthesia states have the BIS values from 0 to 40, moderate anaesthesia state from 40 to 60, light anaesthesia state from 60 to 80 and awake state from 80 to 100. A statistic comparison of *WDoA* and BIS index for 25 patients undergoing general anaesthesia is presented in Figure 8.12. The boxes illustrate the 25^{th} to the 75^{th} percentiles of the distribution of *WDoA* at each plane of anaesthesia as "defined" by the BIS level on the Y-axis whilst the whiskers illustrate the the range for each distribution (Friis, 2003). Five data groups of *WDoA* and BIS are used in this comparison, corresponding to five states of anaesthesia with BIS index ranges from 0-20, 20-40, 40-60, 60-80, and 80-100. Analysis of variance results in Fig. 8.12 indicate that the *WDoA* distributions at each anaesthesia state level are significantly different (p=0). The *WDoA* can distinguish five depths of anaesthesia in the study.

Table 8.3 presents the lower (L), median (M), and upper values (U) of the box plots, corresponding with five anaesthesia state levels of *WDoA* and BIS ranges. The median *WDoA* value clearly decreases with the depth of anaesthesia. ANOVA analysis in Table 8.4 indicates that the *WDoA* distributions at each anaesthesia state

level are significantly different. We conclude that the *WDoA* can distinguish five depths of anaesthesia in our sample.

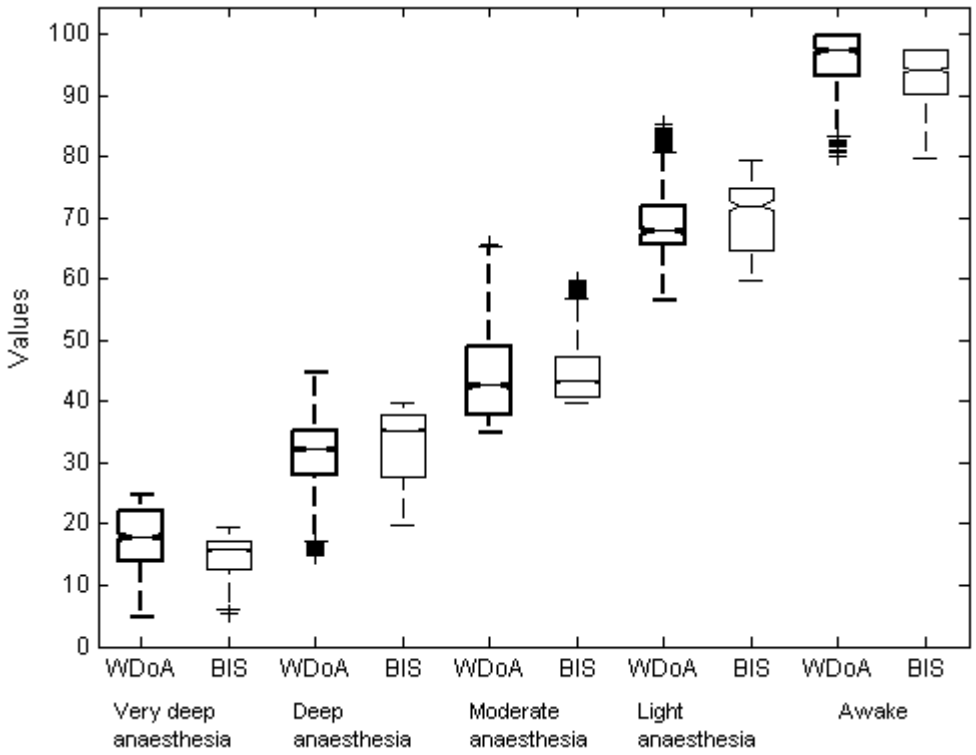

Figure 8.12: The *WDoA* distributions of 25 patients are presented by the box plot in a different anaesthesia state level.

Table 8.3: The lower (*L*), Median (*M*), and Upper (*U*) values between the *WDoA* box plot and the BIS ranges of the patients, corresponding with five anaesthesia state levels

Anaesthesia state levels	**BIS**			***WDoA***		
	L	**M**	**U**	**L**	**M**	**U**
Very deep anaesthesia	12.9	16.0	17.6	14.0	18.2	22.5
Deep anaesthesia	28.1	35.5	38.1	28.2	32.5	35.4
Moderate anaesthesia	41.2	43.5	47.5	38.1	42.9	49.1
Light anaesthesia	64.9	22.3	75.0	65.9	68.1	72.0
Awake	90.5	94.4	97.7	93.5	97.6	100

Table 8.4: ANOVA analysis for *WDoA* distributions at five different depths of anaesthesia, "Source" is the source of the variability; "SS" is the Sum of Squares for each source; "*df"* is the degrees of freedom associated with each source; "MS" is the Mean Squares (*MS*) for each source, which is the ratio *SS/df; "F"* is the F statistic, which is the ratio of the *MS*'s; the *p*-value is derived from the specified cumulative distribution function (*cdf*) of *F*.

Source	SS	df	MS	F	Prob>F
Groups	1.10804×10^{7}	9	1231154.33	39454.62	0
Error	1.39365×10^{6}	44662	31.20		
Total	1.24740×10^{7}	44671			

8.6 CASE STUDIES

Three special cases were reported in section 7.8. In this section, we use *WDoA* index to compare with BIS index in these cases.

8.6.1 The first case

A comparison between the *WDoA* and BIS trends for patient 19 is presented in Figure 8.13. The *WDoA* trend briefly moves into a high range from 9:40:17 to 9:42:08 and thereafter recovers to a range of 48 to 55 during surgery. This trend more accurately reflects clinical observation than does the coincident BIS index.

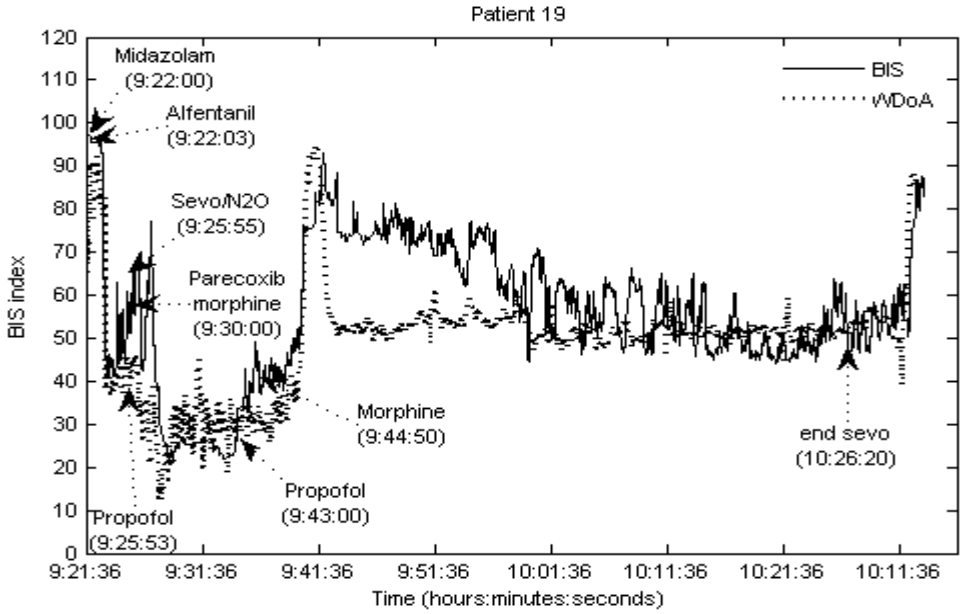

Figure 8.13: Comparison of the *WDoA* and the BIS trends of patient 19.

8.6.2 The second case

Our method can compute (and display) the DoA index at times when the BIS monitor produces the -3276 value representing "non-valid values" and "non supported parameters" (see Figures 8.14(I) and 8.14(II)). *WDoA* does not produce

negative values and outputs remain stable when the BIS monitor output defaults to the -3276 value.

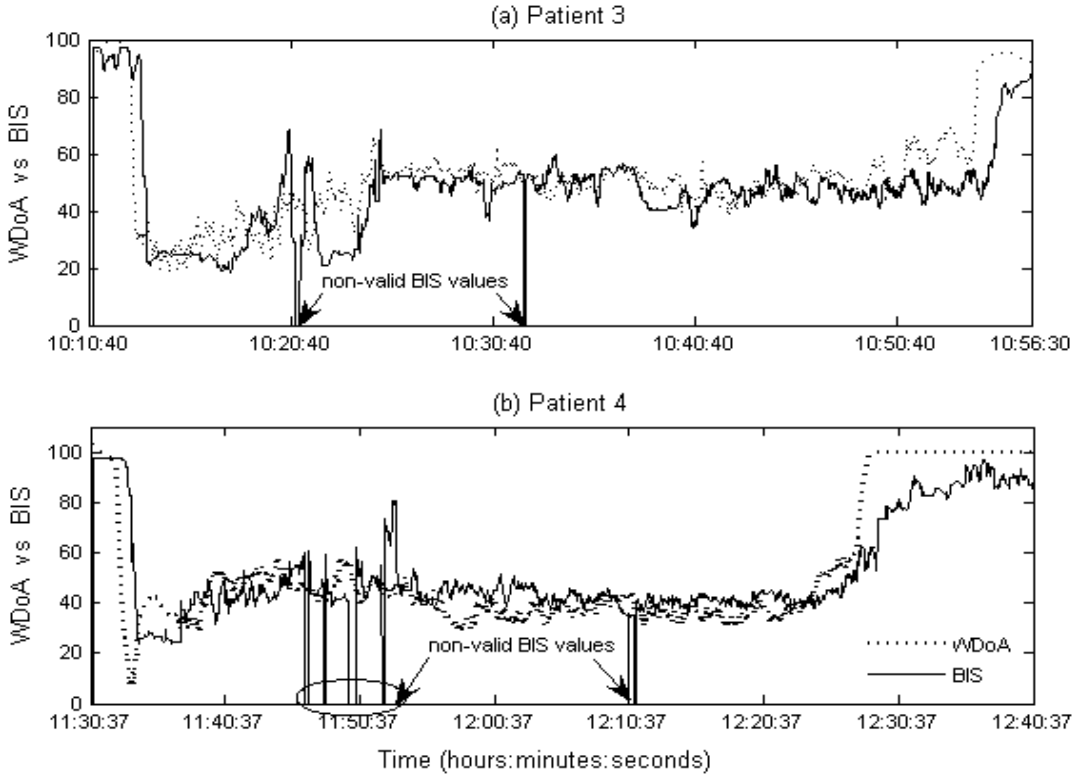

Figure 8.14(I): The *WDoA* and the BIS trends of patient 3 (Figure 8.14 I(a)) and patient 4 (Figure 8.14 I(b)). *WDoA* does not produce negative values and outputs remain stable when the BIS monitor output defaults to the -3276 value.

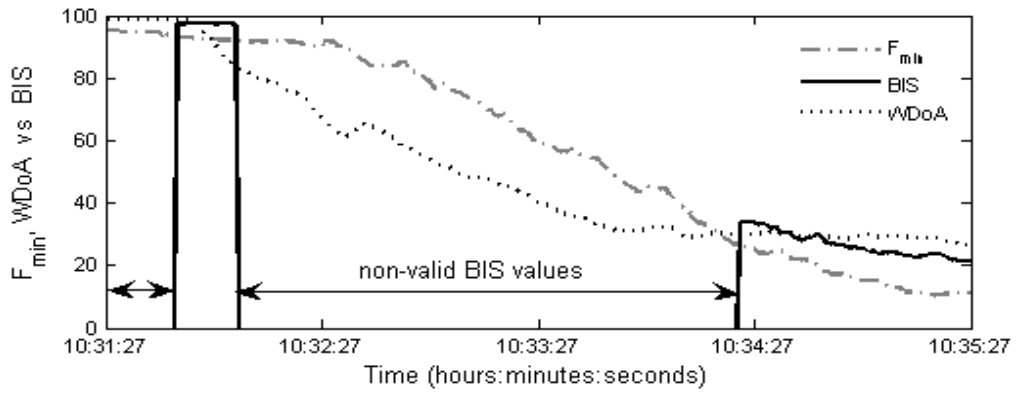

Figure 8.14(II): DoA values in the case of poor signal quality of patient 12: a comparison between *WDoA*, F_{min} and BIS trends.

8.6.3 The third case

A significant criticism of the BIS index is its inherent “time lag". We often see the BIS index change long after an altered state of consciousness is observed. A major aim of this study is to define a method which reflects conscious state changes in “real time” - so as to prevent unintentional lightening of anaesthesia relative to surgical stimulus. Figure 8.15 demonstrates the superiority of *WDoA* over BIS index in this regard in one of the 25 patients. The *WDoA* trend moves intuitively following pharmaceutical administration and appears to track clinically observed changes in conscious state.

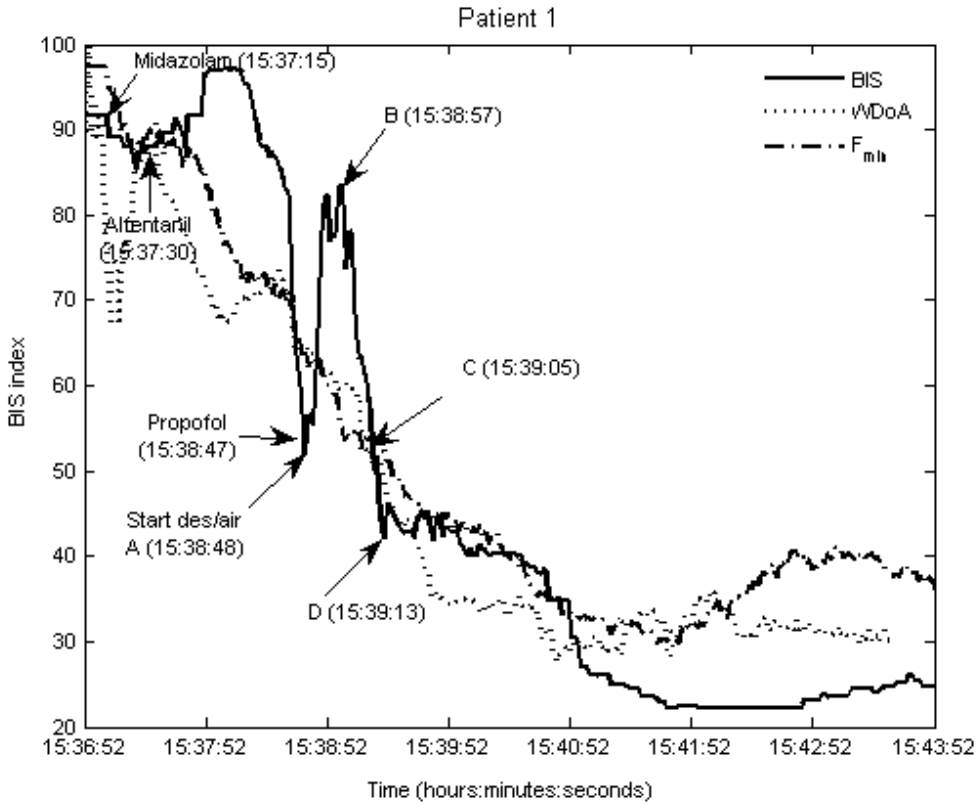

Figure 8.15: A comparison between the *WDoA*, F_{min} and the BIS trends of patient 1 from consciousness to unconsciousness.

Chapter 9

An Improved Chaos Method for Monitoring the DoA

Chaos analysis of EEG signals has been reported by many researchers in recent years (Ogo, 1995; Wang, 2010; Pijn, 1991; Di, 1997; Goodman, 1990; Walling, 2006; Faure, 2001; John, 2003; Korn 2003; Song 1989). A chaotic system is characterized by 'unpredictability', which means simply that one cannot predict how a system will behave in the future on the basis of a series of observations along time. From various experiments, it has been well established that neuronal activity and EEG recordings show many characteristics of chaotic behaviour. In other words, the electrical rhythms of the brain show signs of chaos.

9.1 CHAOS ANALYSIS OF BRAIN FUNCTION

The dynamic of brain electrical activity was presented by Rapp *et al*. (Rapp, 1989; Babloyantz, 1985). In their study, they estimated the correlation dimension of the human EEG signals and event-related brain potentials. Dafilis *et al*. discussed the evidence for the existence of chaos in a theory of brain electrical activity and provide

unique depictions of the dynamics of brain chaotic model (Dafilis, 2002). The aperiodic evolution of brain states through sequences of attractors was studied by Freeman (Freeman, 2003).

Lyapunov exponents estimate the mean exponential convergence of nearby trajectories of the attractor (Blanco, 1997; Fell, 1993). They are defined by:

$$Lp(t) = \frac{1}{t}\sum_{i=0}^{t} \log_2 \left[\frac{D'(t_{i+1})}{D(t_i)} \right] \tag{9.1}$$

Lyapunov exponent (*Lp*) determines the rate of predictability. A positive Lyapunov exponent indicates chaos. It sets the time scale which makes the state of prediction possible.

9.2 MONITORING THE DoA USING HURST EXPONENT IN CHAOS METHOD

The Hurst exponent is directly related to the "fractal dimension", which gives a measure of the roughness of a surface. The fractal dimension has been used to measure the roughness of coastlines. For example, the relationship between the fractal dimension (*D*) and the Hurst exponent (*H*) is:

$$D = 2 - H \tag{9.2}$$

Hurst exponent can distinguish fractal from random time series, or find the long memory cycles. The values of the Hurst Exponent range between 0 and 1. If the value of H=0.5, the time series is normally distributed, or has no long memory process. A Hurst Exponent value H between 0 and 0.5 exists for time series with "anti-persistent behaviour". A Hurst Exponent value H between 0.5 and 1 indicates "persistent behavior", that is, the time series is trending. Sum of the accumulated deviation from the mean of the time series x_i having length L is:

$$Y(i) = \sum_{i=1}^{L} [x_i - \langle x \rangle], \qquad i = 1,..., L \tag{9.3}$$

where <x> is the average of the time series, that is

$$\langle x \rangle = \frac{1}{L} \sum_{i=1}^{L} x_i \tag{9.4}$$

The range $R(i)$ is the difference between the maximum and the minimum of value $Y(i)$, over the length L is:

$$R(i) = \max_{1 \le i \le L}(Y(i)) - \min_{1 \le i \le L}(Y(i)) . \tag{9.5}$$

Standard deviation over the length L is:

$$S(i) = \sqrt{\frac{1}{L} \sum_{i=1}^{L} (x_i - \langle x \rangle)^2} \tag{9.6}$$

The rescaled range is calculated by dividing the range R by the standard deviation:

$$R / S = \frac{R(i)}{S(i)} \tag{9.7}$$

The Hurst exponent is estimated by calculating the average rescaled range over multiple regions of the data. Call the average (mean) of a data set x is $E[x]$, the expected value of R/S is calculated over a set of regions. It converges on the Hurst exponent power function as:

$$E\left[\frac{R(i)}{S(i)}\right] = Ci^H \tag{9.8}$$

The constant C influences the value of H.

Hurst exponent (H) is computed by:

$$H(i) = \frac{\log(R / S)}{\log(i)} \tag{9.9}$$

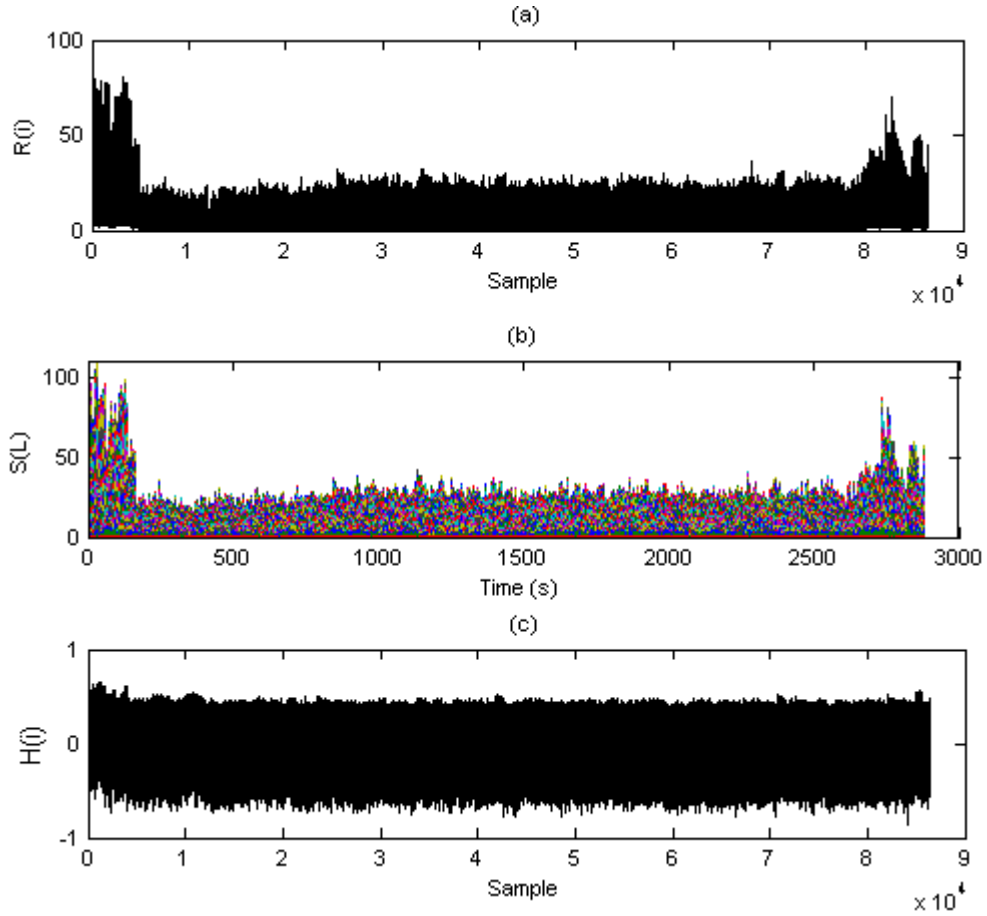

Figure 9.1:

(a) $R(i)$ is the difference between the maximum and the minimum of value $Y(i)$, over the length L = 2881 and window length m = 30, the sample = L x m = 2881 x 30 = 86430.

(b) $S(L)$ is the standard deviation over the length (L=2881) of the signal.

(c) The Hurst exponent $H(i)$ is estimated by calculating the average rescaled range over multiple regions of the data. The length L = 2881 and window length m = 30. The sample = L x m = 2881 x 30 = 86430.

Figure 9.1 presents $R(i)$, $S(L)$ and $H(i)$ of the EEG signal of patient 3, respectively. The information of patient 3 was presented in the previous chapter (section 7.2). The maximum values of $S(L)$ and $R(i)$ in this figure have the relationship with the change of DoA of patient 3. When the patient's state have changed from consciousness to unconsciousness, maximum values of $S(L)$ and $R(i)$ reduced from 100 to 22, corresponding to BIS values reducing from 97 to 20. During the deep anaesthesia time, maximum values of $S(L)$ and $R(i)$ have values between 20 and 30. When the patient's state have changed from unconsciousness to consciousness, maximum values of $S(L)$ and $R(i)$ increase from 20 to 80 in Figures 9.1(a) and 9.1(b).

However, the Hurst exponent $H(i)$ in Figure 9.1(c) does not show the relationship with the clinical state of patient 3. $H(i)$ could not not directly reflect the patient's clinical states from awake to deep anaesthesia and vice versa. In the next section, a modification from Hurst parameters is proposed for monitoring the DoA.

9.3 MODIFIED HURST EXPONENT FOR MONITORING THE DoA

The discussion of results above was based on Hurst parameters which were presented in (9.3) to (9.9). As the results in Figure 9.1, the maximum values of $S(L)$ and $R(i)$ have the relationship with the clinical states of patient 3. Therefore,

we set:

$$mSS = \frac{\max(S) + mean(S)}{2} \tag{9.10}$$

$$mS = \max(mSS) \tag{9.11}$$

$$mR = \max(R) \tag{9.12}$$

We compute the value H_S by:

$$H_S = \max\left(1 - \frac{\log\left(\frac{R}{mean(S)}\right)}{\log(i)}\right) \tag{9.13}$$

Figures 9.2(a) and 9.2(b) represent the diagrams of *mS* and *mR*, respectively. In Figure 9.2, when the patient's states have changed from consciousness to unconsciousness, *mS* decreased from 60 to 10 and *mR* decreased from 100 to 40. During the deep anaesthesia time, *mS* fluctuate from 10 to 20, and *mR* fluctuates from 35 to 45. In emergence time, when the patient's states changed from unconsciousness to consciousness, *mS* increased from 10 to 50 and *mR* increased from 40 to 90. However, during deep anaesthesia, *mS* and *mR* fluctuate widely in the range of 10. To reduce this fluctuation, *mS* and *mR* are divided for H_S values.

Define *CDoA* and *CsDoA* be the DoA indices, we have:

$$\begin{aligned} CDoA &= k_{mR}\frac{mR}{H_S} + V_{OFFSET}^{mR} \\ CsDoA &= k_{mS}\frac{mS}{H_S} + V_{OFFSET}^{mS} \end{aligned} \tag{9.14}$$

k_{mR}, k_{mS}, V_{OFFSET}^{mR}, and V_{OFFSET}^{mS} are the values calculated in the offline analysis. Empirically, values like $k_1=1$, $k_2=2$, $V_{OFFSET}^{mR}=5$, and $V_{OFFSET}^{mS}=20$ produced the best results. These constant values are merely estimates of a unit of measure, to fix the *CDoA* and *CsDoA* values in the range of 0-100.

In order to estimate the results on anaesthesia states of the patients, *CDoA* and *CsDoA* trends were compared with BIS trends, covering the whole scale from 100 to 0 with a full recording time. The *CDoA* and *CsDoA* trends are close to BIS trend in the whole time range in Figure 9.3 and Figure 9.4.

When the patient's states changed from consciousness to unconsciousness, *CDoA* values decreased from 100 to 40 and *CsDoA* values decreased from 90 to 30. During the deep anaesthesia time, *CDoA* values fluctuate from 45 to 50, and *CsDoA* values fluctuate from 35 to 45. In emergence time, when the patient's states have changed from unconsciousness to consciousness, *CDoA* values increased from 40 to 100 and *CsDoA* values increased from 35 to 110. Comparing with BIS trends, covering the whole scale from 100 to 0 with a full recording time, *CDoA* and *CsDoA* trends are close to BIS trend in this time range. Therefore, *CDoA* and *CsDoA* can be used to monitor the depth of anaesthesia.

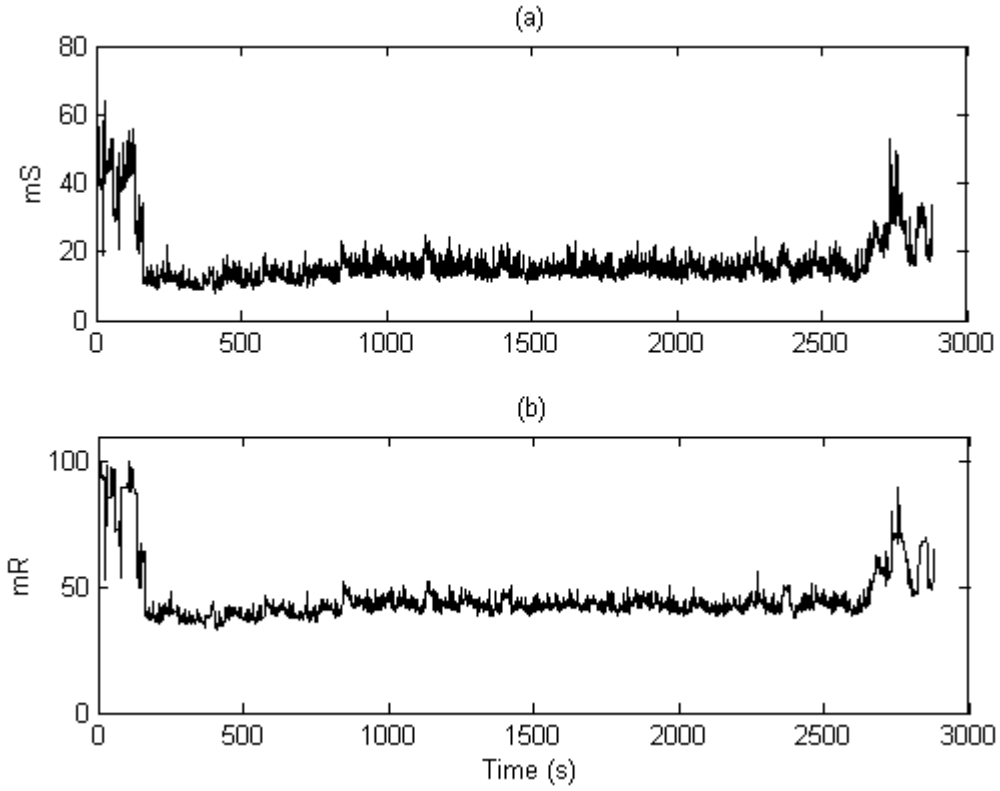

Figure 9.2:

(a) *mS* is the maximum values of *S*(*L*) when the patient's states have changed from consciousness to unconsciousness, *mS* values decreased from 60 to 10. During the deep anaesthesia time, *mS* values fluctuate from 10 to 20. In emergence time, when the patient's states have changed from unconsciousness to consciousness, *mS* values increased from 10 to 50.

(b) *mR* is the maximum values of *R*(*i*). When the patient's states have changed from consciousness to unconsciousness, *mR* decreased from 100 to 40. During the deep anaesthesia time, *mR* fluctuated from 35 to 45. In emergence time, when the patient's states have changed from unconsciousness to consciousness, *mR* increased from 40 to 90.

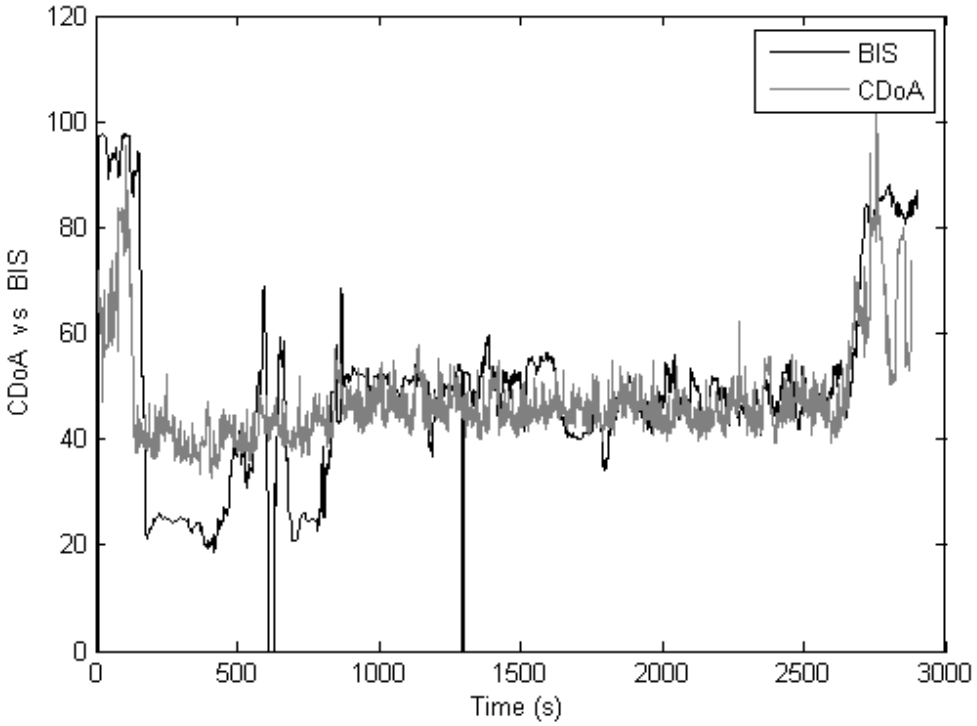

Figure 9.3: CDoA trend are compared with BIS trend. When the patient's states changed from consciousness to unconsciousness, *CDoA* values decreased from 100 to 40. During the deep anaesthesia time, *CDoA* values fluctuate from 45 to 50. In emergence time, when the patient's states have changed from unconsciousness to consciousness, *CDoA* values increased from 40 to 100.

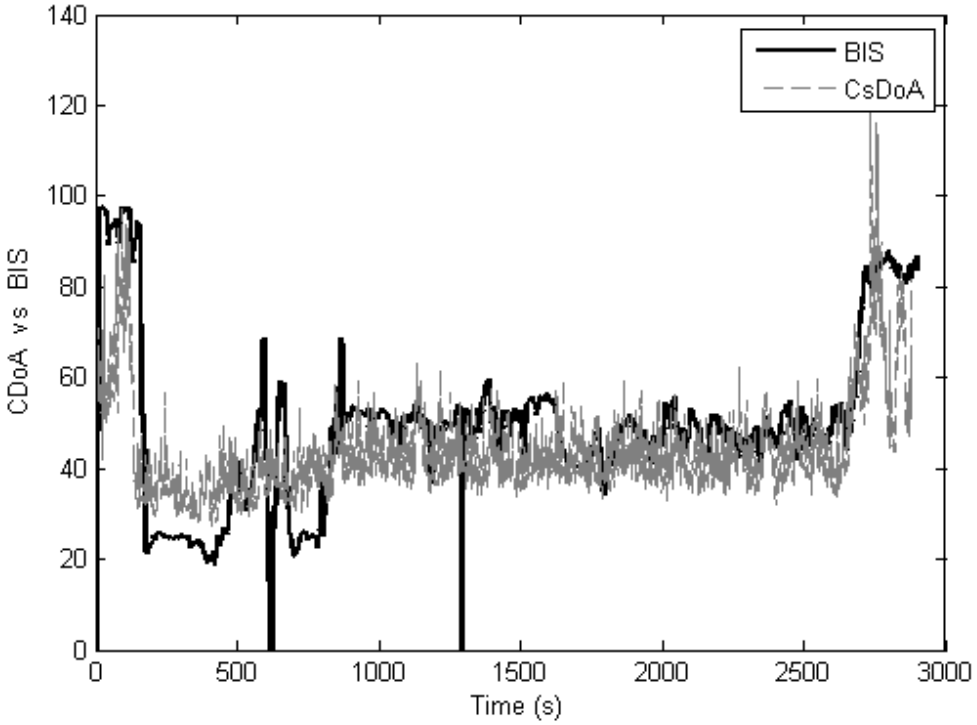

Figure 9.4: CsDoA trend are compared with BIS trend. When the patient's states changed from consciousness to unconsciousness, CsDoA values decreased from 90 to 30. During the deep anaesthesia time, CsDoA values fluctuate from 35 to 45. In emergence time, when the patient's states have changed from unconsciousness to consciousness, CsDoA values increased from 35 to 110.

9.4 COMBINATION OF CHAOS AND MDMA METHODS

Although CDoA and CsDoA trends are close with BIS trend, they are more fluctuation during general anaesthesia as shown in Figures 9.3 and 9.4. In order to reduce this fluctuation, a combination of Chaos and MDMA methods is applied for monitoring the DoA. The detail of MDMA method was presented in Chapter 7. The new method is called as Ch-MDMA.

In Ch-MDMA, the MDMA is chosen as a feature function. $R(i)$ in (9.5) is used as input signal. The diagram for this combination is:

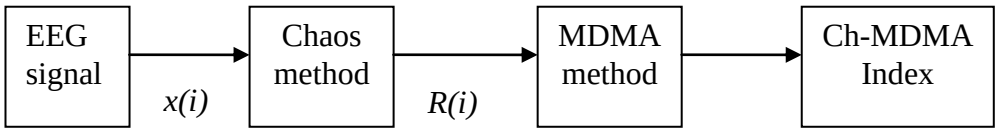

Figure 9.5: The diagram of Ch-MDMA method.

In order to estimate the result on anaesthesia states of the patients, Ch-MDMA trend is compared with BIS trend, covering the whole scale from 100 to 0 with full recording time. Figure 9.5 shows the comparision of Ch-MDMA trend and BIS trend of patient 3 in the 2809 second recording time. In this figure, the Ch-MDMA trend closes with BIS trend in this time range. The fluctuation of Ch-MDMA trend is lower than the fluctuation of CDoA and CsDoA in Figures 9.3 and 9.4.

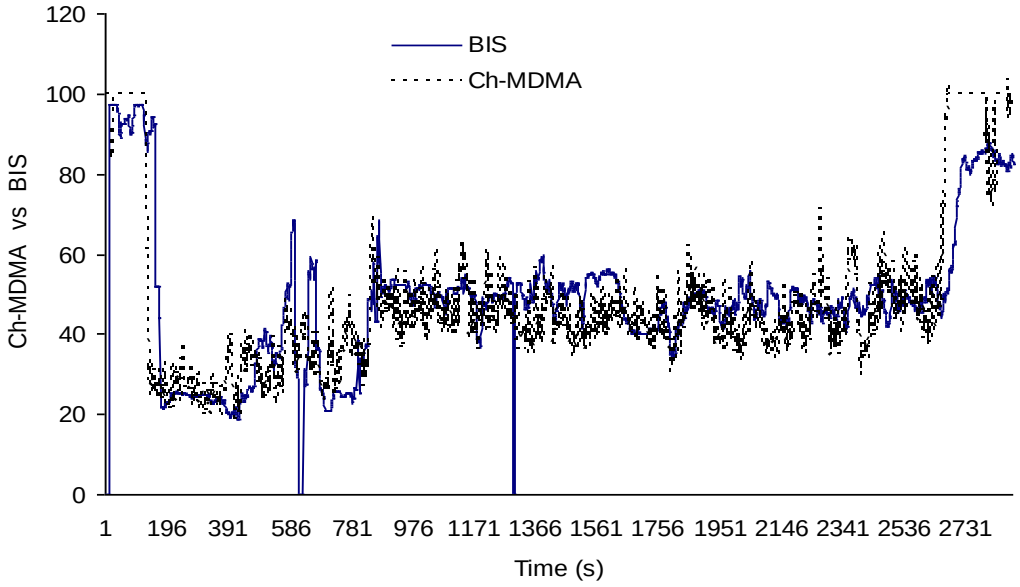

Figure 9.6: A comparison between Ch-MDMA trend and BIS trend.

Chapter 10

Conclusions

10.1 INTRODUCTION

This study was approved by the University of Southern Queensland Human Research Ethics Committee (No: H09REA029) and the Toowoomba and Darling Downs Health Service District Human Research Ethics Committee (No: TDDHSD HREC 2009/016). The raw EEG data and the BIS data were collected from Toowoomba Base Hospital, Toowoomba city, Queensland. This research was carried out at University of Southern Queensland (USQ) and supported by an Australia Research Council Discovery Program grant (DP0665216).

The main purpose of this study is to monitor the DoA based on simplified EEG signals. The EEG signals are investigated in both the time domain and the time-frequency domain. The Detrended Fluctuation Analysis (DFA), the Detrended Moving Averaged (DMA), the Chaos method (in the time domain) and the Wavelet methods (in the time-frequency domain) are modified and applied to study the scaling behavior of the EEG as a measure of the DoA.

A literature review of the DoA assessment is introduced in the chapter 2. This chapter briefly introduces an overview of clinical viewpoint, DoA monitoring, basic methods and statement of the problems for monitoring the DoA. Chapter 3 focuses on data acquisition, research objectives, medothologies and thesis outline. Chapter 4 describes the basic techniques in EEG signal de-noising. This chapter also presents a new denoise threshold T_{WE} which is a function of wavelet entropy and window length m for an EEG segment.

Chapters 5 and 6 propose two modifications of the DFA method. Theoretical basis for the MDFA algorithms is based on the DFA algorithm. The motivation of the modifications is to separate the $F(s)$ of the moderate anaesthesia and light anaesthesia states. These two states appear in a short time and are difficult to detect them. The limitation of these methods is that the states of anaesthesia must be identified before using the modified DFA equations. Therefore, the methods to identify the states of anaesthesia such as the FFT, filter banks and modified DFA methods ars proposed. Finally, a new DoA index is proposed and implemented.

Chapter 7 presents a modified DMA method to assess the DoA. The proposed MDMA method is developed by computing the scaling exponent α and minimum lnF_{MDMA} value. The wavelet energy entropy E_m is used to separate the different states of anaesthesia. Two new indices (F_α, F_{min}) are used to monitor the DoA. The limitation of this method is the chosen region. Regions 1 and 2 are selected based on the practical experience from the analysed data. Although this choice was consistent with the result in (Ferree, 2002), F_α still has more fluctuation.

In chapter 8, the discrete wavelet transforms (DWT) and power spectral density (PSD) function are applied to compute the DoA. The change of PSD for the wavelet coefficients has a relation with the change of patient's states. The means and

the standard deviations of *EAj* and ED_j move from high to low when the patient state moves from consciousness to unconsciousness and vice versa. Chapter 9 presented a modified Chaos method. A combination of the Chaos and MDMA methods is applied for monitoring the DoA.

The limitation of the proposed methods in chapters 7, 8 and 9 are the set of constants and V_{offset} in the equations of DoA index. The other limitation of this research is the off-line analysing. Therefore, the results can not be compared with the clinical states in the real time.

10.2 CONTRIBUTIONS AND PUBLICATIONS

The significant achievements and contributions of this dissertation are presented in chapter 4 to 9 which introduce five new methods to monitor the depth of anaesthesia. In addition, a algorithm has been developed to de-noise and pre-process the EEG signals. Details of the research contributions in each chapter are summarized as follows:

Chapter 4

The main results in this chapter are the wavelet transform based denoising algorithm and the new threshold T_{WE} which are proposed to de-noise the raw EEG signal. The results have been published in a conference paper:

- Nguyen-Ky, T., Wen, P. and Li, Y. (2010a). "De-noising a raw eeg signal and measuring depth of anaesthesia for general anaesthesia patients." *The 2010 IEEE/ICME International Conference on Complex Medical Engineering (CME2010) in Gold Coast, Australia.*

Chapter 5

In this chapter, we proposes a modifid detrended fluctuation analysis (MDFA I) and to apply it to monitor the DoA. In this method, we optimise the box size to achieve performance. The results demonstrate that the new method can clearly discriminate the awake state, light anesthesia, moderate anesthesia, deep anesthesia and very deep anesthesia state based on the raw EEG data. Therefore, this method provides a better solution in DoA assessment. The results have been published in one journal paper and one conference paper:

- Nguyen-Ky, T., Wen, P. and Li, Y. (2009b). "Theoretical basis for identification of different anaesthetic states based on routinely recorded EEG during operation." *Computers in Biology and Medicine* 39(1): 40-45.
- Nguyen-Ky, T., Wen, P. and Li, Y. (2008). "Modified detrended fluctuation analysis method in depth of anaesthesia assessment application." *Proceeding of the 2008 International Conference on bioinformatics & computational biology, Las Vegas, Nevada, USA*: 279-284.

Chapter 6

The main result in this chapter is another modified detrended fluctuation analysis (MDFA II) which is used to improve the monitoring accuracy of the depth of anaesthesia. This new method extends the ranges of the moderate anaesthesia, deep anaesthesia and very deep anaesthesia. This extension is significant from a clinical perspective as these states are within the ranges for operations. The results have been published in a journal paper:

- Nguyen-Ky, T., Wen, P. and Li, Y. (2010b). "Improving the accuracy of depth of anaesthesia using modified detrended fluctuation analysis method." *Biomedical Signal Processing and Control* 5(1): 59-65.

Chapter 7

The main contribution in this chapter is the modified detrended moving average (MDMA) method for monitoring the DoA. Two new indices (Fα, Fmin) are responsive to the anaesthetic agent and can estimate a patient's hypnotic state when signal quality is poor. This new method also reduces the time delay during which the patient's hypnotic state changes from consciousness state to unconsciousness state, and vice versa. Three special cases were analysed in comparison with BIS. The results of our methods are better correlation with the patient's hypnotic state in clinical observation. The results have been published in a journal paper.

- Nguyen-Ky, T., Wen, P. and Li, Y. (2010c). "An improved de-trended moving average method for monitoring the depth of anaesthesia." *IEEE Transactions on biomedical engineering*, 57(10): 2369-2378.

Chapter 8

The key contribution in this chapter is to propose a new wavelet-based depth of anaesthesia (WDoA) index for monitoring the DoA. This index is based on the discrete wavelet transforms (DWT) and power spectral density (PSD) function. During computation, an adaptive window length (AWL) was applied to reduce the time delay. AWL is a function of the wavelet energy entropy and adapts to the clinical state of the patient. Three special cases were analysed in comparison with

BIS. The results have been published in a conference paper and also accepted for publication in a journal.

- Nguyen-Ky, T., Wen, P., Li, Y., *et al.* (2010d). "Measuring and reflecting depth of anaesthesia using wavelet and power spectral density techniques." IEEE *Transactions on Information Technology in BioMedicine,* accepted 2011.
- Nguyen-Ky, T., Wen, P. and Li, Y. (2009a). "Monitoring the depth of anaesthesia using discrete wavelet transform and power spectral density." *Proceeding of the fourth International Conference on Rough Sets and Knowledge Technology (RSKT2009), Gold Coast, Australia*. (The best student paper award).

Chapter 9

The main contribution in this chapter is to modify the Hurst parameters in Chaos method for monitoring the DoA. Two new indices (*CDoA* and *CsDoA*) are proposed in order to estimate the anaesthesia states of the patients. In order to reduce the fluctuation of *CDoA* and *CsDoA* trends, a combination of Chaos and MDMA methods (Ch-MDMA) is applied for monitoring the DoA. Comparing with BIS trends, *CDoA, CsDoA* and Ch-MDMA trends are close to BIS trend. The results are under a journal submission and also will be submitted to a conference.

10.3 FUTURE WORK

10.3.1 Improvement and combination of the new methods in this dissertation

In future research, with increased number of patients, these factors { K_{α}^{Modify}, $K_{\min}^{Modify}$, k_1, k_2, k_3, k_{Mr}, k_{Ms}, and V_{offset} } in Chapters 7, 8, and 9 may become a function of patient's age, weight, protocol or all of them.

The trend of WDoA index is smoother than F_{α} and F_{min} trends. Therefore, it is suggested that F_{α} and F_{min} can be used to reflect the patient's changes from consciousness to unconsciousness; and WDoA index can be used during general of anaesthesia. Therefore, method III and method IV can be coordinated by two new functions: *mean*(WDoA, F_{α}) and *mean*(WDoA, F_{min}).

10.3.2 Combination of EEG signal with other signals for DoA monitoring

This research uses simplified EEG signals to monitor the depth of anaesthesia. In future research, EEG, ECG and blood pressure will be combined as the input signals for monitoring the DoA.

EEG can be used simultaneously with Functional magnetic resonance imaging (fMRI), Positron Emission Tomography (PET), and Single Photon Emission Computed Tomography (SPECT) so that high-temporal-resolution data can be recorded at the same time as high-spatial-resolution data**.** Combination of EEG source with above imaging techniques may be advantageous to increase the validity of the depth of anaesthesia assessment (Peyron, 2000; Richard, 2004).

.

10.4 SUMMARY

This research has proposed and applied novel signal processing techniques, which are better suited for non-stationary EEG signals than currently established methods, to monitor the DoA using simplified EEG signals. Firstly, we collect the EEG data from hospital, and convert it into the decimal number for processing. Secondly, the new denoising algorithm and new adaptive threshold are proposed for denoising the raw EEG signal. Thirdly, we propose and develop five new methods for identifying, classifying and monitoring the DoA. Finally, three special cases are studied. These cases demonstrade the advantages of proposed methods and limitations of the current BIS index in the cases of poor signal quality, time delay and reflect administered drugs. The new methods are not only used for monitoring the DoA but can also be used for analysing the ECG signal, controlling DoA, and detecting epileptic seizure.

References

Agarwal, M. and Griffiths, R. (2004). "Monitoring the depth of anaesthesia." Anaesthesia & intensive care medicine 5(10): 343-344.

Alkire, M. T. (1998). "Quantitative eeg correlations with brain glucose metabolic rate during anesthesia in volunteers." *Anesthesiology* 89(2): 323-333.

Alvarez-Ramirez, J., Alvarez, J., Dagdug, L., et al. (2008). "Long-term memory dynamics of continental and oceanic monthly temperatures in the recent 125 years." Physica A: Statistical Mechanics and its Applications 387(14): 3629-3640.

Anderson, R. E., Barr, G., Assareh, H., *et al*. (2003). "The aaitm index, the bis index and end-tidal concentration during wash in and wash out of sevoflurane." *Anaesthesia* 58(6): 531-535.

Anderson, R. E., Barr, G., Assareh, H., *et al*. (2005). "Cerebral state index during anaesthetic induction: A comparative study with propofol or nitrous oxide." *Acta Anaesthesiologica Scandinavica* 49(6): 750-753.

Anderson, R. E. and Jakobsson, J. G. (2004). "Entropy of eeg during anaesthetic induction: A comparative study with propofol or nitrous oxide as sole agent " British journal of anaesthesia 92(2): 167-170.

Anderson, R. E. and Jakobsson, J. G. (2006). "Cerebral state index response to incision: A clinical study in day-surgical patients." *Acta Anaesthesiologica Scandinavica* 50(6): 749-753.

Andrew, J. D., Huang, G. H., Czarnecki, C., *et al.* (2005). "Awareness during anesthesia in children: A prospective cohort study." *Anaesthesia & Analgesia* 100(3): 653-661.

Arianos, S. and Carbone, A. (2007). "Detrending moving average algorithm: A closed-form approximation of the scaling law." *Physica A: Statistical Mechanics and its Applications* 382(1): 9-15.

Aspect, M. S. (2008). " Bis monitor export data technical specification.". Aspect Medical Systems.

Attwood, H. L. and Mackay, W. A. (1989). "Essentials of neurophysiology." B. C. Decker, Hamilton, Canada.

Aydın, S., Saraoğlu, H. and Kara, S. (2009). "Log energy entropy-based eeg classification with multilayer neural networks in seizure." *Annals of Biomedical Engineering* 37(12): 2626-2630.

Babloyantz, A., Salazar, J. M. and Nicolis, C. (1985). "Evidence of chaotic dynamics of brain activity during the sleep cycle." *Physics Letters A* 111(3): 152-156.

Bajekal, R. (2004). "Eye signs in anaesthesia and intensive care." *Anaesthesia & intensive care medicine* 5(9): 310-311.

Banjanin, B., Gergic, B., Planinsic, P., *et al*. (2001). "Entropy-threshold method for best basis selection." *Image and Vision Computing* 19(7): 477-484.

Bardet, J. M. and Kammoun, I. (2008). "Asymptotic properties of the detrended fluctuation analysis of long-range-dependent processes." *Information Theory, IEEE Transactions on* 54(5): 2041-2052.

Barr, G., Jakobsson, J. G., Owall, A., *et al*. (1999). "Nitrous oxide does not alter bispectral index: Study with nitrous oxide as sole agent and as an adjunct to i.V. Anaesthesia." *British journal of anaesthesia* 82(6): 827-830.

Bauerle, K., Greim, C.-A., Schroth, M., et al. (2004). "Prediction of depth of sedation and anaesthesia by the narcotrendtm eeg monitor." *Br. J. Anaesth*. 92(6): 841-845.

Bhagat, M., Bhushan, C., Saha, G., *et al*. (2009). "Investigating neuromagnetic brain responses against chromatic flickering stimuli by wavelet entropies." *PLoS ONE* 4(9): e7173.

Bibian, S., Zikov, T., Dumon, G. A. T., *et al.* (2008). "Method and apparatus for the estimation of anaesthetic depth using wavelet analysis of the electroencephalogram." *US Patent* #7,373,198.

BIS, M. (2008). "Export data technical specification." Aspect Medical Systems.

BIS sensor for Aspect Medical Systems, Inc.

Bischoff, P., Schmidt, G. N., Schulte, A. E., *et al.* (2000). "Assessment of depth of anaesthesia." *Best Practice & Research Clinical Anaesthesiology* 14(2): 321-334.

Blanco, S., Figliola, A., Kochen, S., et al. (1997). "Using nonlinear dynamic metric tools for characterizing brain structures." *Engineering in Medicine and Biology Magazine, IEEE* 16(4): 83-92.

Blesic, S., Miloševic, S., Stratimirovic, D., Ljubisavljevic, M. (1999). "Detrended fluctuation analysis of time series of a firing fusimotor neuron." *Physica A: Statistical Mechanics and its Applications* 268(3-4): 275-282.

Bøggild-Madsen, N. and Cargnelli, T. (1978). "Accidental over-dose of alfathesin under general anaesthesia: Case report." *Canadian Journal of Anesthesia / Journal canadien d'anesthésie* 25(3): 245-246.

Bojanic, S., Simpson, T. and Bolger, C. (2001). "Ocular microtremor: A tool for measuring depth of anaesthesia?" *Br. J. Anaesth*. 86(4): 519-522.

Boyd, S. and Vandenberghe, L. (2004). "Convex optimization." Cambridge University Press.

Breckenridge, J. L. (1983). "Awareness during anaesthesia: A review " *Annals of the Royal College of Surgeons of England* 65.

Brice, D. D., Hetherington, R. R. and Utting, J. E. (1970). "A simple study of awareness and dreaming during anaesthesia." *Br. J. Anaesth*. 42(6): 535-542.

Brigham, E. O. (1988). "The fast fourier transform and its applications." Prentice-Hall, Inc..

Bruhn, J., Myles, P. S., Sneyd, R., *et al.* (2006). "Depth of anaesthesia monitoring: What's available, what's validated and what's next?" *Br. J. Anaesth*. 97(1): 85-94.

Buldyrev, S. V., Dokholyan, N. V., Goldberger, A. L., *et al.* (1998). "Analysis of DNA sequences using methods of statistical physics." *Physica A: Statistical Mechanics and its Applications* 249(1-4): 430-438.

Buldyrev, S. V., Goldberger, A. L., Havlin, S., *et al.* (1995). "Long-range correlation properties of coding and noncoding DNA sequences: Genbank analysis." *PHYSICAL REVIEW E* 51(5): 5084.

Carbone, A. (2009). Detrending moving average algorithm: A brief review. *Science and Technology for Humanity (TIC-STH), 2009 IEEE Toronto International Conference*.

Chen, S.-W., Chen, H.-C. and Chan, H.-L. (2006). "A real-time qrs detection method based on moving-averaging incorporating with wavelet denoising." *Computer Methods and Programs in Biomedicine* 82(3): 187-195.

Chen, Z., Ivanov, P. Ch., Hu, K., *et al.* (2002). "Effect of nonstationarities on detrended fluctuation analysis." *PHYSICAL REVIEW E* 65(4): 041107.

Chernik, M. R. and Friis, R. H. (2003). "Introductory biostatistics for the health sciences." A John Wiley & Son Publication.

Coakley, D. and Thomas, J. (1977). "The ocular microtremor record and the prognosis of the unconscious patient." *The Lancet* 309(8010): 512-515.

Coifman, R. R. and Wickerhauser, M. V. (1992). "Entropy-based algorithms for best basis selection." *Information Theory, IEEE Transactions on* 38(2): 713-718.

Cork, R. C., DiNardo, J. A., Hilwig, R. W., *et al.* (1990). "A1077 effects of anaesthetic overdose with isoflurare and sevo-flurane oh hehodyhahics and oxygenation." *Anesthesiology* 73(3A): NA.

Dafilis, M. P., Bourke, P. D., Liley, D. T. J., *et al.* (2002). "Visualising chaos in a model of brain electrical activity." *Computers & Graphics* 26(6): 971-976.

Daubechies I. (1992). "Ten lectures on wavelets." SIAM, Society for Industrial and Applied Mathematics, Philadelphia, Pennsylvania.

De Moura, E. P., Vieira, A. P., Irmão, M. A. S., *et al.* (2009). "Applications of detrended-fluctuation analysis to gearbox fault diagnosis." *Mechanical Systems and Signal Processing* 23(3): 682-689.

Di, X., Hao, Y. and Shouchang, Z. (1997). "Extraction of 40 hz eeg bursts for chaos analysis of brain function." *Engineering in Medicine and Biology Magazine, IEEE* 16(4): 27-32.

Donoho, D. L. (1995a). "De-noising by soft-thresholding." *Information Theory, IEEE Transactions on* 41(3): 613-627.

Donoho, D. L. and Johnstone, I. M. (1995b). "Adapting to unknown smoothness via wavelet shrinkage." *Journal of the American Statistical Association* 90(432): 1200-1224.

Donoho, D. L. and Johnstone, J M. (1994). "Ideal spatial adaptation by wavelet shrinkage." *Biometrika* 81(3): 425-455.

Dorlas, J. C. and Nijboer, J. A. (1985). "Photo-electric plethysmography as a monitoring device in anaesthesia: Application and interpretation." *Br. J. Anaesth*. 57(5): 524-530.

Doufas, A. G., Bakhshandeh, M., Bjorksten, A. R., *et al.* (2001). "Automated responsiveness test (art) predicts loss of consciousness and adverse physiologic responses during propofol conscious sedation." *Anesthesiology* 94(4): 585-592.

Drover, D. and Ortega, H. R. (2006). "Patient state index." *Best Practice & Research Clinical Anaesthesiology* 20(1): 121-128.

Eger, E. I. I., Saidman, L. J. and Brandstater, B. (1965). "Minimum alveolar anaesthetic concentration: A standard of anaesthetic potency." *Anesthesiology* 26(6): 756-763.

Eriksson, A., Stoica, P. and Soderstrom, T. (1994). "Markov-based eigenanalysis method for frequency estimation." *Signal Processing, IEEE Transactions on* 42(3): 586-594.

Evans, J. M., Bithell, J. F. and Vlachonikolis, I. G. (1987). "Relationship between lower oesophageal contractility, clinical signs and halothane concentration during general anaesthesia and surgery in man." *Br. J. Anaesth*. 59(11): 1346-1355.

Evans, J. M., Davies, W. L. and Wise, C. C. (1984). "Lower oesophageal contractility: A new monitor of anaesthesia." *The Lancet* 323(8387): 1151-1154.

Faure, P. and Korn, H. (2001). "Is there chaos in the brain? I. Concepts of nonlinear dynamics and methods of investigation." *Comptes Rendus de l'Académie des Sciences - Series III - Sciences de la Vie* 324(9): 773-793.

Fell, J., Röschke, J. and Beckmann, P. (1993). "Deterministic chaos and the first positive lyapunov exponent: A nonlinear analysis of the human electroencephalogram during sleep." *Biological Cybernetics* 69(2): 139-146.

Ferenets, R., Tarmo, L., Anier, A., *et al.* (2006). "Comparison of entropy and complexity measures for the assessment of depth of sedation." *Biomedical Engineering, IEEE Transactions on* 53(6): 1067-1077.

Ferree, T. C. and Hwa, R. C. (2002). "Fluctuation analysis of human electroencephalogram." Nonlinear Phenomena Complex Syst. 5(3): 302-307.

Ferree, T. C. and Hwa, R. C. (2003). "Power-law scaling in human eeg: Relation to fourier power spectrum." *Neurocomputing* 52-54: 755-761.

Freeman, W. J. (2003). "Evidence from human scalp electroencephalograms of global chaotic itinerancy." *Chaos: An Interdisciplinary Journal of Nonlinear Science* 13(3): 1067-1077.

Fu, Q., Xue, Z., Zhu, J., *et al.* (2005). "Anaesthesia record system on handheld computers--pilot experience and uses for quality control and clinical guidelines." *Computer Methods and Programs in Biomedicine* 77(2): 155-163.

Gibbs, F. A., Gibbs, E. L. and Lennox, W. G. (1937). "Effect on the electro-encephalogram of certain drugs which influence nervous activity." *Arch Intern Med* 60(1): 154-166.

Gifani, P., Rabiee, H. R., Hashemi, M. H., *et al.* (2007). "Optimal fractal-scaling analysis of human eeg dynamic for depth of anesthesia quantification." *Journal of the Franklin Institute* 344(3-4): 212-229.

Glass, P. S. A. (1998). "Anaesthetic drug interactions: An insight into general anesthesia-its mechanism and dosing strategies." *Anesthesiology* 88(1): 5-6.

Gollamudi, S., Nagaraj, S., Kapoor, S., et al. (1998). "Set-membership filtering and a set-membership normalized lms algorithm with an adaptive step size." Signal Processing Letters, IEEE 5(5): 111-114.

Goodman, N. W. (1990). "Chaos in anaesthesia." *Anaesthesia* 45(3): 187-188.

Grau-Carles, P. (2001). "Long-range power-law correlations in stock returns." *Physica A: Statistical Mechanics and its Applications* 299(3-4): 521-527.

Grote, L., Zou, D., Kraiczi, H., *et al.* (2003). "Finger plethysmography--a method for monitoring finger blood flow during sleep disordered breathing." *Respiratory Physiology & Neurobiology* 136(2-3): 141-152.

Hall, J. D. and Lockwood, G. G. (1998). "Bispectral index: Comparison of two montages." *Br. J. Anaesth*. 80(3): 342-344.

Haykin, S. (1991). "Adaprive filter theory." NJ: Prentice-Hall.

He, Z., Chen, X. and Qian, Q. (2007). "A study of wavelet entropy measure definition and its application for fault feature pick-up and classification." *Journal of Electronics (China)* 24(5): 628-634.

Heaney, M., Kevin, L. G., Manara, A. R., *et al.* (2004). "Ocular microtremor during general anesthesia: Results of a multicenter trial using automated signal analysis." *Anesthesia & Analgesia* 99(3): 775-780.

Hilgenberg, J. C. (1981). "Intraoperative awareness during high-dose fentanyl-oxygen anesthesia." *Anesthesiology* 54(4): 341-342.

Horner, R. L., Innes, J. A., Holden, H. B., *et al.* (1991). "Afferent pathway(s) for pharyngeal dilator reflex to negative pressure in man: A study using upper airway anaesthesia." *The Journal of Physiology* 436(1): 31-44.

http://www.hhdsoftware.com/free-hex-editor

http://www.articlesbase.com/personal-injury-articles/anesthesia-overdose-risks-and-medical-malpractice-2254011.html

Huang, J. W., Ying-Ying, L., Nayak, A., *et al.* (1999). "Depth of anesthesia estimation and control " *Biomedical Engineering, IEEE Transactions on* 46(1): 71-81.

Hug, C. C. J. (1990). "Does opioid "Anesthesia" Exist?" *Anesthesiology* 73(1): 1-4.

Isaac, P. A. (1989). "Lower oesophageal contractility and depth of anaesthesia." *Baillière's Clinical Anaesthesiology* 3(3): 533-545.

Isaac, P. A. and Rosen, M. (1990). "Lower oesophageal contractility and detection of awareness during anaesthesia." *Br. J. Anaesth*. 65(3): 319-324.

James, C. J., Hagan, M. T., Jones, R. D., *et al.* (1997). "Multireference adaptive noise canceling applied to the eeg." *Biomedical Engineering, IEEE Transactions on* 44(8): 775-779.

Jensen, E. W. (2005). "Cerebral state monitoring and pharmacodynamic modelling by advanced fuzzy inference - state of the art." http://www.amca2005.unibe.ch.

Johansen, J. W. (2006). "Update on bispectral index monitoring." *Best Practice & Research Clinical Anaesthesiology* 20(1): 81-99.

Johansen, J. W. and Sebel, P. S. (2000). "Development and clinical application of electroencephalographic bispectrum monitoring." *Anesthesiology* 93(5): 1336-1344.

John, D. R., Herv, C. P., Linda, E. K. *et al.* (2003). Using deterministic chaos theory for the analysis of sleep eeg. Formal descriptions of developing systems, *Kluwer Academic Publishers*: 137-149.

Johnson, D. and DeGraaf, S. (1982). "Improving the resolution of bearing in passive sonar arrays by eigenvalue analysis." *Acoustics, Speech and Signal Processing*, IEEE Transactions on 30(4): 638-647.

Joseph, F. A., Earl, E. C. and Douglas, E. R. (2003). "Neural mechanisms of anesthesia.", Humana Press, Totowa, New Jersey.

Jospin, M., Caminal, P., Jensen, E. W., *et al.* (2007). "Detrended fluctuation analysis of eeg as a measure of depth of anesthesia." *Biomedical Engineering, IEEE Transactions on* 54(5): 840-846.

Kane M., Smith A. and Milne R. (2003). "Exploring professional boundaries in anaesthetics." http://www.sdo.nihr.ac.uk/files/project/28-final-report.pdf.

Kantelhardt, J. W., Koscielny-Bunde, E., Rego, H. H. A., *et al.* (2001). "Detecting long-range correlations with detrended fluctuation analysis." *Physica A: Statistical Mechanics and its Applications* 295(3-4): 441-454.

Kaul, H. L. and Neerja, B. (2002). "Monitoring depth of anaesthesia." *Indian J. Anaesth.* 46(2): 323-332.

Kelley, S. D. "Monitoring level of consciousness during anesthesia & sedation:A clinician's guide to the bispectral index." Aspect Medical Systems.

Kim, D. W., Kil, H. Y. and White, P. F. (2002). "Relationship between clinical endpoints for induction of anesthesia and bispectral index and effect-site concentration values." *Journal of Clinical Anesthesia* 14(4): 241-245.

Koitabashi, T. (2004). "Integration of suppression ratio in the bispectral index." *Journal of Anesthesia* 18(2): 141-143.

Korn, H. and Faure, P. (2003). "Is there chaos in the brain? Experimental evidence and related models." *Comptes Rendus Biologies* 326(9): 787-840.

Kortelainen, J., Koskinen, M., Mustola, S., *et al.* (2008). "Remifentanil modifies the relation of electroencephalographic spectral changes and clinical endpoints in propofol anesthesia." *Anesthesiology* 109(2): 198-205.

Kreuer, S. and Wilhelm, W. (2006). "The narcotrend monitor." *Best Practice & Research Clinical Anaesthesiology* 20(1): 111-119.

Kuizenga, K., Wierda, J. M. K. H. and Kalkman, C. J. (2001). "Biphasic eeg changes in relation to loss of consciousness during induction with thiopental, propofol, etomidate, midazolam or sevoflurane." *British journal of anaesthesia* 86(3): 354-360.

Ledowski, T., Preuss, J., Ford, A., *et al.* (2007). "New parameters of skin conductance compared with bispectral index(r) monitoring to assess emergence from total intravenous anaesthesia." *Br. J. Anaesth*. 99(4): 547-551.

Ledowski, T., Paech, M. J., Storm, H., *et al.* (2006). "Skin conductance monitoring compared with bispectral index(r) monitoring to assess emergence from general anaesthesia using sevoflurane and remifentanil." *Br. J. Anaesth*. 97(2): 187-191.

Lee, J.-M., Kim, D-J., Kim, I-Y., *et al.* (2002). "Detrended fluctuation analysis of eeg in sleep apnea using mit/bih polysomnography data." *Computers in Biology and Medicine* 32(1): 37-47.

Lennmarken, C., Bildfors, K., Enlund, G., *et al.* (2002). "Victims of awareness." *Acta Anaesthesiologica Scandinavica* 46(3): 229-231.

Levin, R. I. and Rubin, D. S. (1998). "Statistics for management." Prentice-Hall.

Maj-Lis, L., Stefan, T., Fredrik, G., *et al.* (2009). "Mortality within 2 years after surgery in relation to low intraoperative bispectral index values and preexisting malignant disease " *Anaesthesia & Analgesia* 108(2): 508-512.

Mallat, S. G. (1989). "A theory for multiresolution signal decomposition: The wavelet representation." *IEEE Transactions on Pattern Analysis and Machine Intelligence* 11: 674-693

Mallat, S. G. (1999). "A wavelet tour of signal processing." *Academic Press, San Diego*: 255-258.

Marple, S. L. (1987). "Digital spectral analysis." Englewood Cliffs, NJ, Prentice-Hall.

Mathews, D. M., Rahman, S. S., Cirullo, P. M., *et al.* (2005). "Increases in bispectral index lead to interventions that prevent possible intraoperative awareness." *Br. J. Anaesth.* 95(2): 193-196.

Mekler, A. (2008). "Calculation of eeg correlation dimension: Large massifs of experimental data." *Computer Methods and Programs in Biomedicine* 92(1): 154-160.

Merkel, G. and Eger, E. I. I. (1963). "A comparative study of halothane and halopropane anesthesia: Including method for determining equipotency." *Anesthesiology* 24(3): 346-357.

Mertins, A. (1999). "Signal analysis: Wavelets, Filter banks, Time-frequency Transforms and Applications." John Wiley & Sons Ltd.

Moerman, N., Bonke, B. and Oosting, J. (1993). "Awareness and recall during general anesthesia: Facts and feelings." *Anesthesiology* 79(3): 454-464.

Monk, T. G., Weldon, B. C., Garvan, C. W., *et al.* (2008). "Predictors of cognitive dysfunction after major noncardiac surgery." *Anesthesiology* 108(1): 18-30 10.1097/01.anes.0000296071.19434.1e.

Musshoff, F., Padosch, S. A. and Madea, B. (2005). "Death during patient-controlled analgesia: Piritramide overdose and tissue distribution of the drug." *Forensic Science International* 154(2-3): 247-251.

Nguyen-Ky, T., Wen, P. and Li, Y. (2009). Monitoring the depth of anesthesia using discrete wavelet transform and power spectral density. *Rough sets and knowledge technology, Springer Berlin / Heidelberg*. 5589: 350-357.

Nguyen-Ky, T., Leis, J. and Xiang, W. (2007). "An improved error estimation algorithm for stereophonic acoustic echo cancellation systems." *International conference on signal processing and communication systemss, Australia ICSPCS'2007.*

Nguyen-Ky, T., Leis, J. and Xiang, W. (2010). "An improved new error estimation algorithm for optimal filter lengths for stereophonic acoustic echo cancellation." *Computers & Electrical Engineering* 36(4): 664-675.

Nguyen-Ky, T., Wen, P. and Li, Y. (2008). "Modified detrended fluctuation analysis method in depth of anaesthesia assessment application." *Proceeding of the 2008 International Conference on bioinformatics & computational biology, Las Vegas, Nevada, USA*: 279-284.

Nguyen-Ky, T., Wen, P. and Li, Y. (2009a). "Monitoring the depth of anaesthesia using discrete wavelet transform and power spectral density." *Proceeding of the fourth International Conference on Rough Sets and Knowledge Technology (RSKT2009), Gold Coast, Australia.*

Nguyen-Ky, T., Wen, P. and Li, Y. (2009b). "Theoretical basis for identification of different anaesthetic states based on routinely recorded eeg during operation." *Computers in Biology and Medicine* 39(1): 40-45.

Nguyen-Ky, T., Wen, P. and Li, Y. (2009c). "High reliable anaesthesia index using combined wavelet transform and eigenvector techniques." *Computers in Biology and Medicine*, submited.

Nguyen-Ky, T., Wen, P. and Li, Y. (2010a). "De-noising a raw eeg signal and measuring depth of anaesthesia for general anaesthesia patients." *The 2010 IEEE/ICME International Conference on Complex Medical Engineering (CME2010) in Gold Coast, Australia.*

Nguyen-Ky, T., Wen, P. and Li, Y. (2010b). "Improving the accuracy of depth of anaesthesia using modified detrended fluctuation analysis method." *Biomedical Signal Processing and Control* 5(1): 59-65.

Nguyen-Ky, T., Wen, P. and Li, Y. (2010c). "An improved de-trended moving average method for monitoring the depth of anaesthesia." *IEEE Transactions on biomedical engineering* 57(10): 2369-2378.

Nguyen-Ky, T., Wen, P., Li, Y., *et al.* (2010d). "Measuring and reflecting depth of anaesthesia using wavelet and power spectral density techniques." *Transactions on Information Technology in BioMedicine,* conditionally accepted.

Nieminen, K., Westeren-Punnonen, S., Kokki, H., *et al.* (2002). "Sevoflurane anaesthesia in children after induction of anaesthesia with midazolam and thiopental does not cause epileptiform eeg." *Br. J. Anaesth*. 89(6): 853-856.

Notcutt, W. G., Knowles, P. and Kaldas, R. (1992). "Overdose of opioid from patient-controlled anagesia pumps." *British journal of anaesthesia* 69: 95-97.

Ogo, K. and Nakagawa, M. (1995). "Chaos and fractal properties in eeg data." *Electronics and Communications in Japan (Part III: Fundamental Electronic Science)* 78(10): 27-36.

Oikonomou, V. P., Tzallas, A. T. and Fotiadis, D. I. (2007). "A kalman filter based methodology for eeg spike enhancement." *Computer Methods and Programs in Biomedicine* 85(2): 101-108.

Ortolani, O., Conti, A., Di Filippo, A., *et al.* (2002). "Eeg signal processing in anaesthesia. Use of a neural network technique for monitoring depth of anaesthesia." *Br. J. Anaesth*. 88(5): 644-648.

Pan, C. P., Zheng, B., Wu, Y. Z., *et al.* (2004). "Detrended fluctuation analysis of human brain electroencephalogram." *Physics Letters A* 329(1-2): 130-135.

Panousis, P., Heller, A. R., Koch, T., *et al.* (2009). "Epidural ropivacaine concentrations for intraoperative analgesia during major upper abdominal surgery: A prospective, randomized, double-blinded, placebo-controlled study." *Anesthesia & Analgesia* 108(6): 1971-1976.

Peng, C. K., Buldyrev, S. V., Goldberger, A. L., *et al.* (1995). "Statistical properties of DNA sequences." *Physica A: Statistical Mechanics and its Applications* 221(1-3): 180-192.

Peng, C. K., Buldyrev, S. V., Havlin, S., *et al.* (1994). "Mosaic organization of DNA nucleotides." *PHYSICAL REVIEW E* 49(2): 1685.

Penzel, T., Kantelhardt, J. W., Grote, L., *et al.* (2003). "Comparison of detrended fluctuation analysis and spectral analysis for heart rate variability in sleep and sleep apnea." *IEEE Transactions on Biomedical Engineering,* 50(10): 1143-1151.

Peyron, R., Laurent, B. and Garcia-Larrea, L. (2000). "Functional imaging of brain responses to pain. A review and meta-analysis." *Neurophysiol Clin* 30: 263-288.

Pijn, J. P., Van, N. J., Noest, A., *et al.* (1991). "Chaos or noise in eeg signals; dependence on state and brain site." *Electroencephalogr Clin Neurophysiol* . 79(5): 371-81.

Pilge, S., Zanner, R., Schneider, G., *et al.* (2006). "Time delay of index calculation: Analysis of cerebral state, bispectral, and narcotrend indices." *Anesthesiology* 104(3): 488-494.

Poirier, M. P., Gonzalez, D.-R., Javier, A., *et al.* (1998). "Utility of monitoring capnography, pulse oximetry, and vital signs in the detection of airway mishaps: A hyperoxemic animal model." *The American Journal of Emergency Medicine* 16(4): 350-352.

Pomfrett, C. J. D. and Pearson, A. J. (1998). "Eeg monitoring using bispectral analysis." *Engineering Science and Education Journal* 7(4): 155-157.

Prichep, L. S., Gugino, L. D., John, E. R., *et al.* (2004). "The patient state index as an indicator of the level of hypnosis under general anaesthesia." *Br. J. Anaesth*. 92(3): 393-399.

Rampil, I. J. (1998). "A primer for eeg signal processing in anesthesia." *Anesthesiology* 89(4): 980-1002.

Rampil, I. J. and Laster, M. J. (1992). "No correlation between quantitative electroencephalographic measurements and movement response to noxious stimuli during isoflurane anesthesia in rats." *Anesthesiology* 77(5): 920-925.

Rampil, I. J., Mason, P. and Singh, H. (1993). "Anaesthetic potency (mac) is independent of forebrain structures in the rat." *Anesthesiology* 78(4): 707-712.

Rampil, I. J., Sasse, F. J., Smith, N. T., *et al.* (1980). "Spectral edge frequency - a new correlate of anaesthetic depth." *Anesthesiology* 53(3): S12.

Rampil, I. J., Welskopf, R. B., Brown, J. G., *et al.* (1988). "1653 and isoflurane produce similar dose-related changes in the electroencephalogram of pigs." *Anesthesiology* 69(3): 298-302.

Ramsay, M. A. E. and Michael A. E. (2005). "Role of brain function monitoring in the critical care and perioperative settings." *Seminars in Anesthesia, Perioperative Medicine and Pain* 24(4): 195-202.

Rapp, P. E., Bashore, T. R., Martinerie, J. M., *et al.* (1989). "Dynamics of brain electrical activity." *Brain Topography* 2(1): 99-118.

Renna, M., Wigmore, T., Mofeez, A., *et al.* (2002). "Biasing effect of the electromyogram on bis: A controlled study during high-dose fentanyl induction." *Journal of Clinical Monitoring and Computing* 17(6): 377-381.

Rezek, I., Roberts, S. J. and Conradt, R. (2007). "Increasing the depth of anesthesia assessment." *Engineering in Medicine and Biology Magazine, IEEE* 26(2): 64-73.
-1191.

Richard, G. W., Pauline, W. and Irene, T. (2004). "Using fmri to quantify the time dependence of remifentanil analgesia in the human brain." *Neuropsychopharmacology* 29: 626-635.

Rosso, O. A., Blanco, S., Yordanova, J., *et al.* (2001). "Wavelet entropy: A new tool for analysis of short duration brain electrical signals." *Journal of Neuroscience Methods* 105(1): 65-75.

Rundshagen, I., Schroder, T., Prichep, L. S., *et al.* (2004). "Changes in cortical electrical activity during induction of anaesthesia with thiopental/fentanyl and tracheal intubation: A quantitative electroencephalographic analysis." *Br. J. Anaesth.* 92(1): 33-38.

Russell, I. F. (1993). "Midazolam-alfentanil: An anaesthetic? An investigation using the isolated forearm technique." Br. J. Anaesth. 70(1): 42-46.

Sanei, S., Chambers, J. A. (2007). "EEG signal processing." John Wiley & Sons, Ltd.

Sandin, R. H., Enlund, G., Samuelsson, P., *et al.* (2000). "Awareness during anaesthesia: A prospective case study." *The Lancet* 355(9205): 707-711.

Sang, Y.-F., Wang, D. and Wu, J.-C. (2010). "Entropy-based method of choosing the decomposition level in wavelet threshold de-noising." *Entropy* 12(6): 1499-1513.

Schmidt, R. and Franks, R. (1986). "Multiple source df signal processing: An experimental system." *Antennas and Propagation, IEEE Transactions on* 34(3): 281-290.

Schneider, G., Kochs, E. F., Horn, B., *et al.* (2004a). "Narcotrend(r) does not adequately detect the transition between awareness and unconsciousness in surgical patients." *Anesthesiology* 101(5): 1105-1111.

Schneider, G., Schoniger, S., Kochs, E., *et al.* (2004b). "Does bispectral analysis add anything but complexity? Bis sub-components may be superior to bis for detection of awareness." *Br. J. Anaesth*. 93(4): 596-597.

Schneider, G. and Sebel, P. S. (1997). "Monitoring depth of anaesthesia." *European Journal of Anaesthesiology* 14: 21-28.

Scott, D. K. "Monitoring consciousness using the bispectral indextm during anesthesia, a pocket guide for clinicians." 2nd edition, Aspect Medical System.

Sebel, P. S., Bowdle, T. A., Ghoneim, M. M., *et al.* (2004). "The incidence of awareness during anesthesia: A multicenter united states study." *Anesthesia & Analgesia* 99(3): 833-839.

Service information manual, Aspect Medical Systems, Inc.

Shannon, C. E. (1984). "A mathematical theory of communication." The Bell System Technical Journal 27: 379-423, 623-656.

Sicuranza, G. L. and Carini, A. (2004). "Filtered-x affine projection algorithm for multichannel active noise control using second-order volterra filters." Signal Processing Letters, IEEE 11(11): 853-857.

Sleigh, J. W., Steyn-Ross, D. A., Steyn-Ross, M. L., *et al.* (2001). "Comparison of changes in electroencephalographic measures during induction of general anaesthesia: Influence of the gamma frequency band and electromyogram signal." *Br. J. Anaesth*. 86(1): 50-58.

Soong, A. and Stuart, C. (1989). "Evidence of chaotic dynamics underlying the human alpha-rhythm electroencephalogram." *Biological Cybernetics* 62(1): 55-62.

Stengele, E., Winkler, F., Trenk, D., *et al*. (1996). "Digital pulse plethysmography as a non-invasive method for predicting drug-induced changes in left ventricular preload." *European Journal of Clinical Pharmacology* 50(4): 279-282.

Taylor, T. H. and Major, E. (1993). "Hazards and complications of anaesthesia." Churchill Livingstone in Edinburgh.

Tempe, D. K. and Satyanarayana, L. (2004). "Is there any alternative to the bispectral index monitor?" *Br. J. Anaesth*. 92(1): 1-3.

Terri, G. M., Saini, V., Weldon, B. C., *et al.* (2005). "Anaesthetic management and one-year mortality after noncardiac surgery." *Anesthesia & Analgesia* 100 (1): 4-10.

Urban, B. W. and Bleckwenn, M. (2002). "Concepts and correlations relevant to general anaesthesia " *Br. J. Anaesth*. 89(1): 3-16.

Van, S. B. (2006). "A succession of anaesthetic endpoints in the drosophila brain." *Journal of Neurobiology* 66(11): 1195-1211.

Vetterli, M. and Herley, C. (1992). "Wavelets and filter banks: Theory and design." *Signal Processing, IEEE Transactions on* 40(9): 2207-2232.

Viertiö-Oja, H., Maja, V., Särkelä, M., *et al.* (2004). "Description of the entropy™ algorithm as applied in the datex-ohmeda s/5™ entropy module." *Acta Anaesthesiologica Scandinavica* 48(2): 154-161.

Walling, P. T. and Hicks, K. N. (2006). "Nonlinear changes in brain dynamics during emergence from sevoflurane anesthesia: Preliminary exploration using new software." *Anesthesiology* 105(5): 927-935.

Wang, X., Meng, J., Tan, G., *et al.* (2010). "Research on the relation of eeg signal chaos characteristics with high-level intelligence activity of human brain." *Nonlinear Biomedical Physics* 4(1): 2.

Yentis, S. M., Hirsch, N. P. and Smith, G. B., (2009). Anaesthesia and Intensive Care A-Z: An Encyclopedia of Principles and Practice. 4th Ed. Churchill Livingstone.

Yordanova, J., Kolev, V., Rosso, O. A., *et al.* (2002). "Wavelet entropy analysis of event-related potentials indicates modality-independent theta dominance." *Journal of Neuroscience Methods* 117(1): 99-109.

Zanner, R., Pilge, S., Kochs, E. F., *et al.* (2009). "Time delay of electroencephalogram index calculation: Analysis of cerebral state, bispectral, and narcotrend indices using perioperatively recorded electroencephalographic signals." *Br. J. Anaesth*. 103(3): 394-399.

Zhang, X. S., Roy, R. J. and Jensen, E. W. (2001). "EEG complexity as a measure of depth of anesthesia for patients." *Biomedical Engineering, IEEE Transactions on* 48(12): 1424-1433.

Zhong, T., Guo, Q. L., Pang, Y. D., *et al.* (2005). "Comparative evaluation of the cerebral state index and the bispectral index during target-controlled infusion of propofol." *Br. J. Anaesth*. 95(6): 798-802.

Zikov, T., Bibian, S., Dumont, G. A., *et al.* (2006). "Quantifying cortical activity during general anesthesia using wavelet analysis." *Biomedical Engineering, IEEE Transactions on* 53(4): 617-632.